MAGNETIC EXCITATIONS IN THE DILUTED FERROMAGNET $Ni_2Mn_{0.8}V_{0.2}Sn$

By

© KENNETH E. LOCKE, B.Sc., M.Sc.

A Thesis

Submitted to the School of Graduate Studies

in Partial Fulfilment of the Requirements

for the Degree

Doctor of Philosophy

McMaster University

November 1981

MAGNETIC EXCITATIONS IN $Ni_2Mn_{0.8}V_{0.2}Sn$

DOCTOR OF PHILOSOPHY (1981)
(Physics)

McMASTER UNIVERSITY
Hamilton, Ontario

TITLE: Magnetic Excitations in the Diluted Ferromagnet $Ni_2Mn_{0.8}V_{0.2}Sn$

AUTHOR: Kenneth E. Locke, B.Sc. (Dalhousie University)

M.Sc. (McMaster University)

SUPERVISOR: Professor C.V. Stager

NUMBER OF PAGES: ix, 121

ABSTRACT

The magnetic excitation spectrum of the randomly diluted ferromagnet, $Ni_2Mn_{0.8}V_{0.2}Sn$, has been measured by neutron inelastic scattering techniques. The frequencies are reduced from those observed for the non-diluted ferromagnet, Ni_2MnSn, by a factor that depends on wavevector. The shape of the frequency shift is characteristic of an in-band resonance. Computer simulation calculations have been performed for large finite arrays (~15,000 spins) including up to third neighbour interactions. The predicted frequencies agree with experiment. The calculations show a resonant effect however it is not as pronounced as the observed effect.

ACKNOWLEDGEMENTS

First and foremost, I would like to thank my supervisor, Dr. C.V. Stager, for his interest and guidance throughout the course of this research. Secondly, my thanks go to Dr. W.J.L. Buyers for his help and advice concerning the computer simulation theory, and to Drs. M.F. Collins, D.W. Taylor and B.N. Brockhouse for many helpful discussions.

For technical assistance, I am indebted to Mr. J. Couper and Mr. J. Garrett. It has been a pleasure to work with them.

Thanks are due to Atomic Energy of Canada Limited for providing research and computing facilities and to Dr. G. Dolling and the other members of the Neutron Solid State Physics Branch whose helpfulness and friendship was greatly appreciated during my visits to Chalk River.

Finally, I wish to thank Mrs. Helen Kennelly and Ms. Devi Symons for carefully typing the thesis, and the many colleagues and friends who made my stay at McMaster an enjoyable and rewarding experience.

Financial assistance is acknowledged from the McMaster University Physics Department, the Natural Sciences and Engineering Research Council of Canada and the Ontario Graduate Scholarship Program.

To my parents

TABLE OF CONTENTS

LIST OF FIGURES

LIST OF TABLES

CHAPTER 1

INTRODUCTION

There has been considerable experimental and theoretical interest in magnetic excitations in substitutionally disordered alloys. Several mixed and diluted systems of antiferromagnetic insulators have been studied, as reviewed by Cowley and Buyers[1] and Cowley[2], but there has been no experimental investigation of a disordered ferromagnet. This is because suitable alloys have not been available. However, recent magnetic studies have suggested that the Heusler alloy, $Ni_2Mn_{1-x}V_xSn$, is a randomly diluted ferromagnet[3]. The spins reside on the Mn atoms and the interaction between them is Heisenberg in nature[4]. In this work, to study the effect of dilution, the magnetic excitation spectra for $Ni_2Mn_{0.8}V_{0.2}Sn$ has been measured by inelastic neutron scattering techniques and the results compared to a computer simulation calculation.

Heusler alloys are intermetallic compounds, which are metallic in lustre and conductivity but have an ordered structure. Most Heusler alloys have the chemical formula, X_2MnZ, and the $L2_1$ lattice structure, where X is a transition element and Z is an s/p element. Many combinations of X and Z are possible. For example, X can be Cu, Ni, Co, Pd or Pt,

and Z can be Ge, Ga, Sb, Sn or Al. Recent tabulations are given by Campbell[5] and Price *et al.*[6] In the $L2_1$ structure, which is face-centered cubic, the X atoms are arranged on a simple cubic lattice while the Mn and Z atoms occupy alternate body centres. The magnetic properties of these compounds are somewhat surprising. In Ni_2MnSn, which is ferromagnetic (T_C = 344 K), the saturation moment of $\sim$4 μ_B per molecule is localized on the Mn atoms. The Ni atoms carry no appreciable moment, in spite of the fact that elemental Ni is ferromagnetic while Mn is not. The moment of 4 μ_B per Mn atom, which corresponds to a spin S = 2, is characteristic of all Heusler alloys except those containing Co or Fe[7-10] or when Mn is the X atom[11]. Polarized neutron studies of Pd_2MnSn, which is isostructural and isoelectronic with Ni_2MnSn, show that a small moment of $\sim$0.05 μ_B may exist at the Pd site and -0.05 μ_B at the Sn site[9]. The possibility of a small moment on the Ni and Sn atoms is neglected in this work. The Mn atoms form a fcc lattice of spins.

The spin-wave dispersion has been measured in three Heusler alloys; in Pd_2MnSn and Ni_2MnSn by Noda and Ishikawa[4], and in Cu_2MnAl by Tajima *et al.*[12] The results for Ni_2MnSn at 50 K are shown in Fig. 1.1. Noda and Ishikawa observed well defined peaks out to the zone boundary in the $[00\zeta]$, $[\zeta\zeta 0]$ and $[\zeta\zeta\zeta]$ directions. Only one branch was present which is expected if the Mn atoms carry all the moment. No widths

Fig. 1.1 Spin-wave dispersion relations for Ni_2MnSn at 50 K, after Noda and Ishikawa[4]. The solid line is the six-neighbour fit to the Heisenberg model (eqn. 1.2). The corresponding exchange constants are given in Table 1.1.

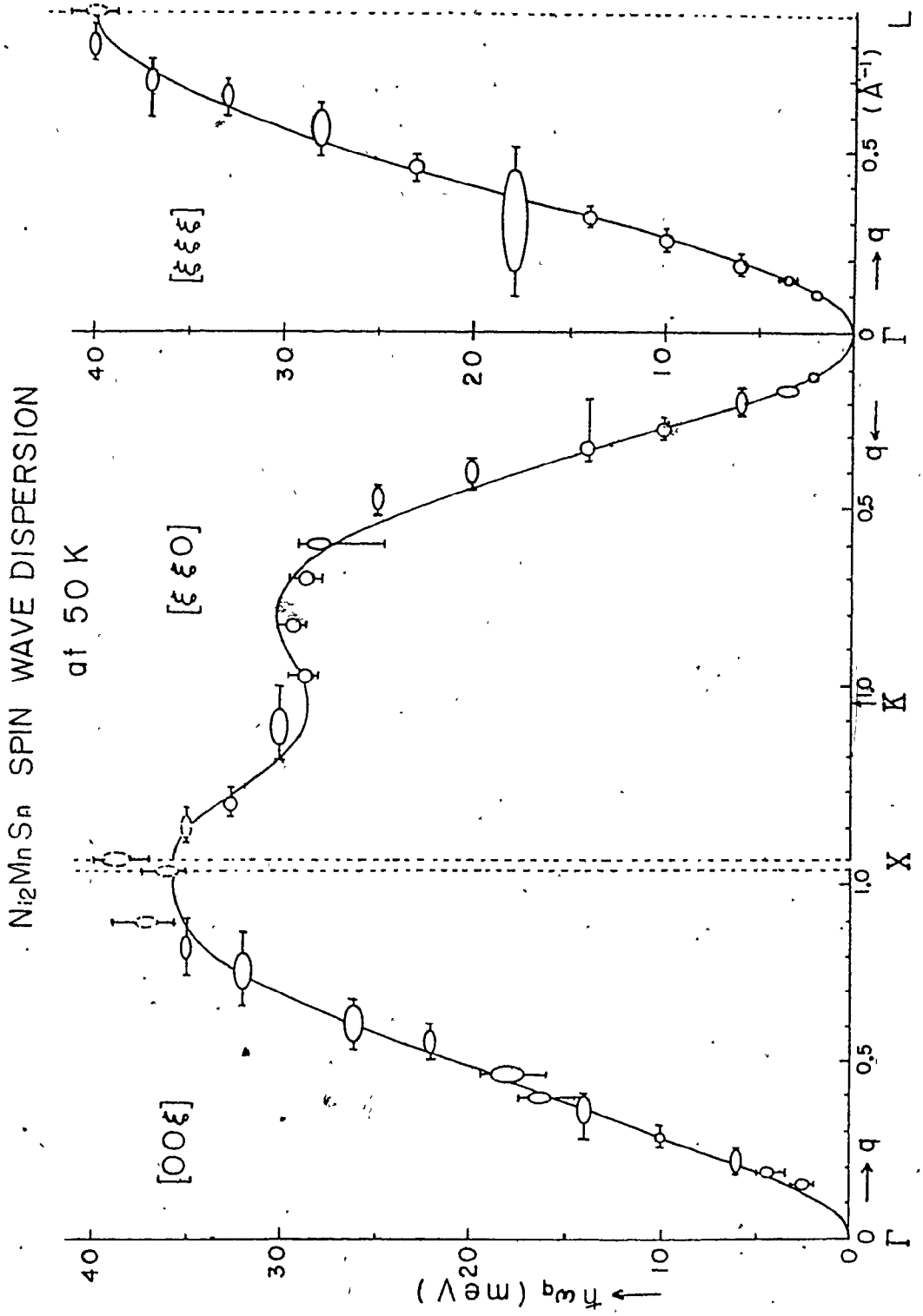
Ni2MnSn SPIN WAVE DISPERSION
at 50 K
[ξ00]
[ξξ0]
[ξξξ]
ħωq (meV)
q → (Å⁻¹)
Γ
X
K
L
0
10
20
30
40
0.5
1.0

intrinsic to the spin waves were observed, although the responses beyond the K-point in the $[\zeta\zeta 0]$ direction were broad, probably due to defocusing of the spectrometer. The dispersion curves in all three materials were similar in shape, increasing in energy from Pd_2MnSn to Ni_2MnSn to Cu_2MnAl. At higher temperatures the dispersion curves for Pd_2MnSn decreased in energy but retained the same shape, implying that the shape is characteristic of the magnon dispersion and not due to a magnon-phonon interaction. These curves were fit to a Heisenberg model where the energy contained in the spins is given by

$$H = -\sum_{ij} J_{ij} \vec{S}_i \cdot \vec{S}_j \qquad (1.1)$$

assuming no anisotropy. Here S_i is the spin at site i and J_{ij} is the exchange constant. For a perfect fcc lattice of localized spins S, the spin-wave energies are given by

$$h\omega_{\bar{q}} = 2S(J(0) - J(\bar{q})) \qquad (1.2)$$

where $J(\bar{q})$ is the Fourier transform of J_{ij}. The fit for Ni_2MnSn is also shown in Fig. 1.1. The dispersion curves are well reproduced by the Heisenberg model. Exchange parameters out to 8 neighbours for Pd_2MnSn, 6 for Ni_2MnSn and 5 for Cu_2MnAl were required for a good fit, implying long range interactions. The exchange constants for Ni_2MnSn are given in Table 1.1. The first three are large and positive (ferromagnetic) however beyond the third neighbour the exchange oscillates with distance. This is characteristic of indirect coupling via the s-d interaction between localized and con-

Table 1.1 Exchange parameters J_i (meV) for Ni_2MnSn determined by a 6 neighbour least squares fit to Noda and Ishikawa's data at 50 K.[4] z_i is the number of i^{th} neighbours. The uncertainty in each parameter is 0.02 meV.

	J_1	J_2	J_3	J_4	J_5	J_6
	0.296	0.283	0.110	-0.095	0.023	-0.015
z_i	12	6	24	12	24	8

duction electrons. The interaction polarizes the conduction band which affects the spins on neighbouring sites. RKKY theory[13-15] for the s-d interaction, based on the nearly free electron model, predicts that the exchange oscillates with distance and falls off as R^{-3} for large R. Caroli and Blandin[16], and later Caroli[17], developed a double resonance exchange model based on the Friedel-Anderson picture of a local moment in a metal[18,19]. The result is similar to the RKKY expression except for an additional phase shift due to the resonant nature of the electron scattering. Noda and Ishikawa fit this expression to their data and obtained good agreement for large R, however the theory predicts the wrong magnitude and sign for the n.n and n.n.n. exchange constants.

Recently two models have been proposed to explain the 3d exchange interactions in Heusler alloys. Price[20] and Malmström *et al.*[21], using the same model as Caroli, calculated the pre-asymptotic part of the interaction and were able to obtain positive values for the first three exchange constants. The single interaction depends only on the average conduction electron concentration. Stearns[22] has suggested that the ferromagnetism is due mainly to Coulomb exchange between itinerant and localized d-electrons. In her model there are three exchange mechanisms: d_i-d_l exchange, indirect s-d_l exchange and antiferromagnetic superexchange via the Z-ligand. Reitz and Stearns[23] have fit this model to the dispersion

curves for the three Heusler alloys and obtained reasonable agreement between theory and experiment by varying only the concentration of d_i electrons, believed to depend strongly on the X atom. However, studies of the magnetic phase transitions in $Pd_{2-x}Cu_xMnIn$[24] and in the series $Pd_2MnIn/Sn/Sb$[25,26] conclude that the overall s conduction electron concentration determines whether these compounds are ferromagnetic or antiferromagnetic, regardless of whether the X or Z atoms are changed. This result favours the Price/Malmström picture, but the presence of other interactions cannot be ruled out.

The electronic structure of Cu_2MnAl[27], Pd_2MnSn and Ni_2MnSn[28] has been calculated by the symmetrized augmented plane wave (SAPW) method. A muffin-tin crystal potential was formed from a superposition of atomic potentials generated from the free atom Hartree-Fock-Slater wave functions and the exchange potential was determined by the χ-α method with an adjustable parameter. In Ni_2MnSn the most appropriate configuration was found to be $3d^6 4s^1$ for Mn and $3d^9 4s^1$ for Ni. For the majority spin states the E(k) curves show flat d-bands for Mn and Ni below the Fermi level whereas for the minority spin states the d-bands of Ni are below the Fermi level but those for Mn lie above. It is obvious from the curves that the main carrier of the magnetic moment in Heusler alloys is Mn and the magnetic moment of the X atom is nearly zero. Calculation of the magnetic form factor agrees with experiment.

Hurd *et al.*[29] have measured the field and temperature dependence of the electrical resistivity, the Hall effect and the transverse magnetoresistance of Ni_2MnSn. Conduction in Ni_2MnSn is dominated by electrons moving in a s/p band but they interact strongly with the lattice and with the magnetic electrons localized on the Mn ions. There is evidence of a resonant s-d-s scattering mechanism, consistent with the Price picture of coupling between the Mn ions, which dominates the resistivity at temperatures above 120 K but operates even at 4.2 K. Estimates of the electron mean free path are 30 A^o at 4.2 K and 6 A^o at 261 K.

In the Heusler alloy, $Ni_2Mn_{1-x}V_xSn$, there is evidence that V is non-magnetic[3]. The magnetization per unit volume and the effective paramagnetic moment per molecule are proportional to the Mn concentration. Also, the Curie temperature decreases linearly with the Mn concentration and extrapolates to zero at a dilution of x = 0.9. This limit agrees favorably with percolation limit calculations for a fcc lattice with n.n. and n.n.n. interactions[30]. The alloy series is ferromagnetic above the critical percolation concentration and retains the Heusler structure for all values of x. As was mentioned above, the spin-wave spectra for the perfect (x = 0) crystal, Ni_2MnSn, has been measured elsewhere and the exchange constants determined. The exchange interaction was found to be Heisenberg in nature and there is some understanding of the coupling mechanism. Furthermore, the material is cubic and has only a small aniso-

tropy energy ($h\omega_{\vec{Q}=0} \sim 10^{-4}$eV)^4. For these reasons the above series is ideal for studying the effect, on the spin-wave spectra of a Heisenberg ferromagnet, of randomly diluting the spins with non-magnetic ions. The spectra can be measured by inelastic neutron scattering techniques.

There are a number of theories[31] that describe the effect of dilution on the T = 0 spin waves in a random lattice. As the spin concentration decreases, the spin-wave frequencies decrease and the response broadens. To treat this effect theoretically is not straightforward because in a random lattice translational symmetry is lost and the crystal momentum, $\vec{Q}$, is no longer a good quantum number for the excitations. There are two simple models. In the "virtual crystal" model the disordered lattice is replaced by a perfect lattice in which all exchange parameters are scaled with the concentration of spins. There is a consequent scaling of the spin-wave frequencies by the same factor but the theory predicts no increase in the widths of the response. The Ising cluster model, on the other hand, recognizes that resonances should occur at frequencies which correspond to the energy required to flip a spin in the field of its reduced number of magnetic neighbours. This theory is useful in predicting the frequencies of localized modes in mixed systems but can give no information about dispersion.

The principal theoretical approach, used to obtain the dispersion in a disordered system, has involved the coherent

potential approximation (CPA). A self-energy is found that minimizes the multiple scattering at a single site. The CPA can be used to determine frequency shifts and widths. This theory was originally developed to treat electrons[32] and phonons[33] and was first extended to magnetic systems by Buyers *et al.*[34,35]. A full comparison of the results with experiments has been made for dilute antiferromagnets[31,35]. CPA results for the response of a three-dimensional diluted ferromagnet have been presented by Tahir-Kheli[36], Harris *et al.*[37], and others[38,39] for the simple cubic case but no full confrontation with experiment has been made. There have been some more recent developments[40,41] but no CPA calculations for the response in a fcc ferromagnet have been reported. Furthermore, the CPA may produce spurious results arising from branch cuts[42] and a pseudopotential may have to be introduced[31,35,37] to remove the unphysical response of the non-magnetic ions at $\omega \sim 0$.

An alternative approach is to solve this type of problem by computer simulation techniques[43-45]. This is the approach chosen in the present work. It involves little more numerical work than the CPA and for large systems tends to the exact result. The technique is used in the form given by Alben *et al.*[45]

A large random array of spins with periodic boundary conditions is generated by the computer program. Using linear spin-wave theory the neutron scattering response, $S(\vec{Q},E)$, is determined numerically for the finite array. The method involves

solving for the correlation functions that describe the spin waves by integrating equations of motion forward in time. These correlation functions are then Fourier transformed in space and time to give $S(\vec{Q},E)$. By averaging the results of several arrays of different dimensions and with different spin configurations an approximation to an infinite crystal is obtained. For three arrays, of ~15,000 spins each, the error in $S(\vec{Q},E)$ is ~5%, but in general the accuracy is limited only by computer memory and time. The error in the frequencies of peaks is considerably less.

As part of this work, a computer program was written to determine $S(\vec{Q},E)$ for a diluted, fcc, ferromagnetic lattice by the numerical method described above. It is assumed that the Heisenberg exchange constants between spins present in the lattice do not change with dilution. Results have been obtained for n.n. and up to third nearest neighbour interactions for dilutions of 20% and 30%. A comparison is made between these calculations and the experimental results for $Ni_2Mn_{0.8}V_{0.2}Sn$.

Chapter 2 describes the inelastic neutron scattering experiment to measure the spin-wave dispersion curves for Ni_2MnSn and $Ni_2Mn_{0.8}V_{0.2}Sn$ including a section on the growth and characterization of the large single crystal samples. Chapter 3 gives an outline of linear spin-wave theory and shows how the scattering function, $S(\vec{Q},E)$, for a diluted Heizenberg ferromagnet can be expressed in terms of correlation functions. Chapter 4 describes the computer simulation technique for calculating

$S(\vec{Q},E)$, paying particular attention to the various types of errors which limit the accuracy of the technique. A description and listing of the computer program is given in the Appendix. The experimental results are presented and compared with the computer simulation results in Chapter 5, and conclusions are presented in Chapter 6.

CHAPTER 2

EXPERIMENT

2.1 Samples

Large single crystals of Ni_2MnSn and $Ni_2Mn_{0.8}V_{0.2}Sn$ were grown for inelastic neutron scattering studies. They were obtained in the following manner. Polycrystalline ingots of alloy were prepared by melting together stoichiometric amounts of elemental material weighed to the nearest 0.0001 g. The elements were premelted, before weighing, as a purifying procedure and to remove any entrapped gas. For Ni_2MnSn a Czochralski growth was begun. The ingots were melted in an r-f furnace in an Al_2O_3 crucible with a graphite susceptor. The furnace was backfilled with argon. An oriented seed was lowered into the melt. The seed and melt were counter-rotated at $\sim$ 0.2 rev/sec. The pulling rate was set at 1" per hour and the boule size was controlled by regulating the power to the r-f coils. The crystal was expanded to about 2 cm in diameter when it caught onto polycrystalline charge freezing in from the circumference of the crucible. The growth was immediately changed to a slow-cooling (Kyropoulos) technique. The crystal was cooled from $\sim$ 1100 C to 300 C over a period of 24 hr. Details on the temperature of the crystal as

a function of time are unknown. Neutron diffraction photographs showed that the center of the boule was a single crystal. There was no further heat treatment.

The $Ni_2Mn_{0.8}V_{0.2}Sn$ crystal was grown by the Bridgman technique. An Al_2O_3 Bridgman crucible (20 mm ID and 100 mm long) was filled with polycrystalline alloy and sealed in a quartz ampoule, backfilled to 0.25 atm of argon. The ampoule was lowered through a platinum resistance furnace at $\sim$ 2 mm per hour. Several tries were necessary to produce a single crystal.

The dimensions of the samples were $\sim$ 25 mm in diameter and 15 mm long for Ni_2MnSn and 15 mm in diameter and 30 mm long for $Ni_2Mn_{0.8}V_{0.2}Sn$. Photographs are shown in Fig. 2.1, (a) and (b). X-ray Laue and neutron diffraction photographs (using a polaroid neutron camera) showed that the samples were single crystals.

The samples were further characterized by measuring the bulk magnetization, the chemical disorder, the mosaic spread and the chemical composition. To determine the magnetization, slabs were removed from the crystals by spark erosion and measurements were taken on a vibrating-sample magnetometer. The results indicate a magnetic moment per Mn atom of $4.1\pm0.1\ \mu_B$ in Ni_2MnSn and $4.0\pm0.1\ \mu_B$ in $Ni_2Mn_{0.8}V_{0.2}Sn$. These results agree with previous measurements[3] and with the general results of $\sim 4\mu_B$ per Mn atom for all Heusler alloys, and are consistent with the nominal concentration of Mn atoms in the samples.

Fig. 2.1 (a) Photograph of the Ni_2MnSn crystal.

(b) Photograph of the $Ni_2Mn_{0.8}V_{0.2}Sn$ crystal.

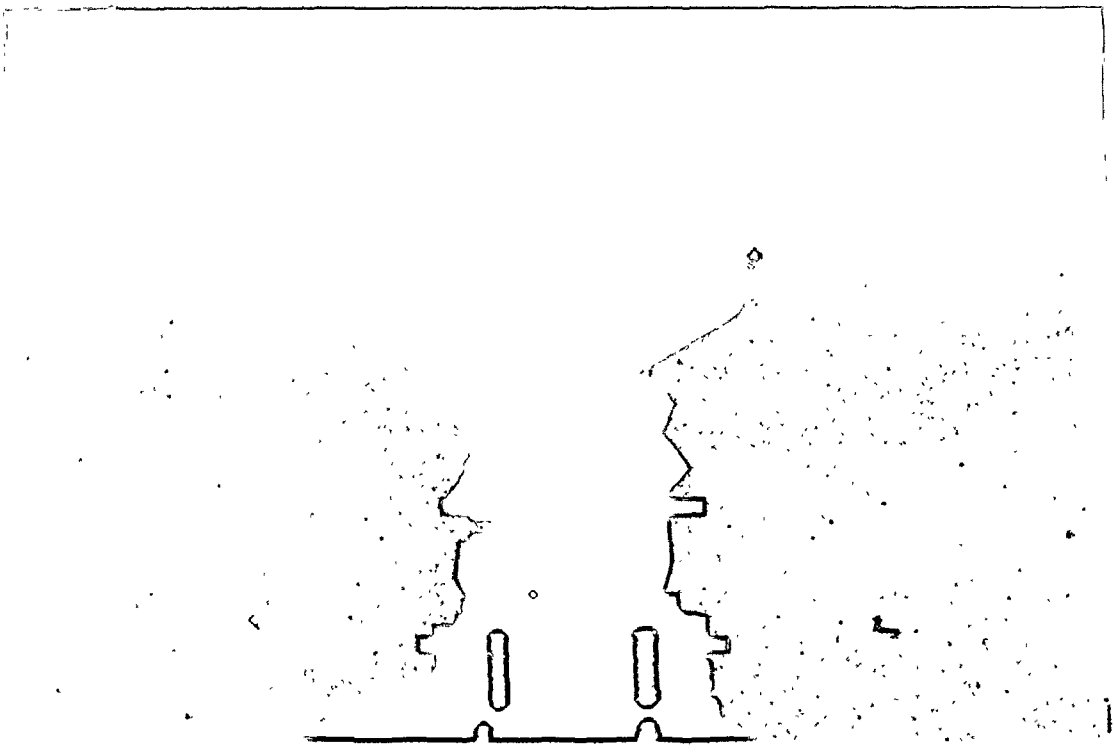

The chemical disorder was determined from elastic neutron diffraction experiments on portions of the samples. These were performed at the McMaster University reactor by Luc Martin. The results indicate a preferential Ni-Mn disorder of 3.5±1.2% for Ni_2MnSn and 0.0±3.0% for $Ni_2Mn_{0.8}V_{0.2}Sn$.

The mosaic spreads of the samples were measured on the double-axis spectrometer at the McMaster University reactor. The monochromator was an Al(200) crystal set at $2\theta = 41.8°$ which selected a wavelength of 1.444 Å. The instrument was set for the focusing condition where the width of the ψ rocking curve depends only on the mosaic spreads of the sample and monochromator and not on collimation. Rocking curves were measured for the 220 reflection of a Ge crystal slab, which had a small mosaic spread, and for the 220 reflection of each of the samples. The mosaic spreads were found to be 32.4±0.9' (minutes) for the monochromator, 18±2' for Ni_2MnSn and 34±4' for $Ni_2Mn_{0.8}V_{0.2}Sn$.

The chemical composition was measured by neutron activation analysis at the McMaster Nuclear Reactors. The results are presented in Table 2.1. In terms of atomic per cent, the compositions were measured to be $Ni_{2.11}Mn_{0.94}Sn_{0.94}$ and $Ni_{2.08}Mn_{0.76}V_{0.20}Sn_{0.95}$. Both samples show an excess of Ni, possibly due to evaporation of the other elements during the crystal growth. The results indicate that $\sim$ 3% of the Mn sites may be occupied by Ni atoms.

For the inelastic scattering experiments the samples were fastened to aluminum posts with vanadium straps and mounted in the vacuum space of a liquid nitrogen dewar (see Fig. 2.2). The

Fig. 2.2 Nitrogen dewar for neutron scattering experiments showing position of sample.

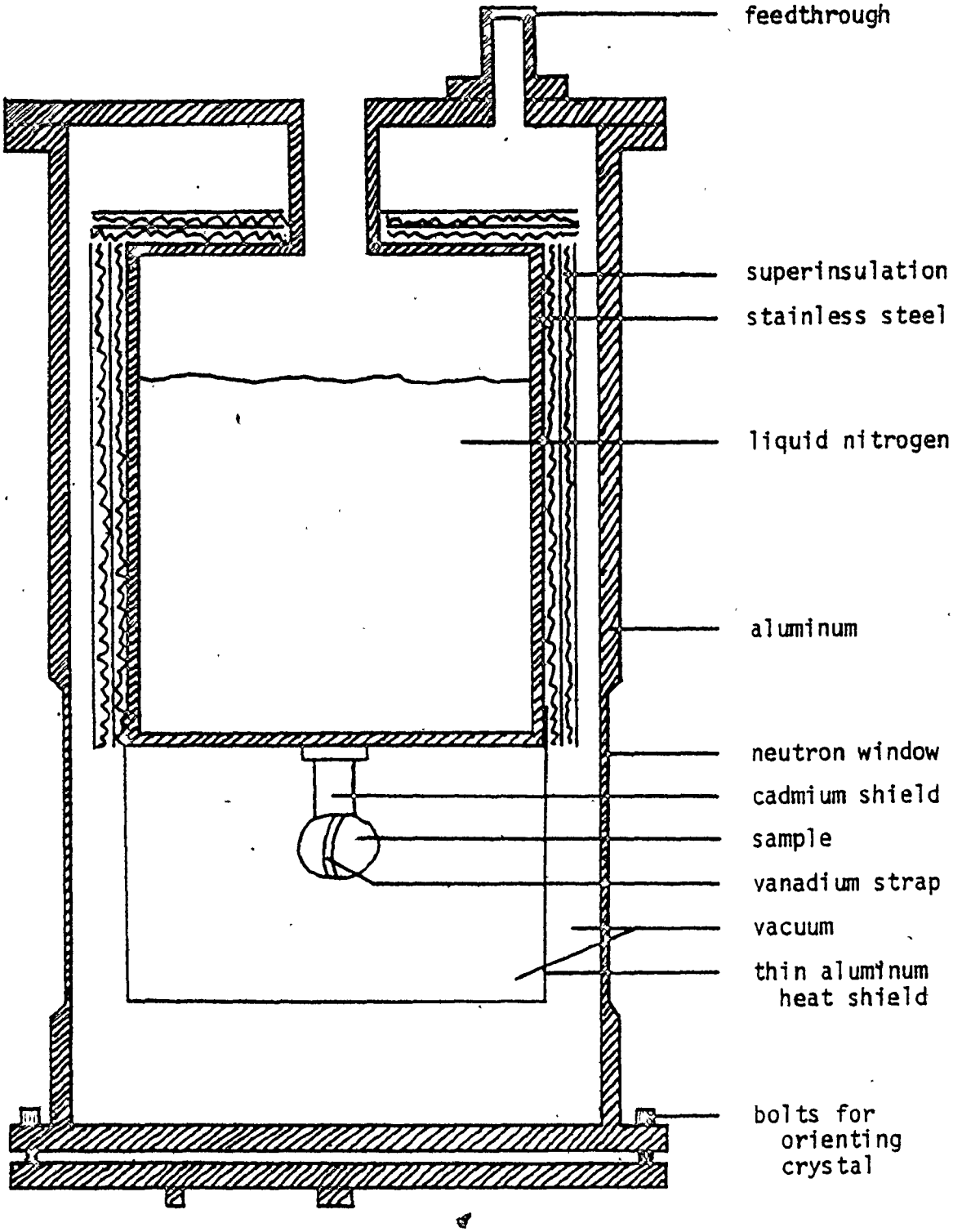
feedthrough
superinsulation
stainless steel
liquid nitrogen
aluminum
neutron window
cadmium shield
sample
vanadium strap
vacuum
thin aluminum heat shield
bolts for orienting crystal

temperature of the sample in this arrangement was measured by a copper-constantan thermocouple and found to be 93 K. The holding time of the dewar was about 20 hr.

Table 2.1 Neutron activation analysis results. Error estimates are based on counting statistics and six replicate analyses

Sample identified as Ni_2MnSn:

	% by weight
Ni	43.2± .8
Mn	18.0± .4
Sn	39.0±1.2

Sample identified as $Ni_2Mn_{0.8}V_{0.2}Sn$:

	% by weight
Ni	42.6±1.1
Mn	14.6± .2
V	3.5± .1
Sn	39.4±1.2

2.2 Inelastic Neutron Scattering Experiment

The neutron scattering was done on the McMaster University triple-axis spectrometer at the N.R.U. reactor in Chalk

River. Detailed descriptions of this spectrometer have been given by Brockhouse[46] and Brockhouse *et al.*[47] A schematic diagram of the spectrometer is shown in Fig. 2.3.

A collimated hole in the wall of a nuclear reactor allows a white beam of neutrons to be extracted. The double-crystal monochromator, consisting of two Cu(220) crystals set at θ_M, selects neutrons of a particular wavelength, λ_0, to be incident on the specimen. ψ is the angle of the specimen with respect to the incoming beam. Neutrons scattered through the angle ϕ are detected by the He^3 counter if they are of the correct wavelength, λ', to be Bragg scattered by the analysing crystal set at θ_A. The analyser used was a Cu(200) crystal. An essential part of the instrument is the thin U^{235} fission counter which monitors the incoming beam intensity. Scattered neutrons are counted for a preset number of monitor counts. The Soller-slit horizontal collimators set the resolution of the spectrometer. Resolution is discussed in more detail in Section 2.3. A photograph of the experimental apparatus is shown in Fig. 2.4.

The neutron is an ideal probe for the study of magnetic excitations in a crystal. It is neutral in charge but has a magnetic moment and therefore can interact with the electron spins in the crystal. A thermal neutron has a momentum and energy comparable to the momentum and energy of a typical magnon. It is therefore scattered through an appreciable angle and undergoes a measurable change in energy when it creates or

Fig. 2.3 Schematic of Chalk River triple-axis spectrometer.

A hole in reactor wall

B double crystal monochromator

C monochromatic beam

D beam incident on specimen

E beam gate

F fission chamber monitor

G Soller-slit collimators

H sample angling apparatus

I counter angling apparatus

J helium counters

K parafin and cadmium shielding barrel

L analysing crystal

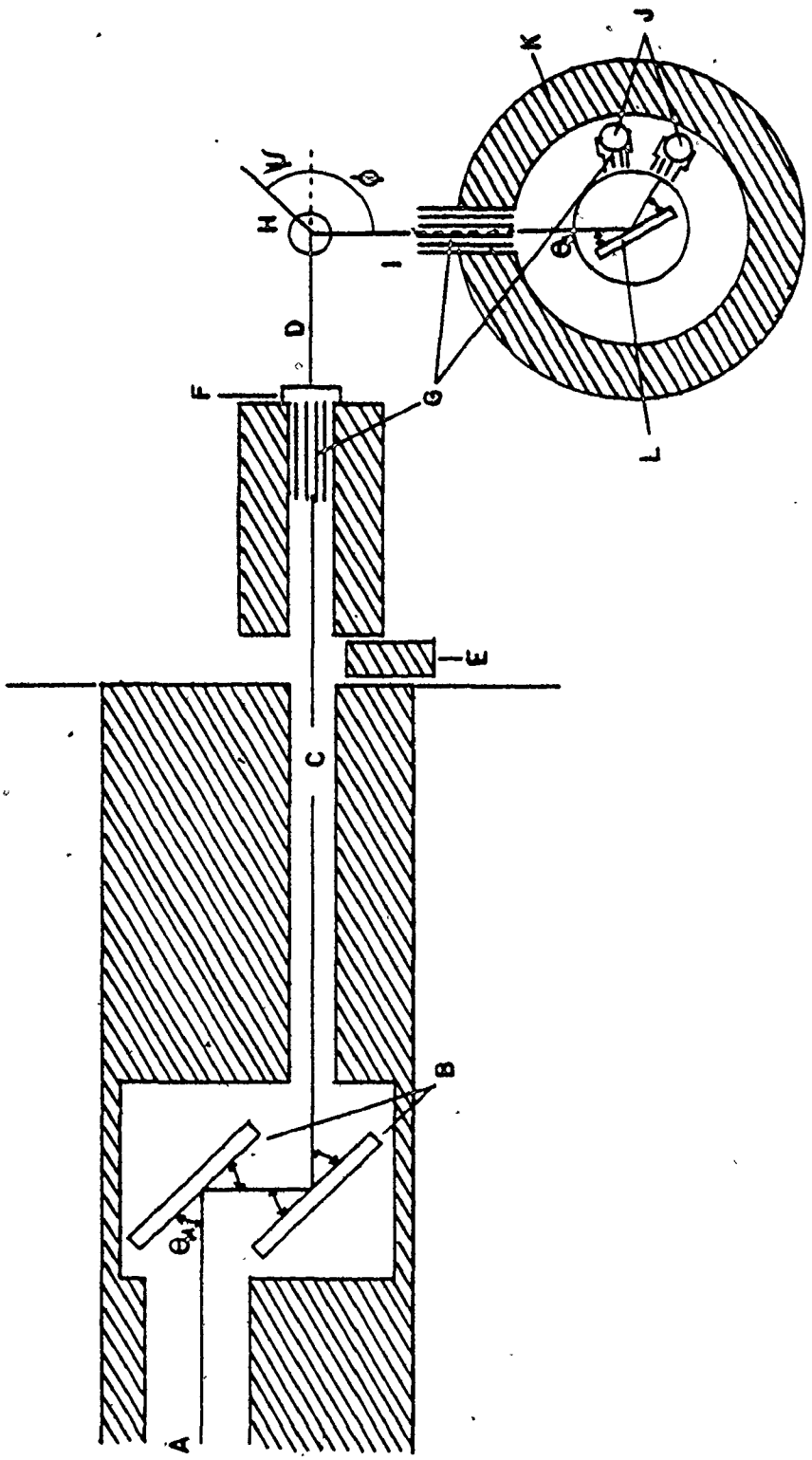
K
J
ψ
φ
H
I
θ
D
F
G
L
E
C
B
θ_M
A

Fig. 2.4 Photograph of the Chalk River triple-axis spectrometer showing the beam port at the reactor face, the nitrogen dewar which holds the sample and the analyser, coated with parafin wax.

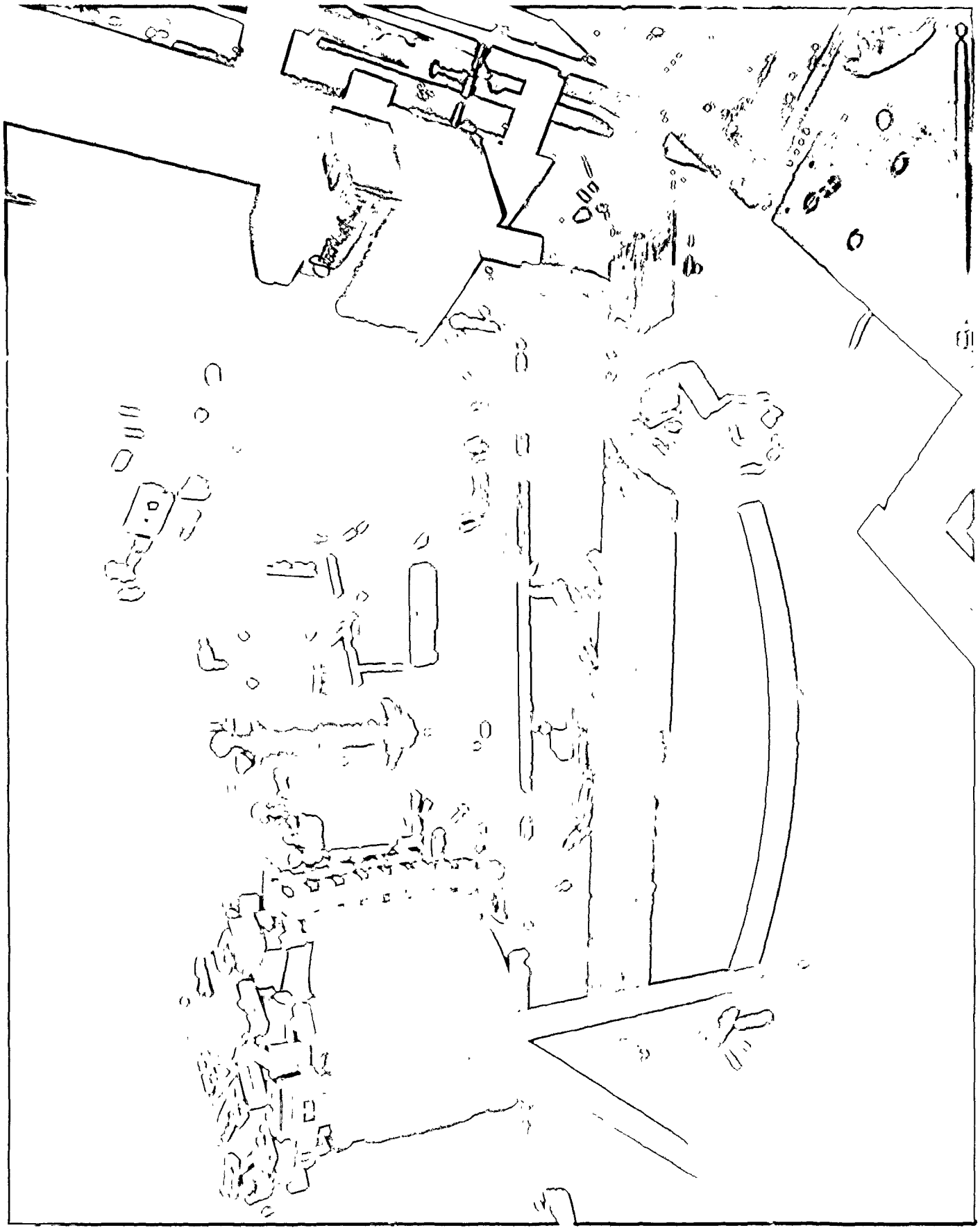

annihilates a magnon. In such a collision, quasi-momentum and energy are conserved. That is,

$$\vec{Q} \equiv \vec{k}_o - \vec{k}' = \vec{\tau} - \vec{q} \tag{2.1}$$

and

$$E \equiv E_o - E' = \hbar\omega, \tag{2.2}$$

where $\hbar\vec{Q}$ is the momentum transfer and E is the energy transfer. $\vec{k}_o$ and $\vec{k}'$ are the wavevectors of the incident and scattered neutrons and E_o and E' are the corresponding energies. $\vec{\tau}$ is a reciprocal lattice vector while $\vec{q}$ and ω are the wavevector and angular frequency of the magnon involved. Brockhouse[46] has emphasized that $\vec{Q}$ and E are the natural variables for the inelastic scattering process.

When momoenergetic neutrons are incident on a crystal, information about the excitations is present in the scattered neutron spectrum in the form of "neutron groups" which are those neutrons scattered by excitations of a particular $\vec{q},\omega$ combination. The neutron groups can be observed if the spectrometer is programmed to sweep through the corresponding area of $\vec{Q}$,E space. A triple-axis spectrometer has the advantage over other spectrometers in that θ_M, θ_A, ϕ and ψ can all be moved independently. There are several special modes of operation possible, most notably the constant $\vec{Q}$ and constant E modes. These are methods for obtaining one point on the dispersion curves of the magnons. Successive and adjacent scans allow the whole dispersion curve to be plotted out. These curves can be com-

pared to theoretical models and fitted to obtain exchange parameters. For these experiments the constant energy mode was more favorable because of the relative steepness of the dispersion curves.

The following is a description of the procedure used for taking constant energy scans of the neutrons scattered by spin-waves in Ni_2MnSn and $Ni_2Mn_{0.8}V_{0.2}Sn$. The samples were oriented so that the $(1\bar{1}0)$ plane coincided with the scattering plane of the spectrometer (defined by $\vec{k}_o$ and $\vec{k}'$). The spin-wave dispersion curves were measured in three symmetry directions about the (111) reciprocal lattice point. At this point there is a low dynamical structure factor for phonon scattering yet $\vec{Q}$ is small enough so that the magnetic form factor does not drastically reduce the intensities. A diagram of the reciprocal lattice is given in Fig. 2.5. On it are shown the centers of observed peaks for constant energy scans in $Ni_2Mn_{0.8}V_{0.2}Sn$.

In the constant E method, $\vec{Q}$ is usually moved along a symmetry direction in reciprocal space while E is held constant. To measure a point on the dispersion curve at energy E, one first chooses the range of $\vec{Q}$ expected to correspond to that E. The wavelength of the incident neutrons is selected by setting θ_M. Knowing λ_o and E, λ' is calculated from

$$E = \frac{h^2}{2m\lambda_o^2} - \frac{h^2}{2m\lambda'^2} \qquad (2.3)$$

and θ_A is set. Finally a triangle is formed from $\vec{Q}$, $\vec{k}_o$ and $\vec{k}'$

Fig. 2.5 Reciprocal lattice of Heusler alloys in the $(\bar{1}10)$ plane. The points are wavevectors of observed neutron scattering peaks.

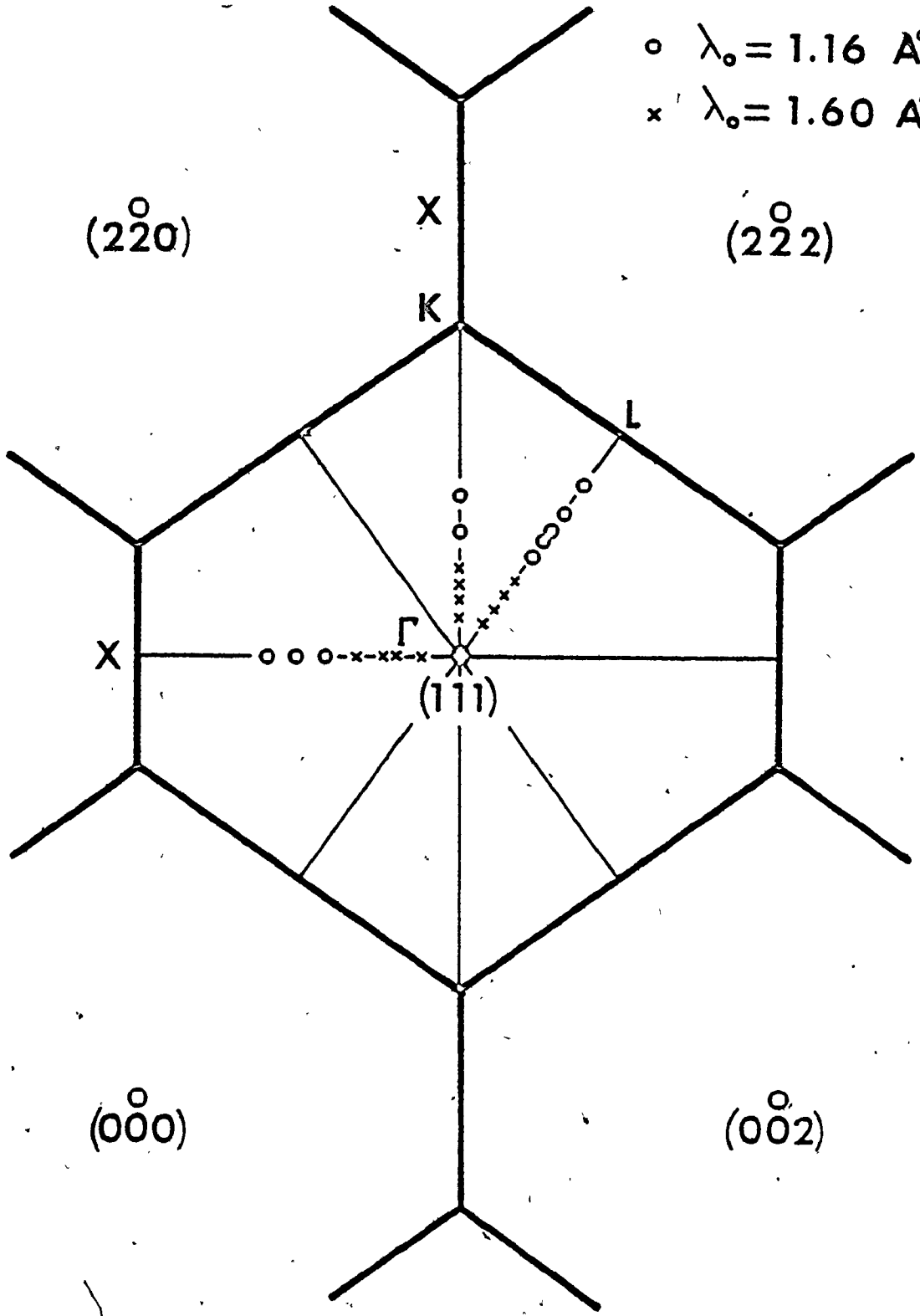
o λ₀ = 1.16 Å°
× λ₀ = 1.60 Å°
(2̄20)
(22̄2)
X
K
L
X
Γ
(111)
(000)
(002)

and the angles ϕ and ψ are calculated. The spectrometer angles can be set to any multiple of 0.1° with a stated accuracy of 0.01°. The calculations are done for all points on the sweep of $\vec{Q}$ by a computer program that produces a paper tape which controls the spectrometer. The scattered neutrons are counted for a preset number of monitor counts at each point. The observed result is a neutron group, such as those shown in Fig. 5.1, and the centre of the peak gives one point on the dispersion curve.

It is possible that the triangle cannot be closed, in which case λ_o must be changed. Resolution is another consideration in choosing the incident wavelength. For weak scattering a small λ_o is desired to decrease the energy resolution in the analyser and increase the intensity. For these experiments a wavelength of 1.6 Å was chosen for energy transfers less than 3 THz and 1.16 Å for transfers greater than 3 THz. The latter corresponds to the largest E_o obtainable from the double monochromator of this instrument.

At the beginning of an experiment it is necessary to accurately determine the incident wavelength, the lattice constant of the sample and the scale readings for the zero positions of all angles. These were obtained by the following procedures. λ_o and ϕ_0 were obtained by measuring the positions of diffraction peaks from Cu powder and least squares fitting the angles to Bragg's Law. The centers of the peaks were estimated to the nearest 0.01°. Five peaks were obtainable for $\lambda_o = 1.16$ Å and four peaks for 1.6 Å. The resulting error in λ_o was

$\pm$ 0.0007 Å and in ϕ_o was $\pm$ 0.01°. a, the lattice constant of the sample, and ψ_o were determined by fitting the ψ angles of Bragg reflections to Bragg's Law. The lattice constants obtained at 93 K were

$$a(Ni_2MnSn) = 6.053 \pm 0.010 \text{ Å}$$

$$a(Ni_2Mn_{0.8}V_{0.2}Sn) = 6.029 \pm 0.010 \text{ Å} .$$

The value for Ni_2MnSn agrees with other results[3] however the value for $Ni_2Mn_{0.8}V_{0.2}Sn$ is slightly less than obtained by previous workers. The error in ψ_o was $\pm$ 0.01°. θ_{A_o} and $2\theta_{A_o}$ were determined to $\pm$ 0.01° by measuring isotropic elastic scattering from V powder.

The samples were oriented by observing the (440), $(\bar{4}\bar{4}0)$, (006) and $(00\bar{6})$ reflections. The vertical collimation in the incoming and outgoing beams was set to 1/160 radians and the crystal orientation was adjusted for a maximum counting rate. The method is thought to be accurate to better than 0.05°.

2.3 Resolution

The resolution of a triple-axis spectrometer is determined by collimation and by the mosaic spreads of the monochromator and analyser crystals. If the scattering function of the sample is independent of ω and $\vec{Q}$ and the spectrometer is set to observe a process $(\omega_o, \vec{Q}_o)$ then the resolution function, $R(\omega, \omega_o, \vec{Q}, \vec{Q}_o)$, is defined as the probability that a detected neutron was scattered with an energy transfer $\hbar\omega$ and

a momentum transfer $\hbar\vec{Q}$. If the transmission functions of all collimators and crystals involved are assumed to be Gaussian then the resolution function can be written in the form

$$R(\omega_o+\Delta\omega,\vec{Q}_o+\Delta\vec{Q}) = R_o\exp\{-\frac{1}{2}\sum_{k=1}^{4}\sum_{\ell=1}^{4} M_{k\ell}X_kX_\ell\} \qquad (2.4)$$

where $X_i = Q_i - Q_{i_o}$ for i = 1,2,3 and $X_4 = \omega-\omega_o$. Conventionally X_1 is parallel to $\vec{Q}_o$ and X_3 is perpendicular to the scattering plane. $M_{k\ell}$ is called the resolution matrix. Cooper and Nathans[48] have derived expressions for the matrix elements in terms of k_o, ω_o and $\vec{Q}_o$; the monochromator and analyser mosaic spreads and plane spacings, η_M, η_A, d_M and d_A; and the horizontal and vertical collimation angles, α_0, α_1, α_2, α_3, β_0, β_1, β_2 and β_3. These expressions were used to choose the constant energy scans most suitable from the standpoint of focusing. The parameters of the spectrometer are listed in Table 2.2.

Table 2.2 Instrumental parameters for the triple-axis spectrometer

	Scattering Plane	Plane Spacing (A)	Mosaic Spread
monochromator	Cu 220	1.278	20'
analyser	Cu 200	1.807	30'
specimen (Ni_2MnSn)	--	--	18'
($Ni_2Mn_{0.8}V_{0.2}Sn$)	--	--	34'

Collimation (FWHM)

	Horizontal (radians)	Vertical (radians)
in pile	$\alpha_0 = 0.1002$	$\beta_0 = 0.1002$
monochromator to sample	$\alpha_1 = 0.0125$	$\beta_1 = 0.0300$
sample to analyzer	$\alpha_2 = 0.0125$	$\beta_2 = 0.0700$
analyser to detector	$\alpha_3 = 0.0833$	$\beta_3 = 0.5000$

Note: α_1 and α_2 are typical for the Soller-slit collimators.

2.4 Spin-Wave Renormalization

The energy required to create a spin-wave decreases with increasing temperature because of interactions between the spin-waves. The spin-wave energies for Ni_2MnSn and $Ni_2Mn_{0.8}V_{0.2}Sn$, measured at 93 K in this experiment, are therefore reduced from the energies at 0 K. To obtain the dispersion curves at T = 0 K, a correction was applied by assuming that the energies drop by the same factor as the bulk magnetization.

The magnetization of the compounds was measured on a vibrating sample magnetometer using pieces cut from the same samples used in the neutron scattering experiments. The results are shown in Fig. 2.6 where the reduced magnetization, M(T)/M(0), is plotted against temperature. The curve for the diluted crystal is a different shape than for the non-diluted crystal, decreasing faster with temperature. At 93 K the magnetization has dropped by 2.0% for Ni_2MnSn, and by $\sim$ 8.0% for $Ni_2Mn_{0.8}V_{0.2}Sn$. The measured spin-wave energies were therefore increased by the corresponding factors to obtain the spin-wave energies at 0 K.

That the dispersion curves have the same temperature dependence as the bulk magnetization is only an approximation. The assumption is supported by the Green function theory of ferromagnetism by H. Callen[49] and follows from the simple physical picture of spin-wave renormalization, given by F. Keffer[50]. As the temperature increases, more spin-waves are

Fig. 2.6 Temperature dependence of the reduced magnetization for Ni_2MnSn and $Ni_2Mn_{0.8}V_{0.2}Sn$.

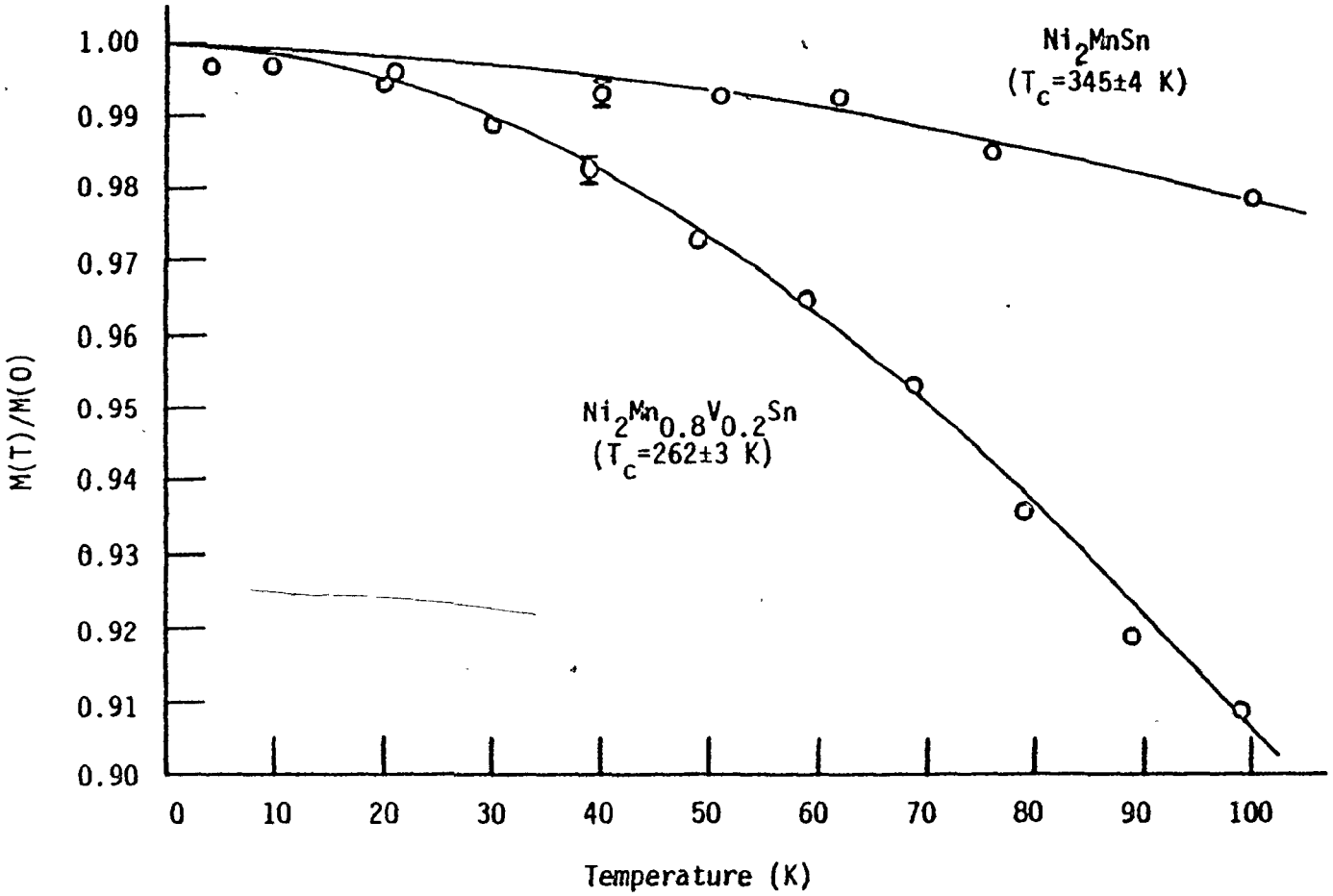
1.00
0.99
0.98
0.97
0.96
0.95
0.94
0.93
0.92
0.91
0.90
M(T)/M(0)
0
10
20
30
40
50
60
70
80
90
100
Temperature (K)
Ni2MnSn
(Tc=345±4 K)
Ni2Mn0.8V0.2Sn
(Tc=262±3 K)

excited and the average angle, ϕ_M, between each spin and the direction of bulk magnetization increases. This causes the total magnetization, M(T), to drop. In the "first random phase approximation" the components of each spin which are perpendicular to $\vec{M}$ are averaged to zero. This results in a system of spins, S cos ϕ_M in length and totally aligned in the magnetic field M(T). The energy required to excite another spin-wave is thereby reduced by the factor M(T)/M(0). This overestimates the renormalization at low temperatures because only long-wavelength spin-waves are excited. A better approximation, called the "second random phase approximation" is obtained by averaging the spin-components perpendicular to the local magnetization. At higher temperatures the two averaging procedures are equivalent and correcting the spin-wave energies by the magnetization should be a good approximation.

The spin-wave dispersion curves for Pd_2MnSn were measured at different temperatures by Noda and Ishikawa[51]. They compared their results with a self-consistent renormalization theory based on the two magnon dynamical interaction and obtained good agreement. However, this theory cannot easily be applied to a diluted ferromagnet. For Pd_2MnSn at $T \sim 0.3\ T_c$ the drop in magnetization exceeds the spin-wave renormalization by about 25%. However the renormalization was

found to be independent of $\bar{q}$. For $Ni_2Mn_{0.8}V_{0.2}Sn$ the possible overcorrection by 25% is thought to be within experimental error, given the suspected deficiency of Mn.

CHAPTER 3

THEORY

This chapter outlines the low temperature theory required to calculate the scattering function, $S(\vec{Q},E)$, for a diluted Heisenberg ferromagnet. These calculations can be compared directly with neutron scattering measurements and they also give qualitative information about the energy of the spin excitations in the diluted crystal. The first step is to obtain the linear Hamiltonian for spin-waves in a Heisenberg ferromagnet. For a perfect crystal the spin-wave dispersion relation follows readily. Next, an expression for the scattering function, $S(\vec{Q},E)$, is derived in terms of correlation functions. This expression simplifies for a perfect crystal but not for a diluted crystal because there is no translational symmetry. However, equations of motions for the correlation functions can be obtained which leads to a computer simulation technique for calculating $S(\vec{Q},E)$. The temperature dependence of spin-waves is discussed in Section 2.4.

3.1 The Linear Spin-Wave Hamiltonian

The treatment below is standard and appears in many places. See, for example, Marshall and Lovesey[52]. According

to the Heisenberg model, a ferromagnetic crystal can be described by a Hamiltonian expressed in terms of spin operators:

$$H = - \sum_{ij} J_{ij} \vec{S}_i \cdot \vec{S}_j \ . \tag{3.1}$$

J_{ij} is the exchange integral between spins at sites i and j. It is positive for ferromagnetic coupling. In eqn. (3.1) all contributions from external magnetic fields and anisotropy have been neglected. If the spin angular momentum raising and lowering operators, S_i^+ and S_i^-, are introduced where

$$S_i^+ = S_i^x + iS_i^y \tag{3.2}$$

and

$$S_i^- = S_i^x - iS_i^y, \tag{3.3}$$

then the Hamiltonian can be written as

$$H = - \sum_{ij} J_{ij} \{S_i^+ S_j^- + S_i^z S_j^z\} \ . \tag{3.4}$$

This can be expressed in terms of spin deviation operators by means of the Holstein-Primakoff transformation[53]:

$$S_i^+ = (2S)^{\frac{1}{2}} [1 - \frac{a_i^+ a_i}{2S}]^{\frac{1}{2}} a_i \tag{3.5a}$$

$$S_i^- = (2S)^{\frac{1}{2}} a_i^+ [1 - \frac{a_i^+ a_i}{2S}]^{\frac{1}{2}} \tag{3.5b}$$

$$S_i^z = S - a_i^+ a_i \ . \tag{3.5c}$$

a_i^+ and a_i are boson creation and destruction operators which obey the commutation relation

$$[a_i, a_j^+] = \delta_{ij} \ . \tag{3.6}$$

Now $n_i \equiv a_i^+ a_i$ is the operator for the number of spin deviations. As the temperature decreases the average value of n_i approaches zero. Therefore in the limit of low temperature and large spins

$$[1 - \frac{a_i^+ a_i}{2S}]^{\frac{1}{2}} = [1 - \frac{n_i}{2S}]^{\frac{1}{2}} \approx 1 \ . \tag{3.7}$$

Eqns. (3.5) become

$$S_i^+ = (2S)^{\frac{1}{2}} a_i \tag{3.8a}$$

$$S_i^- = (2S)^{\frac{1}{2}} a_i^+ \tag{3.8b}$$

$$S_i^z = S - a_i^+ a_i \ . \tag{3.8b}$$

This is the first order Holstein-Primakoff transformation. Substitution of eqns. (3.8) into eqn. (3.4) gives

$$H = - \sum_{ij} J_{ij} S^2 - \sum_{ij} 2SJ_{ij}(a_i^+ a_j - a_i^+ a_i) \ . \tag{3.9}$$

We have used the fact that a_i commutes with a_j^+ for $i \neq j$ and that $J_{ij} = J_{ji}$. A term in $a_i^+ a_i a_j^+ a_j$ has been neglected, which is consistent with the approximations made in the transformation.

The first term of eqn. (3.9) is the zero temperature energy of the lattice. It is a constant, has no effect on spin

excitations, and is therefore neglected. Eqn. (3.9) becomes

$$H = \sum_{ij} 2SJ_{ij}(a_i^+ a_i - a_i^+ a_j) \quad . \tag{3.10}$$

This is the quadratic, linear spin-wave Hamiltonian. It will be used below to derive linear equations of motion for the spins.

3.2 The Spin-Wave Dispersion Relation

To obtain the dispersion relation for spin-waves in the perfect crystal we introduce the operators $b_{\bar{q}}^-$ and $b_{\bar{q}}^+$ through the Fourier expansions

$$a_i = \frac{1}{\sqrt{N}} \sum_{\bar{q}} \exp(i\bar{q}\cdot\vec{R}_i) b_{\bar{q}}^- \tag{3.11a}$$

and

$$a_i^+ = \frac{1}{\sqrt{N}} \sum_{\bar{q}} \exp(-i\bar{q}\cdot\vec{R}_i) b_{\bar{q}}^+ \quad . \tag{3.11b}$$

$b_{\bar{q}}^+$ and $b_{\bar{q}}^-$ create or destroy a magnon of wavevector $\bar{q}$. The following properties can be shown to hold:

$$[b_{\bar{q}}^-, b_{\bar{q}}^-,] = [b_{\bar{q}}^+, b_{\bar{q}}^+,] = 0 \quad ; \quad [b_{\bar{q}}^-, b_{\bar{q}}^+,] = \delta_{\bar{q},\bar{q}'} \tag{3.12}$$

$$\sum_i a_i^+ a_i = \sum_{\bar{q}} b_{\bar{q}}^+ b_{\bar{q}}^- \tag{3.13}$$

$$\frac{1}{N} \sum_i \exp\{i(\bar{q}'-\bar{q})\cdot\vec{R}_i\} = \delta_{\bar{q},\bar{q}'} \tag{3.14}$$

Substituting eqns. (3.11) into eqn. (3.10) and using (3.13) and

(3.14) gives

$$H = \sum_{\bar{q}} 2S(J(o)-J(\bar{q}))b_{\bar{q}}^{+}b_{\bar{q}} \qquad (3.15)$$

where

$$J(\bar{q}) = \sum_{\bar{\delta}} J(\bar{\delta})\exp(-i\bar{q}\cdot\bar{\delta}) \ . \qquad (3.16)$$

$\bar{\delta}$ is the neighbour vector

$$\bar{\delta} = \vec{R}_i - \vec{R}_j \ . \qquad (3.17)$$

The Hamiltonian is a sum of terms, each of which involves only one $\bar{q}$. There are no cross terms. Therefore the spin-waves do not interact. This is a consequence of linear spin-wave theory. A magnon is a quantized spin-wave. If eqn. (3.15) is written as

$$H = \sum_{\bar{q}} \hbar\omega_{\bar{q}} n_{\bar{q}} \qquad (3.18)$$

where $\hbar\omega_{\bar{q}}$ is the energy of one magnon and $n_{\bar{q}} \equiv b_{\bar{q}}^{+}b_{\bar{q}}$ is the number operator for magnons of wavevector $\bar{q}$, then the magnon dispersion curve is given by

$$\hbar\omega_{\bar{q}} = 2S(J(o)-J(\bar{q})) \ . \qquad (3.19)$$

3.3 The Scattering Function, $S(\vec{Q},E)$

Neutrons can scatter off spin-waves because there is a magnetic interaction between the neutrons and the unpaired electron spins. The scattering function, $S(\vec{Q},E)$, is that part of the scattering cross-section that depends on the dynamics of the spin system and not on the properties of the incident radiation.

For a system of spins localized on the sites $\vec{R}_i$ of a Bravais lattice, $S(\vec{Q},E)$ is given by

$$S(\vec{Q},E) = \frac{1}{4\pi N\hbar S}\int_{-\infty}^{\infty} dt\, \exp(\frac{iEt}{\hbar}) \sum_{ij} \exp\{-i\vec{Q}\cdot(\vec{R}_i-\vec{R}_j)\} \times$$

$$\times \langle S_i^+(t)S_j^-(o) + S_i^-(t)S_j^+(o)\rangle \ . \qquad (3.20)$$

If $\bar{k}_o$ is the wavevector of the incident neutrons and $\bar{k}'$ is the wavevector of the scattered neutrons, then the scattering vector, $\vec{Q}$, is given by

$$\vec{Q} = \bar{k}_o - \bar{k}' \ . \qquad (3.21)$$

E is the energy transferred to the system and can be written as

$$E = \frac{\hbar^2 k_o^2}{2m} - \frac{\hbar^2 k'^2}{2m} \ . \qquad (3.22)$$

It is related to the energy of the excitation involved by conservation of energy. N is the total number of spins and S is the spin quantum number. S_i^+ and S_i^- are the raising and lowering operators for the spin at site i. $S_i^+(t)$ is the time dependent operator in the Heisenberg representation:

$$S_i^+(t) = e^{iHt/\hbar} S_i^+ e^{-iHt/\hbar} \ . \qquad (3.23)$$

The triangular brackets imply the thermal average over all states at some temperature T. At T = 0 this becomes the expectation value in the ground state.

Neutron scattering experiments measure the cross section which is proportional to $S(\vec{Q},E)$. The partial differential cross-section for inelastic scattering by spin waves is given by

$$\frac{d^2\sigma}{d\Omega dE'} = N\left(\frac{\gamma e^2}{m_e c^2}\right)^2 \left\{\frac{1}{2} g F(\vec{Q})\right\}^2 \frac{k'}{k_o} \frac{S}{2} (1+\tilde{Q}_z^2) \exp\{-2W(\vec{Q})\} S(\vec{Q},E) \quad (3.24)$$

This cross section is the number of neutrons scattered into the solid angle $d\Omega$, about Ω, with energy between E' and E'+dE'. $S(\vec{Q},E)$ is the function given by eqn. (3.20). $\gamma = 1.913$, g is the Landé splitting factor and $F(\vec{Q})$ is the magnetic form factor. $F(\vec{Q})$ is the Fourier transform of the spin density about an ion and causes the intensity of scattering to decrease with increasing $|\vec{Q}|$. $(1+\tilde{Q}_z^2)$ is a factor that depends on the orientation of the magnetization of the sample (z-direction) with respect to the scattering vector $\vec{Q}$. For a cubic crystal with many ferromagnetic domains the factor averages to 4/3. $\exp\{-2W(\vec{Q})\}$ is the Debye-Waller factor.

To obtain the linear spin-wave expression for $S(\vec{Q},E)$, eqn. (3.20) is rewritten in terms of spin deviation operators. Thus

$$S(\vec{Q},E) = \frac{1}{2\pi N\hbar} \int_{-\infty}^{\infty} dt \exp\left(\frac{iEt}{\hbar}\right) \sum_{ij} \exp\{-i\vec{Q}\cdot(\vec{R}_i-\vec{R}_j)\} \times$$

$$\times \langle a_i(t) a_j^+(o) + a_i^+(t) a_j(o) \rangle \ . \quad (3.25)$$

This expression is applicable to diluted lattices as well as to perfect lattices. For the perfect lattice, however, the expression can be simplified.

3.4 $S(\vec{Q},E)$ for a Perfect Crystal

We wish to simplify eqn. (3.25) for a perfect lattice by introducing the operators $b_{\bar{q}}^{+}$ and $b_{\bar{q}}^{-}$. For the Heisenberg representation of the operator, $b_{\bar{q}}^{+}(t)$, the time derivative is given by

$$i\hbar \frac{d}{dt} b_{\bar{q}}^{+}(t) = [b_{\bar{q}}^{+}(t), H] \quad . \tag{3.26}$$

Using eqn. (3.18) for H this becomes

$$i\hbar \frac{d}{dt} b_{\bar{q}}^{+}(t) = i\omega_{\bar{q}} b_{\bar{q}}^{+}(t) \quad . \tag{3.27}$$

We can therefore write

$$b_{\bar{q}}^{+}(t) = \exp(i\omega_{\bar{q}} t) b_{\bar{q}}^{+} \tag{3.28}$$

and

$$b_{\bar{q}}^{-}(t) = \exp(-i\omega_{\bar{q}} t) b_{\bar{q}}^{-} \quad . \tag{3.29}$$

These can be used with eqns. (3.11) to obtain

$$a_i^{+}(t) = \frac{1}{\sqrt{N}} \sum_{\bar{q}} \exp\{-i(\bar{q}\cdot\bar{R}_i - \omega_{\bar{q}} t)\} b_{\bar{q}}^{+} \tag{3.30a}$$

and

$$a_i(t) = \frac{1}{\sqrt{N}} \sum_{\bar{q}} \exp\{i(\bar{q}\cdot\bar{R}_i - \omega_{\bar{q}} t)\} b_{\bar{q}}^{-} \quad . \tag{3.30b}$$

We therefore have that

$$\langle a_i(t) a_j^{+}(o)\rangle = \frac{1}{N} \sum_{\bar{q}} \exp\{-i(\bar{q}\cdot(\vec{R}_j - \vec{R}_i) + \omega_{\bar{q}} t)\} \langle n_{\bar{q}} + 1\rangle \tag{3.31a}$$

and

$$\langle a_i^{+}(t) a_j(o)\rangle = \frac{1}{N} \sum_{\bar{q}} \exp\{i(q\cdot(\vec{R}_j - \vec{R}_i) + \omega_{\bar{q}} t)\} \langle n_{\bar{q}}\rangle \tag{3.31b}$$

where the thermal average, $\langle n_{\bar{q}} \rangle$, is given by

$$\langle n_{\bar{q}} \rangle = \{\exp(\hbar\omega_{\bar{q}}/kT)-1\}^{-1} \quad . \tag{3.32}$$

Substituting eqns. (3.31) into (3.25) gives the linear spin-wave scattering function for a perfect crystal:

$$S(\vec{Q},E) = \sum_{\bar{\tau},\bar{q}} \{\delta(\vec{Q}-\bar{q}-\bar{\tau})\,\delta(E-\hbar\omega_{\bar{q}})\langle n_{\bar{q}}+1\rangle + \delta(\vec{Q}+\bar{q}-\bar{\tau})\,\delta(E+\hbar\omega_{\bar{q}})\langle n_{\bar{q}}\rangle\}. \tag{3.33}$$

$\bar{\tau}$ is a reciprocal lattice vector.

Eqn. (3.33) shows that the cross-section is the sum of two terms. The first corresponds to the creation and the second to the destruction of one magnon. The delta-functions insure conservation of momentum and energy. The two conditions must be satisfied simultaneously for scattering to occur.

It can be seen that for a particular $\vec{Q}$ in a perfect crystal, $S(\vec{Q},E)$ shows sharp peaks at the energies that correspond to the excitations whose wavevector is selected by fixing $\vec{Q}$. In an inelastic neutron scattering experiment it is possible to measure the cross-section as a function of $\vec{Q}$ and E and determine the dispersion relation of the magnons.

Eqn. (3.33) is only valid at low temperatures. At $T = 0$, $\langle n_{\bar{q}} \rangle = 0$ and the probability of destroying a magnon is zero simply because there are none present. $S(\vec{Q},E)$ is given by

$$S(\vec{Q},E) = \sum_{\bar{\tau},\bar{q}} \delta(\vec{Q}-\bar{q}-\bar{\tau})\,\delta(E-\hbar\omega_{\bar{q}}) \quad . \tag{3.34}$$

Notice that $S(\vec{Q},E)$ is normalized so that the integral of $S(\vec{Q},E)$ over energy is unity.

3.5 $S(\vec{Q},E)$ for the Diluted Lattice

If the crystal lattice is diluted, that is if a certain fraction of the magnetic ions are randomly replaced by non-magnetic ions, then we cannot proceed as above to obtain an expression for the dispersion relation of the magnetic excitations. This is because a diluted lattice does not have translational symmetry and therefore the Fourier expansion technique does not work. The operators a_i^+ and a_i for a vacant site are non-physical because they create or destroy a spin deviation where a spin doesn't exist. Hence the operators $b_{\bar{q}}^+$ and $b_{\bar{q}}$ are also non-physical as they involve complete sums over all the a_i^+ or a_i. As a result, $\bar{q}$ is not a good quantum number for the spin excitations in a diluted crystal.

It is possible, however, to obtain qualitative information about the normal modes of a diluted crystal from neutron scattering measurements of $S(\vec{Q},E)$. This is because, although in general, all modes participate in the scattering at a particular $\vec{Q}$, certain modes contribute more strongly than others. The energies of the contributing modes are usually concentrated about some average value.

It would be useful to calculate $S(\vec{Q},E)$ to interpret neutron scattering measurements and to obtain information about

the low temperature magnetic excitations. $S(\vec{Q},E)$ can be calculated for the linear spin-wave model of a diluted ferromagnet by the equation of motion procedure[44] described below.

In the following, the diluted lattice is viewed as a three-dimensional array of spins in which the location of every spin vacancy is known. The interaction between every pair of spins in the array is also assumed to be known. A numerical calculation of $S(\vec{Q},E)$ can be performed for a finite array.

Consider the correlation functions, $g_{i\vec{Q}}(t)$, which are defined as

$$g_{i\vec{Q}}(t) = \langle a_i(t) \sum_j e^{i\vec{Q}\cdot\vec{R}_j} a_j(o) \rangle . \qquad (3.35)$$

There is a $g_{i\vec{Q}}$ for every occupied site i in the array. Eqn. (3.25) for $S(\vec{Q},E)$ can be written in terms of the $g_{i\vec{Q}}$ as

$$S(\vec{Q},E) = \frac{1}{2\pi N\hbar} \int_{-\infty}^{\infty} dt \exp(\frac{iEt}{\hbar}) \sum_i e^{-i\vec{Q}\cdot\vec{R}_i} g_{i\vec{Q}}(t) . \qquad (3.36)$$

The procedure is to determine the $g_{i\vec{Q}}$ as functions of time by solving their equations of motion and hence obtain $S(\vec{Q},E)$. The equations of motion are found by differentiating eqn. (3.35). One obtains

$$i\hbar \frac{dg_{i\vec{Q}}(t)}{dt} = \langle (i\hbar \frac{da_i(t)}{dt}) \sum_j e^{i\vec{Q}\cdot\vec{R}_j} a_j^+(o) \rangle . \qquad (3.37)$$

Now

$$i\hbar \frac{da_i(t)}{dt} = [a_i(t),H] = e^{\frac{iHt}{\hbar}} [a_i(o),H] e^{\frac{iHt}{\hbar}} \qquad (3.38)$$

where H is the Hamiltonian of eqn. (3.10). The commutator can be evaluated as

$$[a_i,H] = \sum_{j'} 2S J_{ij'} [a_i - a_{j'}] \qquad (3.39)$$

and eqn. (3.37) becomes

$$i\hbar \frac{dg_{i\vec{Q}}}{dt} = \sum_j 2S J_{ij} (g_{i\vec{Q}} - g_{j\vec{Q}}) \qquad (3.40)$$

The time derivative of $g_{i\vec{Q}}$ for the site i depends on the $g_{j\vec{Q}}$'s of its neighbours through the interaction of the spin at that site with the spins on the neighbouring sites. Furthermore, from the definition of $g_{i\vec{Q}}$ and the commutation rules for the spin deviation operators,

$$g_{i\vec{Q}}(t=0) = e^{i\vec{Q}\cdot\vec{R}_i} . \qquad (3.41)$$

For a given array the $g_{i\vec{Q}}$'s are calculated by beginning with this initial condition and integrating the coupled equations of motion forward in time. The calculations are performed on a computer and the details are presented in Chapter 4.

Eqn. (3.36) for $S(\vec{Q},E)$ can be further simplified by dividing the integral $\int_{-\infty}^{\infty} dt$ into two integrals, $\int_0^{\infty} dt$ and $\int_{-\infty}^{0} dt$. By changing the variable of integration in the second integral from t to -t and recognizing that

$$\sum_{ij} e^{-i\vec{Q}\cdot\vec{R}_i} g_{i\vec{Q}}(-t) = \{\sum_{ij} e^{-i\vec{Q}\cdot\vec{R}_i} g_{i\vec{Q}}(t)\}^*, \qquad (3.42)$$

(3.36) becomes

$$S(\vec{Q},E) = \frac{1}{\pi N\hbar} \mathrm{Re} \int_0^\infty dt \exp(\frac{iEt}{\hbar}) [\sum_i e^{-i\vec{Q}\cdot\vec{R}_i} g_{i\vec{Q}}(t)] \ . \qquad (3.43)$$

$S(\vec{Q},E)$ in this form is more convenient.

CHAPTER 4

COMPUTER SIMULATION TECHNIQUE

This chapter describes a computer simulation technique used to calculate the scattering law, $S(\vec{Q},E)$, for low-temperature magnetic excitations in disordered systems. The system is assumed to be at T = 0 K and to consist of localized spins coupled by the Heisenberg exchange interaction. Near neighbour (n.n.) and three neighbour (including all n.n., n.n.n. and third n.n. interactions) calculations were performed for a diluted fcc ferromagnet. The choice of various parameters and the errors involved in these calculations are discussed. The program, along with a description, is given in the Appendix. The input data for the various runs is presented at the end of the chapter to illuminate the use of the program. The technique is very similar to that reported by Alben *et al.*[45]

4.1 Computer Simulation Technique

(a) Equations of Motion

The normalized scattering intensity, $S(\vec{Q},E)$, is given in eqn. (3.43) and can be written as

$$S(\vec{Q},E) = \lim_{T\to\infty} \lim_{\lambda\to 0^+} \frac{1}{\pi N\hbar} \mathrm{Re} \int_0^T dt \exp\left(\frac{iEt}{\hbar}\right) \left[\sum_i \exp(-i\vec{Q}\cdot\vec{R}_i) g_{i\vec{Q}}\right] \exp(-\lambda t^2) \tag{4.1}$$

where the correlation functions, $g_{i\vec{Q}}$, are defined by

$$g_{i\vec{Q}}(t) = \langle a_i(t) \sum_j e^{i\vec{Q}\cdot\vec{R}_j} a_j^+(0) \rangle \qquad (4.2)$$

a_i^+ and a_i are Boson creation and destruction operators. At T = 0 K the triangular brackets imply the expectation value in the ground state and equations of motion can be obtained for the $g_{i\vec{Q}}$ using linear spin-wave theory. They are

$$i\hbar \frac{dg_{i\vec{Q}}}{dt} = \sum_j 2SJ_{ij}(g_{i\vec{Q}} - g_{j\vec{Q}}) \qquad (4.3)$$

with the initial condition that

$$g_{i\vec{Q}}(t=0) = \begin{cases} \exp(i\vec{Q}\cdot\vec{R}_i) & \text{(magnetic site)} \\ 0 & \text{(non-magnetic site)} \end{cases} \qquad (4.4)$$

The procedure is to integrate these coupled differential equations forward in time to obtain the $g_{i\vec{Q}}$ as functions of time. These functions are then substituted into eqn. (4.1) to obtain $S(\vec{Q},E)$.

(b) Numerical Method

The integrations are performed numerically using the finite difference formula

$$g_{i\vec{Q}}(t+\Delta t) = g_{i\vec{Q}}(t-\Delta t) + 2\Delta t \frac{dg_{i\vec{Q}}(t)}{dt} . \qquad (4.5)$$

A Taylor expansion is used for the first time step:

$$g_{i\vec{Q}}(\Delta t) = g_{i\vec{Q}}(0) + \Delta t \frac{dg_{i\vec{Q}}(0)}{dt} + \frac{\Delta t^2}{2} \frac{d^2 g_{i\vec{Q}}(0)}{dt^2} . \qquad (4.6)$$

Both of these equations are correct to 2nd order in Δt. The time step, Δt, can be written as

$$\Delta t = \frac{1}{n} \frac{2\pi}{\omega_{max}} \tag{4.7}$$

where ω_{max} is the upper frequency bound of the magnon spectrum. It has been reported that $n \sim 15\text{-}20$ gives sufficient accuracy[44].

The limits in eqn. (4.1) correspond to infinite resolution. In practice, only a finite resolution is required. The parameters T and λ are chosen to give the desired resolution. A finite T cuts off the time Fourier transform integral causing a broadening of the spectrum and "cut-off ripples". The apodizing function, $\exp(-\lambda t^2)$, introduces further broadening in the form of a Gaussian but reduces the cut-off ripples. A non-zero λ smooths out the spectrum and eliminates non-physical negative values of $S(\vec{Q},E)$.

The results for each calculation are in the form of a plot of $S(\vec{Q},E)$ vs. E for a particular $\vec{Q}$. The calculations are performed for one $\vec{Q}$ at a time. For a perfect crystal the response is a delta-function at the energy of the magnon designated by the particular $\vec{Q}$. The response of a diluted crystal is lower in energy and extends over a finite energy range. However, the response is usually concentrated about some frequency, say ω'. This implies that most of the $g_{i\vec{Q}}$ vary as $\exp(-i\omega' t)$. Therefore the functions

$$h_{i\vec{Q}} \equiv \exp^{(i\omega' t)} g_{i\vec{Q}} \tag{4.8}$$

will vary slowly with time. It is computationally more effective to solve for the quantities $h_{i\vec{Q}}$, rather than for the $g_{i\vec{Q}}$, because a larger time interval, Δt, can be used in the numerical integration.

The equations of motion for the $h_{i\vec{Q}}$ are

$$i\hbar \frac{dh_{i\vec{Q}}}{dt} = \sum_j 2SJ_{ij}(h_{i\vec{Q}} - h_{j\vec{Q}}) - \hbar\omega' h_{i\vec{Q}} \qquad (4.9)$$

with

$$h_{i\vec{Q}}(t=0) = \begin{cases} \exp(i\vec{Q}\cdot\vec{R}_i) & \text{(magnetic site)} \\ 0 & \text{(non-magnetic site)} \end{cases} \qquad (4.10)$$

The $h_{i\vec{Q}}$ are multiplied by $\exp(-i\omega' t)$ before substitution into (4.1). Note also that

$$i\hbar \frac{d^2 h_{i\vec{Q}}}{dt^2} = \sum_j 2SJ_{ij}\left(\frac{dh_{i\vec{Q}}}{dt} - \frac{dh_{j\vec{Q}}}{dt}\right) - \hbar\omega' \frac{dh_{i\vec{Q}}}{dt} \qquad (4.11)$$

The model lattices on which the calculations are performed are large, 3-dimensional fcc arrays in which a fraction x of the spins have been removed. For the purposes of indexing, the fcc array is viewed as a sc lattice of dimension N1×N2×N3 in which half the sc sites are missing. A lattice vector, $\vec{R}_{JKL}$, is given by

$$\vec{R}_{JKL} = J\frac{a}{2}\hat{x} + K\frac{a}{2}\hat{y} + L\frac{a}{2}\hat{z} \qquad (4.12)$$

where J, K and L are integers and J+K+L must be even. a is the

lattice spacing of the fcc lattice. An example is given in Fig. 4.1(a). To remain within the array, J, K and L can take on values from 1 to N1, 1 to N2 and 1 to N3 respectively. As periodic boundary conditions are used, N1, N2 and N3 must be even.

A reciprocal lattice vector is given by

$$\vec{G}_{hk\ell} = \frac{2\pi}{a} (h\hat{x} + k\hat{y} + \ell\hat{z}) \tag{4.13}$$

where h, k and ℓ are all even or all odd integers. The reciprocal lattice is shown in Fig. 4.1(b).

Consider the wave, $e^{i\vec{Q}\cdot\vec{R}_{JKL}}$. $\vec{Q}$ is the wavevector. For an infinite lattice, $\vec{Q}$ can be any vector in reciprocal space. However, if periodic boundary conditions are imposed on the wave, $\vec{Q}$ must take the form

$$\vec{Q} = \frac{2\pi}{a} \left(\frac{2n1}{N1} \hat{x} + \frac{2n2}{N2} \hat{y} + \frac{2n3}{N3} \hat{z}\right) \tag{4.14}$$

where n1, n2 and n3 are integers. The wave can be written

$$e^{i\vec{Q}\cdot\vec{R}_{JKL}} = e^{2\pi i\cdot(\frac{Jn1}{N1})} \cdot e^{2\pi i\cdot(\frac{Kn2}{N2})} \cdot e^{2\pi i\cdot(\frac{Ln3}{N3})} \tag{4.15}$$

The program calculates $S(\vec{Q},E)$ for one $\vec{Q}$ at a time for each array. N1, N2 and N3 determine the size of the array and n1, n2 and n3 define $\vec{Q}$. The integers, J, K and L, specify a particular lattice point. The exponentials in (4.15) do not have to be calculated every time they are required. The factors are calculated at the beginning of the program and stored in look-

Fig. 4.1 (a) A fcc lattice array (N1=6, N2=4) illustrating the J,K,L indexing of the lattice sites. $\vec{R}_{JKL}$ is a real lattice vector and a is the fcc lattice spacing.

(b) The reciprocal lattice which corresponds to the lattice in (a). $\vec{G}_{hk\ell}$ is a reciprocal lattice vector. Some special points in reciprocal space are also listed.

(a) fcc lattice (N1 = 6, N2 = 4)

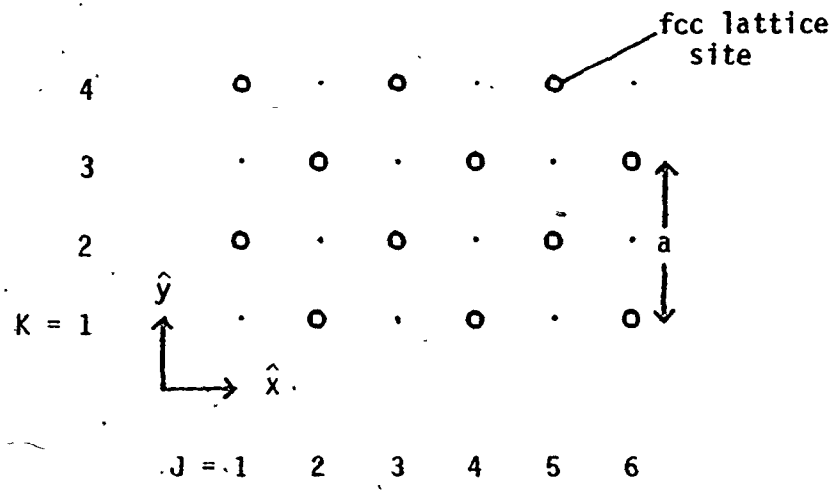

$$\vec{R}_{JKL} = J\frac{a}{2}\hat{x} + K\frac{a}{2}\hat{y} + L\frac{a}{2}\hat{z}$$

(J+K+L = 2n, n an integer)

(b) reciprocal lattice

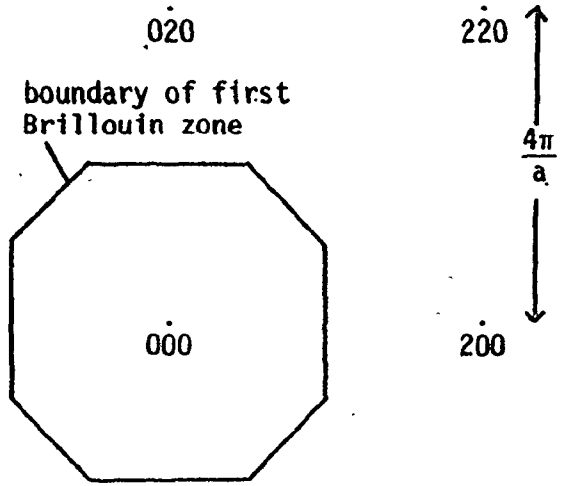

$$\vec{G}_{hk\ell} = \frac{2\pi}{a}(h\hat{x} + k\hat{y} + \ell\hat{z})$$

(h,k,ℓ all even or all odd)

Z.B. at $\frac{2\pi}{a}$ (.5,.5,.5) in (111) direction.

L point at $\frac{2\pi}{a}$ (1,1,0) in (110) direction.

Z.B. at $\frac{2\pi}{a}$ (1,0,0) in (100) direction.

up tables.

4.2 Errors

There are several sources of error in the computer simulation technique. A slight broadening of the spectrum and small ripples occur because λ^* is greater than zero and T is finite (see eqn. (4.1)). These parameters determine the energy resolution of the calculation. There is an error that arises from the integration procedure which causes a small shift in the response to higher frequencies. This error can be reduced by decreasing the time step, Δt. Wiggles occur in the response of diluted arrays, some of which are caused by the periodic boundary conditions, and some arise from the particular disordered spin configuration chosen. These wiggles are errors in the sense that they would not be present if the calculation were performed for an infinite crystal. All of these errors can be quantified and reduced to within certain limits. We now discuss the choice of the various parameters that set these limits.

To check the accuracy of the program, calculations are performed for perfect crystal cases ($x = 0$) and compared with the analytic solution for the dispersion curves (eqn. (3.19)). For example, Fig. 4.2 shows a plot of $S(\vec{Q},E)$ for $\vec{Q} = \frac{2\pi}{a}(0,0,1)$ as a function of the reduced energy $\tilde{E} = E/12SJ_1$. The result is from a n.n. calculation with $x = 0$ for an array of dimension $28\times38\times26$. $\vec{Q}$ is at the zone boundary in the $[00\zeta]$ direction, so from eqn. (3.19) a delta function is expected at $\tilde{E} = 2.6667$. The result of the program is a narrow Gaussian, with some rip-

Fig. 4.2 Computer simulation result for the normalized scattering law, $S(\vec{Q},E)$, as a function of normalized energy, $\tilde{E} = E/12SJ_1$, for a pure (x=0) fcc model of dimension N1×N2×N3 = 28×38×26 (3458 fcc unit cells). $\vec{Q}$ is at the zone boundary in the (001) direction. There is only a single mode excited. The result is a narrow Gaussian, with some ripple, centered at $\tilde{E} = 2.6679$. The analytic result is a delta function at $\tilde{E} = 2.6667$.

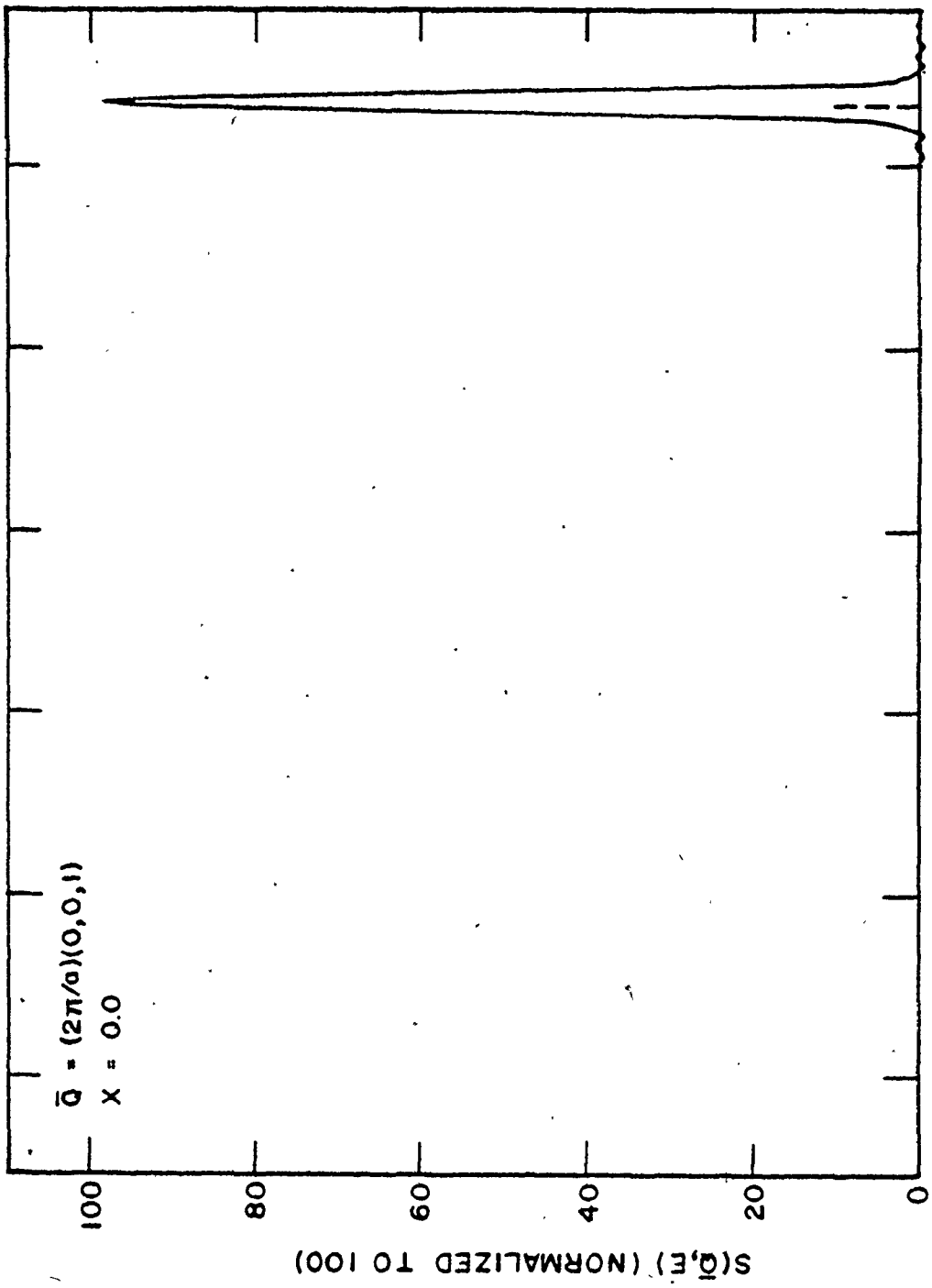
$\bar{Q} = (2\pi/a)(0,0,1)$
X = 0.0
0.0
0.5
1.0
1.5
2.0
2.5
E/12SJ$_1$
0
20
40
60
80
100
S($\bar{Q}$,E) (NORMALIZED TO 100)

ple, centered at $\tilde{E} = 2.6679$, very close to the correct energy.

The apodizing constant, λ, and the cut-off time, T were chosen so that the width of the Gaussian in the perfect crystal calculation was $\sim$ 2 % of the full spectral width (ω_{max}) and the ripple was < 0.5% of the peak height. For these specifications, λ is readily calculated to be

$$\lambda = \left[\frac{0.02\times\omega_{max}}{3.330}\right]^2 \qquad (4.16)$$

T was obtained empirically by repeating the calculation with different values. A value of

$$T = 50\cdot\left[\frac{2\pi}{\omega_{max}}\right] \qquad (4.17)$$

satisfied the ripple criterion given above.

In the example of Fig. 4.2 there is a slight discrepancy between the energy where the narrow Gaussian occurred and the energy expected from the analytic theory. This shift in energy was found to depend on the time step, Δt, and therefore must arise from the method of integration, i.e. eqn. (4.5). It was found empirically that the value

$$\Delta t \simeq \frac{1}{10}\left[\frac{2\pi}{\omega_{max}}\right] \qquad (4.18)$$

resulted in a frequency shift of less than .05% of ω_{max} over a spectral range $\frac{\omega_{max}}{2}$ centred at ω'. This frequency shift is significant only for the lowest values of $\bar{q}$, where a correction was made.

Wiggles occur in the response because periodic boundary conditions are imposed on the arrays. The location of these wiggles depends on the array dimensions. Therefore, care was taken to insure that N1, N2 and N3 were different, and the results of three arrays of different dimensions were averaged together. The averaging had the effect of smoothing out the response.

To simulate diluted crystals, a certain fraction of the spins in the array are removed by use of a random number routine. The resulting spin configuration contains only a finite sample of the single spin environments present in an infinite crystal. This causes an additional uncertainty in the response. The error from this effect can be reduced by averaging over arrays of different spin configurations. For example, see Fig. 5.5(a) and (b). Here $\vec{Q} = \frac{2\pi}{a}$ (0,0,1) and x = 0.2. In (a), $S(\vec{Q},E)$ is plotted for the n.n. calculation for three different arrays of dimensions 28×38×26, 32×34×30 and 36×24×22, each with a different spin configuration. All the arrays had 20% of the spins removed. The average of the results in (a) is shown in (b). The results in (a) differ from the average by less than 5%. This is taken as a rough estimate of the error in $S(\vec{Q},E)$. The centre frequency of the calculated response was selected by taking the centre of the peak at half height. An uncertainty is assigned by considering the distribution of centre frequencies that arises from the three spin configurations used in the average. This uncertainty was $\sim \pm 0.5\%$ and essentially independent of $\vec{Q}$.

4.3 Calculations

In Tables 4.1 and 4.2 are presented the initial data for the computer simulation calculations of $S(\vec{Q},E)$. ζ is the reduced wavevector; N1, N2 and N3 define the x, y and z dimensions of the array; and n1, n2 and n3 fix $\vec{Q}$. The tables show the number of spin sites, the number of spins present and ENORMP which is related to the ω' in the definition of $h_{i\vec{Q}}$. In most cases the results of three arrays were averaged together. Table 4.1 is for n.n. calculations with $x = 0.2$ for the $[00\zeta]$, $[\zeta\zeta 0]$ and $[\zeta\zeta\zeta]$ directions. Table 4.2 is for three neighbour calculations with $x = 0.2$ for the $[00\zeta]$ direction. For these calculations the exchange constants were $J_1 = 0.296$ meV, $J_2 = 0.283$ meV and $J_3 = 0.110$ meV. Other n.n. calculations with $x = 0.3$ were performed using the same arrays as in Table 4.1. The results of the computer runs are presented in the next chapter.

Table 4.1 Initial data for the n.n. computer simulation calculations of $S(\vec{Q},E)$. The fraction of missing spins is $x = 0.2$.

(a) $\vec{Q} = \frac{2\pi}{a}(0,0,\zeta)$

ζ	N1	N2	N3	n1	n2	n3	number of spin sites	number of spins present	ENORMP
.0	52	28	22	0	0	0	16016	12773	0.0
	46	26	24	0	0	0	14352	11485	
	34	32	30	0	0	0	16320	13802	
.1	20	36	44	1	0	0	15840	12631	0.0
	40	30	26	2	0	0	15600	12493	
	40	32	24	2	0	0	15360	12323	
.2	30	38	26	3	0	0	14820	11776	0.2
	40	28	24	4	0	0	13440	10695	
	50	22	20	5	0	0	11000	8789	
.3	20	36	44	3	0	0	15840	12601	0.3
	40	30	26	6	0	0	15600	12450	
	40	32	24	6	0	0	15360	12275	
.4	30	38	26	6	0	0	14820	11889	0.6
	40	28	24	8	0	0	13440	10730	
	50	22	20	10	0	0	11000	8864	
.5	28	38	26	7	0	0	13832	11031	0.8
	32	34	30	8	0	0	16320	12970	
	36	24	22	9	0	0	9504	7525	
.6	30	38	26	9	0	0	14820	11955	1.0
	40	28	24	12	0	0	13440	10780	
	50	22	20	15	0	0	11000	8791	
.7	20	36	44	7	0	0	15840	12761	1.3
	40	30	26	14	0	0	15600	12492	
	40	32	24	14	0	0	15360	12327	
.8	30	38	26	12	0	0	14820	11925	1.4
	40	28	24	16	0	0	13440	10811	
	50	22	20	20	0	0	11000	8921	
.9	20	36	44	9	0	0	15840	12735	1.5
	40	30	26	18	0	0	15600	12449	
	40	32	24	18	0	0	15360	12249	
1.0	28	38	26	14	0	0	13832	11044	1.6
	32	34	30	16	0	0	16320	13044	
	36	24	22	18	0	0	9504	7608	

Table 4.1 (continued)

(b) $\vec{Q} = \frac{2\pi}{a}(\zeta,\zeta,0)$

ζ	N1	N2	N3	n1	n2	n3	number of spin sites	number of spins present	ENORMP
.0833	24	24	52	1	1	0	14976	11935	0.06
	48	24	28	2	1	0	16128	12929	
	48	24	22	2	1	0	12672	10206	
.1667	36	24	30	3	2	0	12960	10294	0.16
	48	24	28	4	2	0	16128	12885	
	48	36	18	4	3	0	15552	12424	
.2500	32	40	22	4	5	0	14080	11198	0.43
	32	24	34	4	3	0	13056	10397	
	40	24	28	5	3	0	13440	10725	
.3333	48	24	22	8	4	0	12672	10155	0.69
	30	36	28	5	6	0	15120	9458	
	42	30	26	7	5	0	16380	13161	
.4167	24	24	52	5	5	0	14976	11965	0.96
	48	24	28	10	5	0	16128	12814	
	48	24	22	10	5	0	12672	10049	
.5000	28	44	26	7	11	0	16016	12931	1.7
	24	40	30	6	10	0	14400	11543	
	32	36	22	8	9	0	12672	10127	
.5833	24	24	52	7	7	0	14976	12055	1.38
	48	24	28	14	7	0	16128	12903	
	48	24	22	14	7	0	12672	10168	
.6667	48	24	22	16	8	0	12672	10197	1.49
	30	36	28	10	12	0	15120	12149	
	42	30	26	14	10	0	16380	13156	
.7500	32	40	22	12	15	0	14080	11234	1.6
	32	24	34	12	9	0	13056	10421	
	40	24	28	15	9	0	13440	10734	
.8333	36	24	30	15	10	0	12960	10373	1.6
	48	24	28	20	10	0	16128	12906	
	48	36	18	20	15	0	15552	12333	
.9167	24	24	52	11	11	0	14976	12047	1.6
	48	24	28	22	11	0	16128	12788	
	48	24	22	22	11	0	12672	10106	
1.0000	36	34	26	18	17	0	15912	12689	1.6
	32	30	28	16	15	0	13440	10779	
	38	22	24	19	11	0	10032	7995	

Table 4.1 (continued)

(c) $\vec{Q} = \frac{2\pi}{a}(\zeta,\zeta,\zeta)$

ζ	N1	N2	N3	n1	n2	n3	number of spin sites	number of spins present	ENORMP
.0667	30	30	30	1	1	1	13500	10717	0.0
	30	30	30	1	1	1	13500	10743	
	30	30	30	1	1	1	13500	10767	
.0833	48	24	24	2	1	1	13824	10997	0.1
	48	24	24	2	1	1	13824	11000	
	48	24	24	2	1	1	13824	11019	
.1250	48	32	16	3	2	1	12288	9859	0.2
	48	32	16	3	2	1	12288	9794	
	48	32	16	3	2	1	12288	9889	
.1667	48	36	12	4	3	1	12288	8291	0.3
	36	36	24	3	3	2	15552	12366	
	36	24	24	3	2	2	10368	8232	
.2000	50	30	20	5	3	2	15000	12100	0.5
	40	30	20	4	3	2	12000	9635	
	50	20	20	5	2	2	10000	8001	
.2500	48	24	24	6	3	3	13824	11126	0.6
	40	32	24	5	4	3	15360	12295	
	32	32	24	4	4	3	12288	9866	
.2857	42	28	14	6	4	2	8232	6567	0.7
	42	28	14	6	4	2	8232	6614	
	42	28	14	6	4	2	8232	6612	
.3333	48	36	18	8	6	3	15552	12527	0.9
	42	30	24	7	5	4	15120	12075	
	36	30	24	6	5	4	12960	10342	
.3750	48	32	16	9	6	3	15552	9811	1.0
	48	32	16	9	6	3	15552	9844	
	48	32	16	9	6	3	15552	9822	
.4167	48	24	24	10	5	5	13824	10950	1.1
	48	24	24	10	5	5	13824	11140	
	48	24	24	10	5	5	13824	10959	
.4444	36	36	18	8	8	4	11664	9295	1.1
	36	36	18	8	8	4	11664	9363	
	36	36	18	8	8	4	11664	9290	
.5000	44	32	16	11	8	4	11264	9040	1.2
	40	36	20	10	9	5	14400	11468	
	36	32	24	9	8	6	13824	11127	

Table 4.2 Input data for the third neighbour computer simulation calculations of $S(\vec{Q},E)$. The fraction of missing spins is $x = 0.2$. $\vec{Q} = 2\pi/a\ (0,0,\zeta)$.

ζ	N1 N2 N3	n1 n2 n3	number of spin sites	number of spins present	ENORMP
.1	44 36 20	0 0 1	15840	12657	.37
.2	26 38 30	0 0 3	14820	11839	1.38
	24 28 40	0 0 4	13440	10825	
	20 22 50	0 0 5	11000	8764	
.3	44 36 20	0 0 3	15840	12616	2.78
	26 30 40	0 0 6	15600	12488	
	24 32 40	0 0 6	15360	12299	
.4	26 38 30	0 0 6	14820	11876	4.22
	24 28 40	0 0 8	13440	10728	
	20 22 50	0 0 10	11000	8775	
.5	26 38 28	0 0 7	13832	11036	5.43
.6	26 38 30	0 0 9	14820	11847	6.21
	24 28 40	0 0 12	13440	10733	
	20 22 50	0 0 15	11000	8787	
.7	44 36 20	0 0 7	15840	12757	6.54
	26 30 40	0 0 14	15600	12414	
	24 32 40	0 0 14	15360	12340	
.8	26 38 30	0 0 12	14829	11870	6.55
	24 28 40	0 0 16	13440	10810	
	20 22 50	0 0 20	11000	8850	
.9	44 36 20	0 0 9	15840	12658	6.45
	26 30 40	0 0 18	15600	12495	
	24 32 40	0 0 18	15360	12340	
1.0	26 38 28	0 0 14	13832	11129	6.38

CHAPTER 5

RESULTS AND DISCUSSION

5.1 Neutron Scattering Experiment

Inelastic neutron scattering experiments were performed on the non-diluted ferromagnet, Ni_2MnSn, and on the 20% diluted ferromagnet, $Ni_2Mn_{0.8}V_{0.2}Sn$. The samples were oriented with the $[\bar{1}10]$ direction vertical and the spin-wave dispersion curves were measured in three symmetry directions about the (111) reciprocal lattice point. Fig. 2.5 is a diagram of the reciprocal lattice in the $(\bar{1}10)$ plane showing the centres of peaks observed in constant energy scans. The constant energy mode was used because of the steepness of the dispersion curves. The sample temperature was approximately 93 K which is 0.27 T_c for Ni_2MnSn and 0.36 T_c for $Ni_2Mn_{0.8}V_{0.2}Sn$.

Some selected neutron groups are shown in Fig. 5.1 for Ni_2MnSn and Fig. 5.2 for $Ni_2Mn_{0.8}V_{0.2}Sn$. The intensity of the spin-wave scattering is weak compared to the background, and decreases as the frequency transfer increases. Some of this decrease may be intrinsic to the spin-waves, but for constant incident energy, it is mostly due to the decrease in efficiency of the analysing spectrometer. A similar decrease was observed for both crystals. The low signal to background ratio limited mwasurements to frequency transfers of less than 6 THz.

Fig. 5.1 Constant energy scans along the (00ζ) direction in Ni_2MnSn at 93 K. Counts are plotted against the reduced wavevector, ζ, for several energy transfers, ν. The incident neutron wavelength was 1.62 A° for $\nu < 4$ THz and 1.17 A° for $\nu \geq 4$ THz.

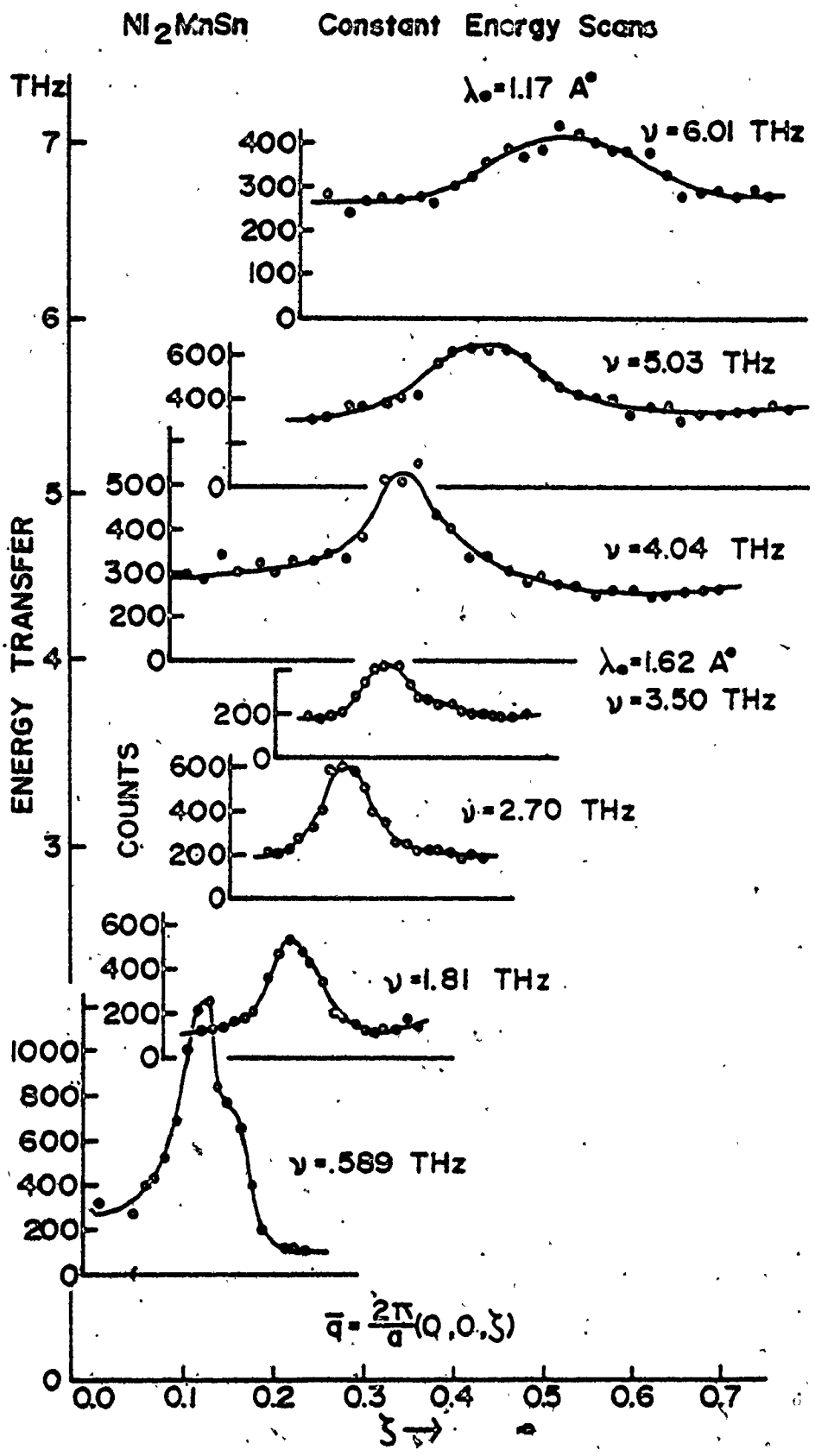
Ni2MnSn Constant Energy Scans
λ₀=1.17 A°
ν=6.01 THz
ν=5.03 THz
ν=4.04 THz
λ₀=1.62 A°
ν=3.50 THz
ν=2.70 THz
ν=1.81 THz
ν=.589 THz
THz
ENERGY TRANSFER
COUNTS
q̄ = 2π/a (0, 0, ζ)
ζ →

Fig. 5.2 Constant energy scans along the $[\zeta\zeta\zeta]$ direction in $Ni_2Mn_{0.8}V_{0.2}Sn$ at 93 K. Counts are plotted against the reduced wavevector, ζ, for several energy transfers, ν. The incident neutron wavelength was 1.60 A° for $\nu < 3$ THz and 1.16 A° for $\nu \geq 3$ THz.

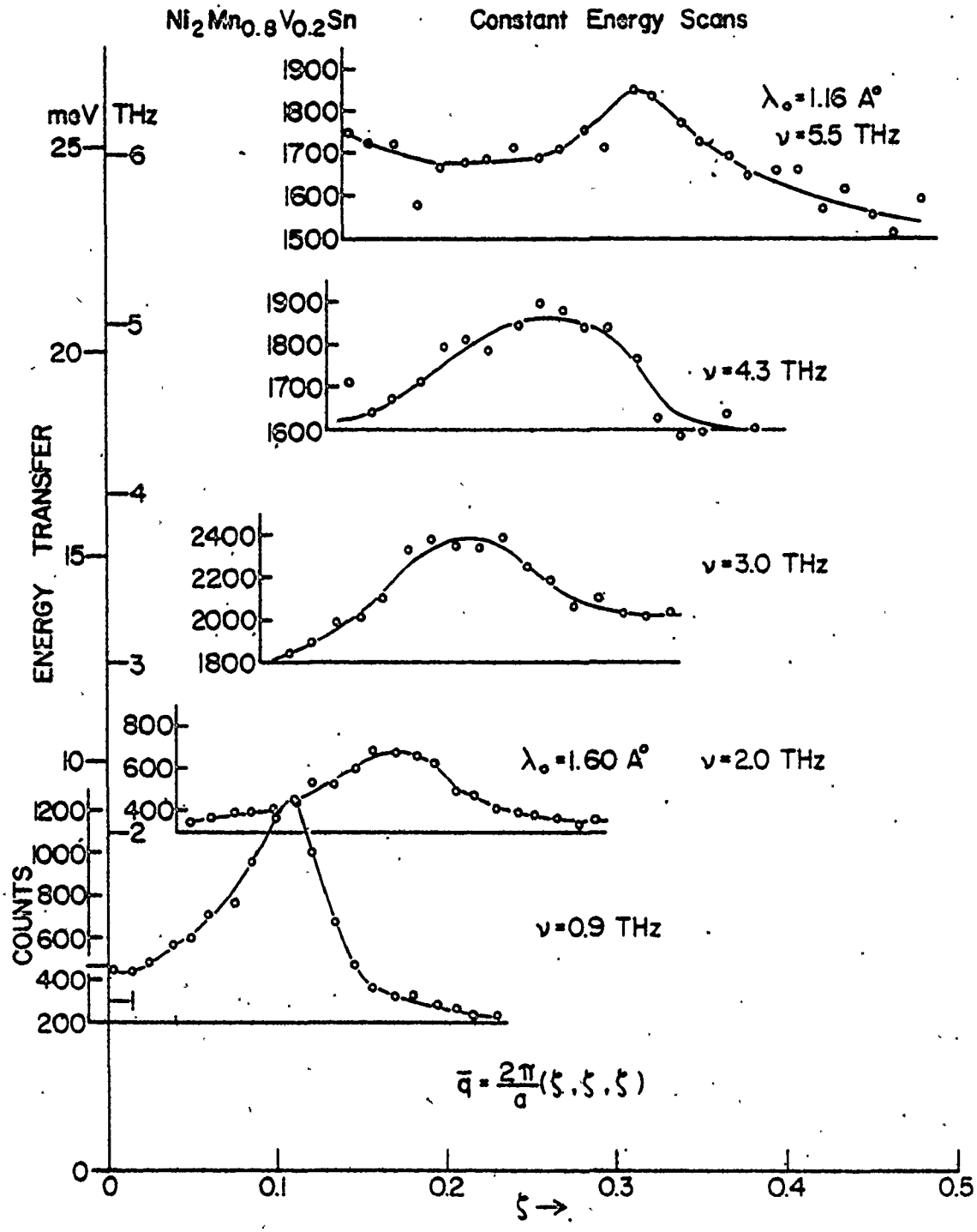
$Ni_2Mn_{0.8}V_{0.2}Sn$
Constant Energy Scans
meV
THz
ENERGY TRANSFER
COUNTS
λ_o=1.16 A°
ν=5.5 THz
ν=4.3 THz
ν=3.0 THz
λ_o=1.60 A°
ν=2.0 THz
ν=0.9 THz
$\vec{q} = \frac{2\pi}{a}(\zeta, \zeta, \zeta)$
ζ →

Points on the dispersion curves were obtained by taking the centre of the observed peak to correspond to the frequency transfer of the scan. Scans at low $\bar{q}$ were repeated with increased horizontal and vertical collimation to check if a resolution correction was necessary in this region. The position of the peaks did not change therefore the correction was not required. The results are given in Table 5.1 for Ni_2MnSn and in Table 5.2 for $Ni_2Mn_{0.8}V_{0.2}Sn$. Also recorded for $Ni_2Mn_{0.8}V_{0.2}Sn$ is R, the ratio of the frequency of the diluted crystal to the frequency of the non-diluted crystal. As measurements for the two crystals were not taken at the same $\bar{q}$ values, interpolated values for Ni_2MnSn, based on the six neighbour fit, were used for the perfect crystal frequency. The uncertainty in the peak position and in R was assigned by considering the statistical error in the number of counts at each point on the scan.

The experimental frequencies for Ni_2MnSn are plotted in Fig. 5.3. Also shown is the six-neighbour fit that Noda and Ishikawa[4] made to their data on the same material. Their data was taken at 50 K whereas this data was taken at 93 K. According to the magnetization curves for Ni_2MnSn (see Fig. 2.5), the ferromagnet is still $\sim$ 98% saturated at 93 K. Therefore the frequencies of the spin-waves should have changed little from their T = 0 K values. Agreement with Noda and Ishikawa's fit is good except in the [00ζ] direction where the

Table 5.1 Spin-excitation frequencies for Ni_2MnSn at 93 K

(a) $\bar{q} = \frac{2\pi}{a}(0,0,\zeta)$

frequency ν (THz)	reduced wavevector ζ
.589	.117(5)
1.342	.197(4)
1.806	.220(7)
2.703	.280(7)
3.495	.326(7)
3.997	.350(10)
4.040	.353(8)
4.503	.408(10)
5.029	.434(16)
6.006	.533(19)

(b) $\bar{q} = \frac{2\pi}{a}(\zeta,\zeta,0)$

ν (THz)	ζ
.543	.081(6)
1.265	.125(6)
1.704	.136(7)
2.496	.180(7)
3.495	.228(10)

(c) $\bar{q} = \frac{2\pi}{a}(\zeta,\zeta,\zeta)$

ν (THz)	ζ
.635	.069(8)
1.418	.105(4)
2.214	.136(4)
3.010	.162(5)
3.495	.184(4)

Table 5.2 Spin-excitation frequencies for $Ni_2Mn_{0.8}V_{0.2}Sn$ at 93 K

(a) $\vec{q} = \frac{2\pi}{a}(0,0,\zeta)$

frequency ν (THz)	reduced wavevector ζ	perfect crystal frequency ν_t (THz)	corrected ratio ν/ν_t
.484	.115(6)	.50075	1.04(10)
.907	.192(9)	1.30842	.75(7)
1.291	.240(5)	1.93492	.72(3)
1.998	.312(8)	2.95592	.73(3)
3.006	.418(10)	4.43428	.73(2)
3.980	.520(15)	5.66791	.76(2)
5.004	.600(15)	6.48400	.83(2)

(b) $\vec{q} = \frac{2\pi}{a}(\zeta,\zeta,0)$

ν (THz)	ζ	ν_t (THz)	ν/ν_2
.484	.085(5)	.55291	.94(12)
.907	.128(3)	1.21185	.81(4)
1.251	.161(3)	1.84959	.73(3)
1.994	.198(3)	2.65889	.81(2)
3.03	.281(7)	4.58018	.71(3)
4.27	.362(10)	6.15169	.75(2)

(c) $\vec{q} = \frac{2\pi}{a}(\zeta,\zeta,\zeta)$

ν (THz)	ζ	ν_t (THz)	ν/ν_t
.484	.071(4)	.58088	.90(11)
.907	.106(2)	1.25868	.78(3)
1.291	.135(2)	1.97680	.70(2)
1.994	.170(3)	2.98208	.72(2)
3.015	.220(10)	4.55292	.71(5)
4.260	.260(20)	5.80103	.79(9)
4.54	.283(12)	6.47445	.76(5)
5.521	.316(10)	7.34924	.81(3)
6.50	.395(15)	8.72707	.80(2)

Fig. 5.3 Spin-wave dispersion relations for $Ni_2Mn_{0.8}V_{0.2}Sn$ and Ni_2MnSn corrected to 0 K. The solid line is the six-neighbour fit to Noda and Ishikawa's data for Ni_2MnSn. The broken line is the result of computer simulation calculations for the 20% diluted ferromagnet. For the $[00\zeta]$ direction the broken line is the three-neighbour calculation plus the virtual crystal result for $4^{\underline{th}}$ to $6^{\underline{th}}$ neighbour contributions. For the $[\zeta\zeta 0]$ and $[\zeta\zeta\zeta]$ directions the line is the nearest neighbour calculation plus 0.8 of the $2^{\underline{nd}}$ to $6^{\underline{th}}$ neighbour non-diluted contributions.

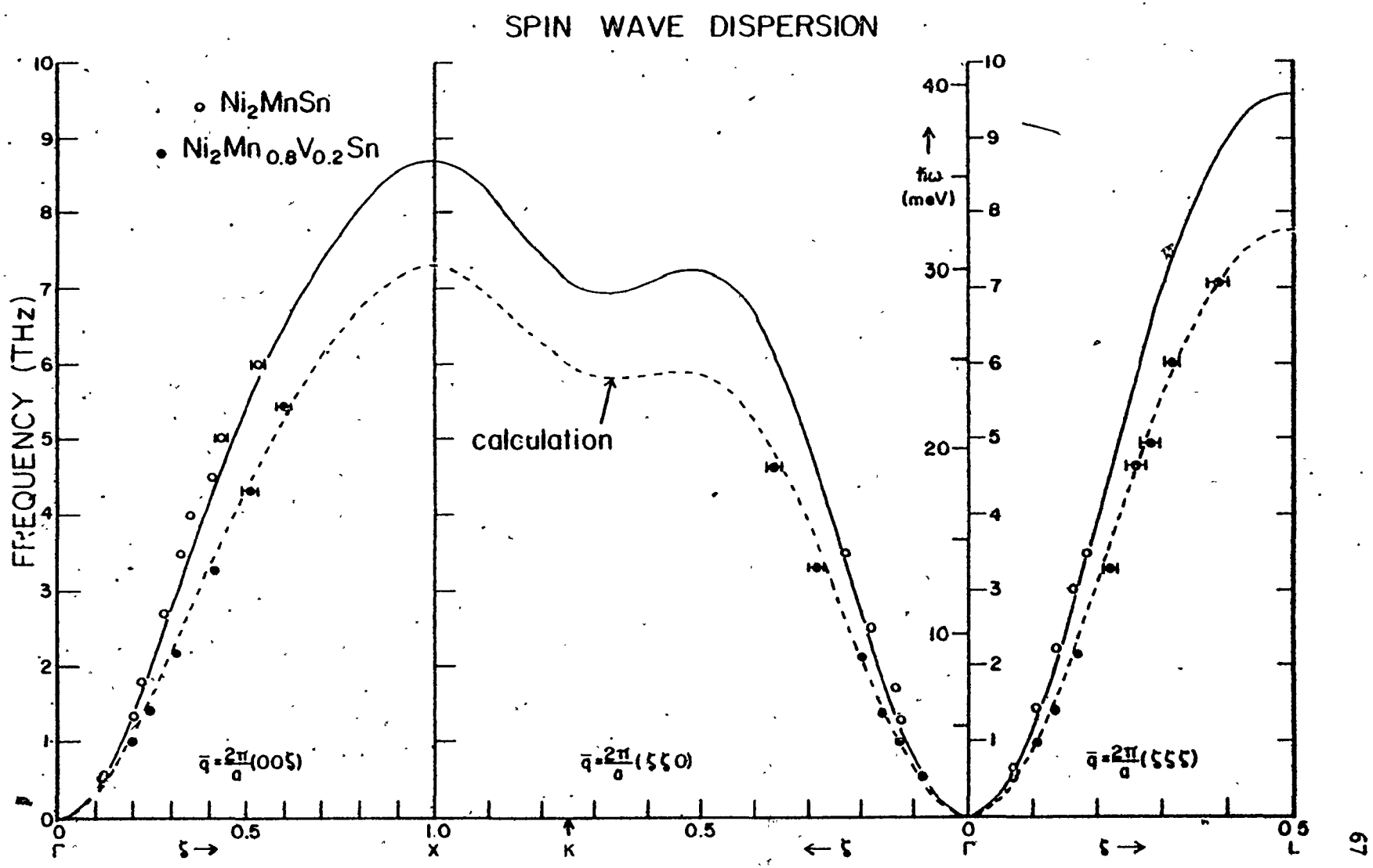
SPIN WAVE DISPERSION
o Ni2MnSn
• Ni2Mn0.8V0.2Sn
FREQUENCY (THz)
ħω (meV)
calculation
q̄ = 2π/a (00ζ)
q̄ = 2π/a (ζζ0)
q̄ = 2π/a (ζζζ)
Γ
X
K
L
ζ →
← ζ

frequencies are slightly higher than the fit. This discrepancy may be due to a disorder effect[4]. Careful examination of the scans shows that there are possibly two peaks suggesting two branches. One of the peaks occurs at the fit frequency. The higher frequencies are as yet unexplained. The values for the exchange constants obtained by Noda and Ishikawa were used in subsequent calculations because their data is more complete.

The spin-wave dispersion relations for $Ni_2Mn_{0.8}V_{0.2}Sn$ are also shown in Fig. 5.3. The experimental frequencies measured at 93 K, have been corrected to 0 K by scaling with the temperature dependence of the magnetization. The correction increased all frequencies by 8.7%. The validity of this temperature correction is discussed in Section 2.4.

It is obvious from Fig. 5.3 that the effect of dilution is to lower the frequencies of the spin-waves. In the virtual crystal model the random removal of a fraction x of the spins lowers the spin-wave frequencies by a factor 1-x. The factor is independent of $\bar{q}$. In contrast, the measured ratio of the frequency for the 20% diluted alloy to that of the non-diluted alloy is found to very with $\bar{q}$. This ratio is plotted in Fig. 5.4(a). The ratio is less than 0.8 for low $\bar{q}$ and greater than 0.8 for high $\bar{q}$. This result is characteristic of an in-band resonance[1]. The virtual crystal model is inadequate to explain this phenomena because it does not properly account for the randomness in the local environment of each spin.

Fig. 5.4 (a) Frequency ratio, $\omega_{dilute}/\omega_{non\text{-}dilute}$, vs. reduced wavevector, ζ, for the $[00\zeta]$, $[\zeta\zeta 0]$ and $[\zeta\zeta\zeta]$ directions. The measured frequencies for $Ni_2Mn_{0.8}V_{0.2}Sn$ were divided by the corresponding frequency of the six-neighbour fit to the data for Ni_2MnSn. The solid line is the ratio obtained from the n.n. computer simulation calculation and the broken line is the result of the three-neighbour calculation.

(b) Width of the response obtained from the computer simulation calculations for n.n. interactions with x=0.2 (solid line) and x=0.3 (dotted line), and for three-neighbour interactions with x=0.2 (dashed line).

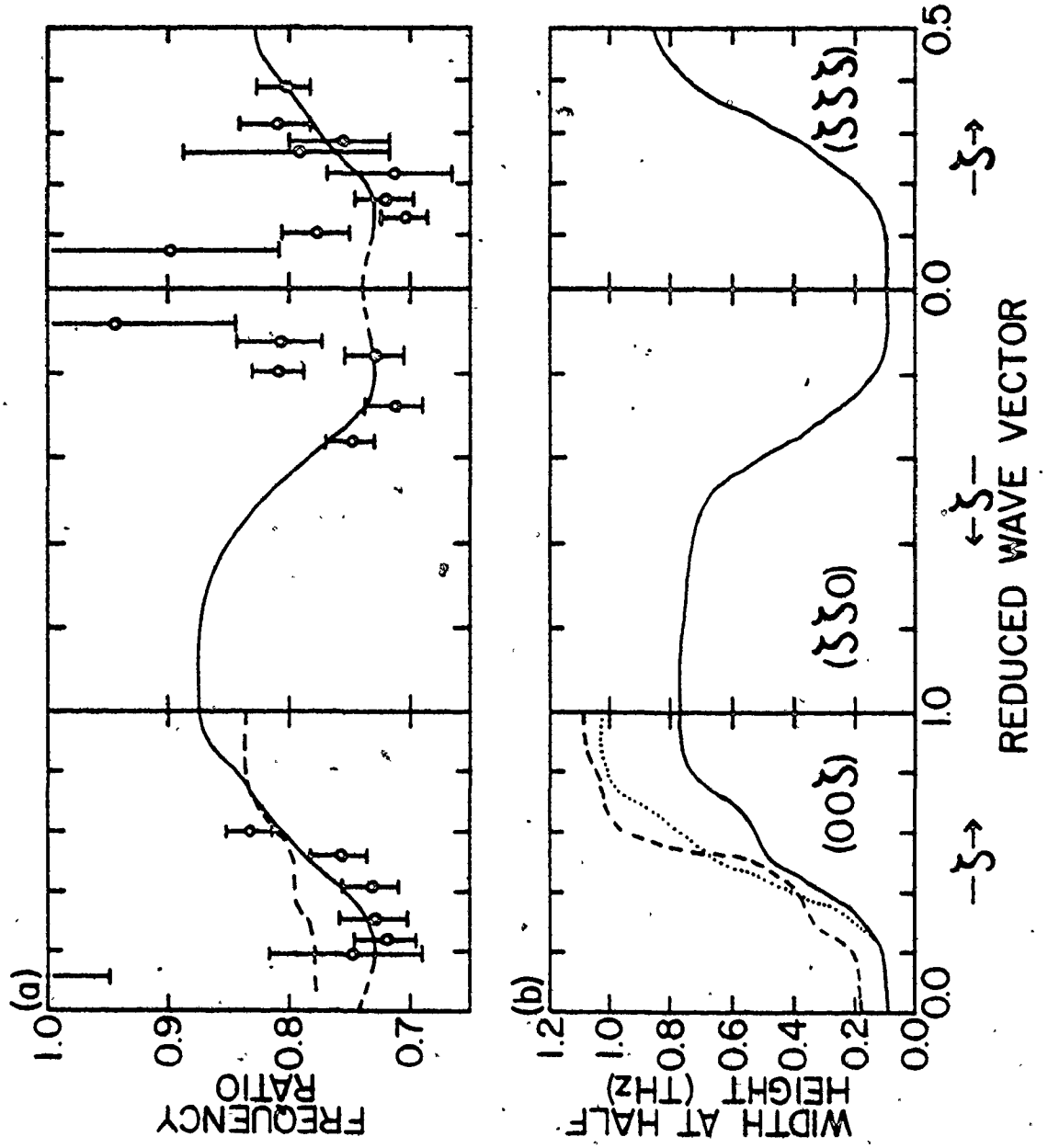
(a)
FREQUENCY RATIO
1.0
0.9
0.8
0.7
(b)
WIDTH AT HALF HEIGHT (THz)
1.2
1.0
0.8
0.6
0.4
0.2
0.0
(00ζ)
(ζζ0)
(ζζζ)
0.0
1.0
0.0
0.5
−ζ→
←ζ→
−ζ→
REDUCED WAVE VECTOR

Another expected effect of dilution is an increase in the width of the response due to a decrease in the lifetime of the excitations. However, the low intensity of the scattering made it necessary to set the spectrometer for low resolution which precluded accurate measurement of the response widths. The expected increase in width was small compared to the resolution width of the instrument.

5.2 Computer Simulation Results

The effects of dilution were first examined in a n.n. model. Fig. 5.6 shows results of the computer simulation for a fcc lattice, including only n.n. matrices, with $x = 0.2$ (20% diluted). In the figure are plots of $S(\vec{Q},E)$, normalized to 100, vs. the reduced energy $\tilde{E} = E/12SJ_1$, as $\vec{Q}$ increases towards the zone boundary in the $[00\zeta]$ direction. The results are averages of three different arrays, each with a different configuration of spins selected by a random number generator. By averaging the three calculations, boundary effects are minimized and $\sim$ 40,000 single spin environments are considered. The error in $S(\vec{Q},E)$ estimated from the difference in the results from the three arrays, is approximately 5%.

The graphs in Fig. 5.5 show that the diluted crystal responses broaden and decrease in frequency from the non-diluted results, which are delta-functions at the frequencies indicated by bars. The centre frequency of the calculated response was selected by taking the centre of the peak at

Fig. 5.5 $S(\vec{Q},E)$ for various $\vec{Q}$'s in the [00ζ] direction from the n.n. computer simulation calculations. The vertical bars are the delta-function responses for the non-diluted crystal. (a) $S(\vec{Q},E)$ for three different arrays (28×38×26, 32×34×30 and 36×24×22) at the same $\vec{Q}$. (b) Average of the three arrays in (a). (c),(d),(e) and (f) $S(\vec{Q},E)$ for various $\vec{Q}$'s in the [00ζ] direction.

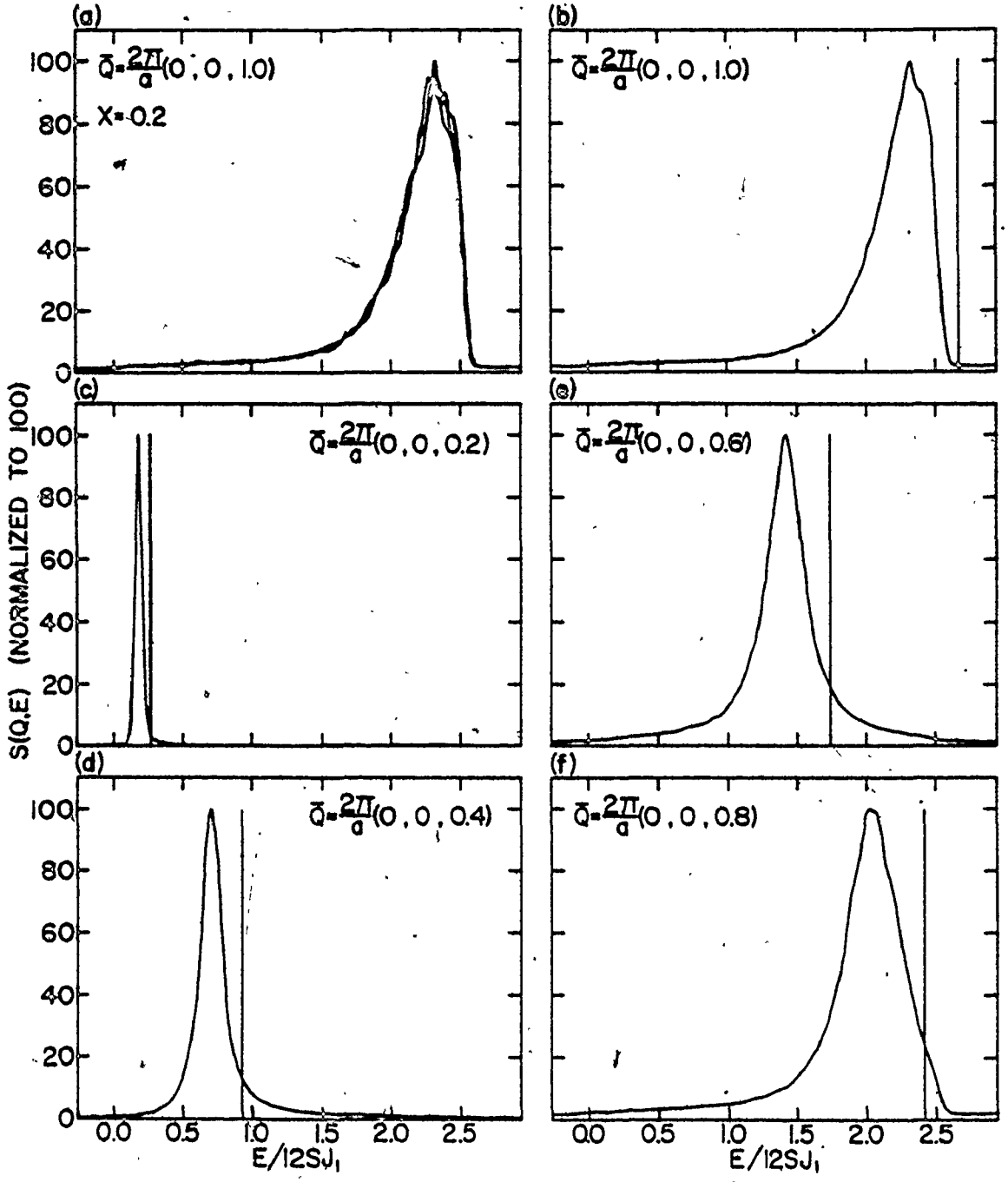
(a)
$\vec{Q}=\frac{2\pi}{a}(0,0,1.0)$
X=0.2
(b)
$\vec{Q}=\frac{2\pi}{a}(0,0,1.0)$
(c)
$\vec{Q}=\frac{2\pi}{a}(0,0,0.2)$
(e)
$\vec{Q}=\frac{2\pi}{a}(0,0,0.6)$
(d)
$\vec{Q}=\frac{2\pi}{a}(0,0,0.4)$
(f)
$\vec{Q}=\frac{2\pi}{a}(0,0,0.8)$
S(Q,E) (NORMALIZED TO 100)
0
20
40
60
80
100
0.0
0.5
1.0
1.5
2.0
2.5
E/12SJ1

half height. An uncertainty is assigned by considering the distribution of centre frequencies that arise from the three spin configurations used in the average. This uncertainty was $\sim$ 0.5% and essentially independent of $\vec{Q}$. The frequencies, frequency ratios and widths are presented in Table 5.3.

The frequency ratios for the n.n. calculation are also plotted in Fig. 5.4(a). The shape of the measured ratio, characteristic of an in-band resonance, is well reproduced by the calculated curves of $S(\vec{Q},E)$ for the n.n. model. However, because the alloy is a metal and the exchange interactions are long range, the contribution to the spin-wave frequencies from further neighbours cannot be neglected. To examine the effects of including more neighbours in the computer simulation, a calculation was done for the [00ζ] direction which included up to third neighbours. These results are presented in Table 5.4. The frequency ratios for this calculation are also shown in Fig. 5.4(a) (broken lines). It can be seen that the ratios are closer to 0.8 and the resonance behavior is not as pronounced. This is to be expected because the larger number of neighbours makes for smaller fluctuations in the number of neighbours interacting with each spin. However, the calculated resonance is now smaller than the measured resonance, and there is not as good agreement with experiment. Note that the inclusion of neighbours more distant than third should have little effect on the ratios

Table 5.3. Spin-excitation frequencies, in THz, for a diluted fcc lattice with n.n. exchange interactions, from computer simulation calculations. The fraction of missing spins is x = 0.2 and the exchange constant is J_1 = 0.0716 THz

(a) $\bar{q} = \frac{2\pi}{a}(0,0,\zeta)$

reduced wavevector ζ	frequency ν	perfect crystal frequency ν_1	ratio ν/ν_1	width of response W	6-neighbour frequency ν_{total}
uncertainty:	±.5%		±.5%	±1%	
0	0	0	--	.0933	0
.1	.0831	.11210	.741	.0940	.2291
.2	.3176	.43744	.726	.102	1.0939
.3	.689	.94416	.730	.165	2.1602
.4	1.195	1.58266	.755	.295	3.2845
.5	1.786	2.29045	.780	.465	4.3084
.6	2.42	2.99824	.808	.526	5.2116
.7	3.00	3.63675	.825	.603	5.9687
.8	3.49	4.14347	.843	.781	6.6173
.9	3.87	4.46880	.865	.793	7.1106
1.0	4.00	4.58091	.873	.724	7.2933

(b) $\bar{q} = \frac{2\pi}{a}(\zeta,\zeta,0)$

ζ	ν	ν_1	ν/ν_1	W	ν_{total}
.0833	.1162	.15476	.751	.0940	.4180
.1667	.433	.59317	.730	.112	1.5330
.2500	.916	1.24347	.737	.202	3.0086
.3333	1.524	2.00415	.760	.360	4.4480
.4167	2.19	2.76615	.792	.559	5.4499
.5000	2.83	3.43568	.824	.692	5.8777
.5833	3.34	3.95178	.844	.729	5.8578
.6667	3.70	4.29460	.862	.749	5.8019
.7500	3.89	4.48266	.869	.749	5.9957
.8333	3.96	4.56035	.869	.749	6.4890
.9167	3.97	4.57958	.866	.769	7.0237
1.0000	3.98	4.58091	.869	.733	7.2763

Table 5.3 (continued)

(c) $\bar{q} = \frac{2\pi}{a}(\zeta,\zeta,\zeta)$

ζ	ν	ν_1	ν/ν_1	W	ν_{total}
.0667	.1089	.14852	.733	.0943	.4009
.0833	.1686	.23015	.733	.0948	.6192
.1250	.3687	.50314	.733	.106	1.3384
.1667	.626	.85892	.729	.135	2.2440
.2000	.873	1.18700	.735	.202	3.0561
.2500	1.301	1.71784	.757	.304	4.3235
.2857	1.621	2.10009	.772	.398	5.1824
.3333	2.03	2.57676	.786	.533	6.1697
.3750	2.35	2.93254	.801	.702	6.8578
.4167	2.60	3.20553	.812	.769	7.3478
.4444	2.74	3.33208	.822	.813	7.5804
.5000	2.84	3.43568	.826	.864	7.7511

Table 5.4 Spin-excitation frequencies, in THz, for a diluted fcc lattice with n.n., n.n.n. and third n.n. exchange interactions, from computer simulation calculations. The fraction of missing spins is $x = 0.2$ and the exchange constants are $J_1 = 0.0716$ THz, $J_2 = 0.0684$, $J_3 = 0.02660$ THz, $\vec{q} = 2\pi/a\ (0,0,\zeta)$

reduced wavevector ζ	frequency ν	perfect crystal frequency ν_3	ratio ν/ν_3	width of response W	6 neighbour frequency ν_{total}
uncertainty:	±.5%		±.5%	±1%	
.1	.3596	.46254	.777	.1901	.2952
.2	1.347	1.72900	.779	.206	1.0901
.3	2.72	3.47675	.782	.332	2.1651
.4	4.21	5.28910	.796	.390	3.3336
.5	5.41	6.79011	.797	.523	4.3361
.6	6.29	7.75683	.811	.980	5.2708
.7	6.79	8.17058	.831	1.013	6.1289
.8	6.85	8.18951	.836	1.029	6.7307
.9	6.69	8.05733	.830	1.079	7.0614
1.0	6.64	7.98563	.831	1.012	7.2073

because their contributions to the spin-wave frequencies are small.

The computer simulation results for the spin-wave dispersion curves are shown in Fig. 5.3. For those neighbours not included in the simulation the contributions were taken to be 0.8 of their contribution to the spin-wave frequencies in the non-diluted Ni_2MnSn. It was found that the frequencies obtained for the [00ζ] direction by using the three-neighbour simulation results plus 0.8 of the rest were not significantly different from those obtained by using the n.n. calculation plus 0.8 of the 2nd to 6th neighbour contributions. Therefore the three-neighbour calculation was not done for the other directions. The frequencies are shown in Fig. 5.3. The experimental data for the spin-wave dispersion curves in the diluted ferromagnet is in good agreement with the curves predicted by the computer simulation technique.

The computer simulation calculations can be compared to other theories. Fig. 5.6 shows n.n. frequency ratios in the [00ζ] direction for two spin-vacancy concentrations, $x = 0.2$ and $x = 0.3$. (The $x = 0.3$ results are presented in Table 5.5). Also plotted are the ratios for a n.n. CPA calculation using the method of L.A. Roth[41]. The calculation was performed by D.W. Taylor[54]. Resonant frequency shifts are evident for all sets of data. For $x = 0.2$, the CPA results agree very well with the simulation results but there is some discrepancy at

Fig. 5.6 Frequency ratios in the [00ζ] direction for a n.n. fcc lattice for two spin-vacancy concentrations, $x = 0.2$ and $x = 0.3$. The open circles or triangles are the computer simulation calculation results and the continuous lines are from a CPA calculation. The solid points are the results of a low q, high spin-concentration theory by Izyumov[55].

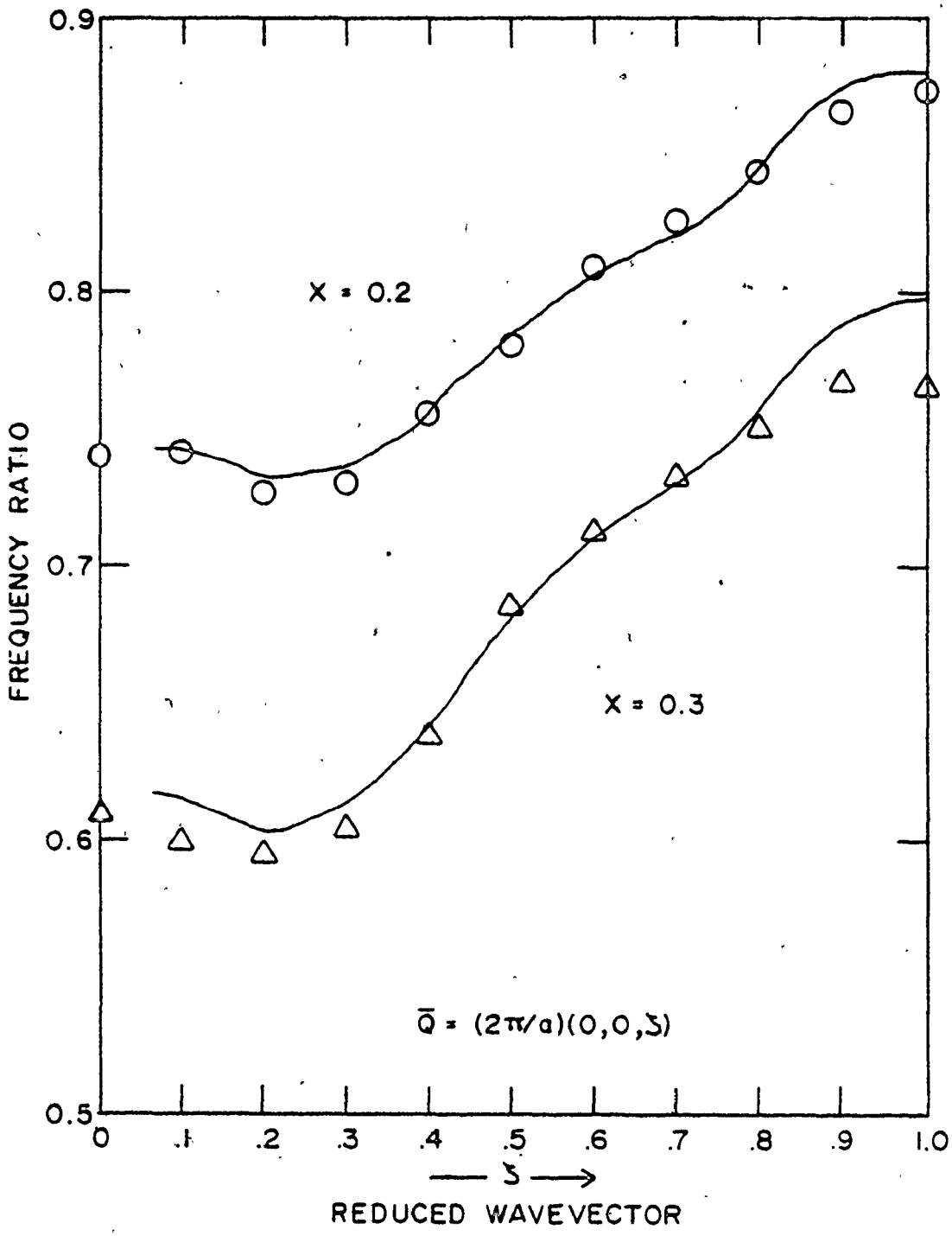
0.9
0.8
0.7
0.6
0.5
FREQUENCY RATIO
X = 0.2
X = 0.3
$\bar{Q} = (2\pi/a)(0,0,\zeta)$
0
.1
.2
.3
.4
.5
.6
.7
.8
.9
1.0
— ζ →
REDUCED WAVEVECTOR

Table 5.5 Spin-excitation frequencies in THz for a diluted fcc lattice with n.n. exchange interactions, from computer simulation calculations. The fraction of missing spins is $x = 0.3$ and the exchange constant is $J_1 = 0.0716$ THz. $\underline{q} = 2\pi/a\ (0,0,\zeta)$

reduced wavevector ζ	frequency ν	perfect crystal frequency ν_1	ratio ν/ν_1	width of response W
uncertainty:	±.5%		±.5%	±1%
0	0	0	--	.0935
.1	.0671	.11210	.599	.0940
.2	.260	.43744	.595	.1071
.3	.570	.94416	.604	.206
.4	1.010	1.58266	.638	.434
.5	1.569	2.29045	.685	.644
.6	2.13	2.99824	.712	.772
.7	2.66	3.63675	.732	.931
.8	3.11	4.14347	.750	1.044
.9	3.43	4.46880	.767	1.005
1.0	3.50	4.58091	.765	.966

low $\bar{q}$ for $x = 0.3$. In this region the computer simulation technique is least accurate. However an analytic theory by Izyumov[55], good at low spin-vacancy concentrations, calculates the zero frequency response at low $\bar{q}$ and gives $R = 0.740$ for $x = 0.2$ and $R = 0.610$ for $x = 0.3$. These points agree with an extrapolation of the computer simulation results to $\bar{q} = 0$.

The widths of the response for these calculations are plotted in Fig. 5.4(b), although there is no experimental data to compare. At large $\bar{q}$ the widths are large but at low $\bar{q}$ the widths approach the resolution of the program. In general the responses are wider for lower concentrations. The three neighbour calculations predict a wider response than the n.n. calculation, however the increase is small. The addition of n.n.n. and third n.n. ferromagnetic interactions does not increase the width by much but does increase the frequencies significantly. Therefore the relative width, W/ν, decreases tending to the virtual crystal or molecular field result of zero width. This is another indication that increasing the number of neighbours that interact causes the results to be more molecular field-like.

CHAPTER 6

CONCLUSIONS

The spin-wave dispersion in the 20% diluted ferromagnet, $Ni_2Mn_{0.8}V_{0.2}Sn$, has been measured at 93 K, by neutron inelastic scattering techniques, and corrected to 0 K. Excitations were observed only part way to the zone boundary because the efficiency of the analysing spectrometer was low for large energy transfers. The frequencies of the spin waves are reduced from those observed in Ni_2MnSn and the frequency shifts exhibit a resonant behaviour.

Frequencies for the diluted crystal have been calculated by numerical simulation on a large lattice, including full randomness in the large near-neighbour interactions, while the virtual crystal energies are used for further neighbour interactions. The experimental frequencies for $Ni_2Mn_{0.8}V_{0.2}Sn$ agree with the frequencies obtained in this manner.

To examine the resonance effect the ratio of the frequencies for the diluted to the non-diluted crystal is calculated as a function of $\vec{Q}$. The effect is more pronounced in the n.n. calculation than in a three-neighbour calculation. A careful examination of the data shows that the measured

frequency ratio shows more of a resonant effect than expected from the three-neighbour calculation. This result is not understood. One possible explanation is that the exchange interactions change with dilution, which could happen if, for example, the substitution of V for Mn changed the average conduction electron concentration. A shift in the relative magnitudes of the exchange constants would change the shape of the dispersion curves, conceivably in such a way as to resemble an increased resonant effect. However, because of the uncertainties in the model with respect to other sample characteristics, for example, chemical disorder, the Mn concentration and the temperature dependence of the dispersion, it is not possible to make any definite conclusions regarding the discrepancy. The answers lie in better experiments using a more suitable spectrometer. The dispersion should be measured over the complete Brillouin zone at liquid helium temperatures. Better characterization of the samples, possibly using a polarized neutron beam, would also be necessary.

The computer simulation technique for disordered crystals can be used to compare with other theories. The results agree very well with those from a CPA calculation. The technique also gives information about response shapes

and widths. It can easily be extended to include many neighbours for long-range interactions and is reasonable in terms of computer time and memory.

BIBLIOGRAPHY

1. R.A. Cowley and W.J.L. Buyers, Rev. Mod. Phys. 44, 406 (1972).
2. R.A. Cowley, AIP Conf. Proc. 29, 243 (1976).
3. C.C.M. Campbell and C.V. Stager, Can.J. Phys. 54, 2197 (1976).
4. Y. Noda and Y. Ishikawa, J. Phys. Soc. Japan 40, 690 (1976).
5. C.C.M. Campbell, J. Phys. F 5, 1931 (1975).
6. D.C. Price, J.D. Rush, C.E. Johnson and M.F. Thomas, J. de Physique, 37, C6-317 (1976).
7. P.J. Webster and R.S. Tebble, Phil. Mag. 16, 347 (1967).
8. P.J. Webster, Contemp. Phys. 10, 559 (1969).
9. Y. Ishikawa, K. Tajima and P. Radhakrishna, J.Phys. Soc. Japan 40, 1597 (1976).
10. P.J. Webster, J. Phys. Chem. Sol. 32, 1221 (1971).
11. M. Kawakami, Y. Yoshida, T. Nakamichi, S. Ishida and H. Enokiya, J. Phys. Soc. Japan 50, L1041 (1981).
12. K. Tajima, Y. Ishikawa, P.J. Webster, M.W. Stringfellow, D. Tocchetti and K.R.A. Zeabeck, J. Phys. Soc. Japan 43, 483 (1977).
13. M.A. Ruderman and C. Kittel, Phys. Rev. 96, 99 (1954).
14. T. Kasuya, Progr. Theor. Phys. 16, 45 (1956).
15. K. Yosida, Phys. Rev. 106, 893 (1957).
16. B. Caroli and A. Blandin, J. Phys. Chem. Solids 27, 503 (1966).
17. B. Caroli, J. Phys. Chem. Solids 28, 1427 (1967)
18. J. Friedel, Nuovo Cim. Suppl. 7, 287 (1958).

19. P.W. Anderson, Phys. Rev. 124, 41 (1961).

20. D.C. Price, J. Phys. F. 8, 933 (1978).

21. G. Malmström, D.J.W. Geldart and C. Blomberg, J.Phys. F. 6, 233 (1976a); 6, 1953 (1976b).

22. M.B. Stearns, J. Appl. Phys. 50, 2060 (1979).

23. J.R. Reitz and M.B. Stearns, J. Appl. Phys. 50, 2066 (1979).

24. P.J. Webster, J. Appl. Phys. 52, 2040 (1981).

25. P.J. Webster and M.R.I. Ramadam, J. Magn. Magn. Mat. 5, 51 (1977).

26. P.J. Webster and M.R.I. Ramadam, J. Magn. Magn. Mat. 13, 301 (1979).

27. S. Ishida, J. Ishida, S. Asano and J. Yamashita, J. Phys. Soc. Japan, 45, 1239 (1978).

28. S. Ishida, Y. Kubo, J. Ishida and J. Asano, J. Phys. Soc. Japan, 48, 814 (1980).

29. C.M. Hurd, I. Shiozaki, S.P. McAlister and C.V. Stager, J. Phys. F. 11 (1981), (in press).

30. K.J. Duff, V. Cannella, AIP Conf. Proc. 10, 541 (1972).

31. G.J. Coombs, R.A. Cowley, W.J.L. Buyers, E.C. Svensson, T.M. Holden and D.A. Jones, J. Phys. C 9, 2167 (1976).

32. P. Soven, Phys. Rev. 156, 809 (1967).

33. D.W. Taylor, Phys. Rev. 156, 1017 (1967).

34. W.J.L. Buyers, D.E. Pepper and R.J. Elliott, J. Phys. C. 5, 2611 (1972).

35. W.J.L. Buyers, D.E. Pepper and R.J. Elliott, J. Phys. C. 6, 1933 (1973).

36. R.A. Tahir-Kheli, Phys. Rev. B 6, 2809 (1972).

37. A.B. Harris, P.L. Leath, B.G. Nickel and R.J. Elliott, J. Phys. C 7, 1693 (1974).

38. B.G. Nickel, J. Phys. C 7, 1719 (1974).

39. A. Theuman and R.A. Tahir-Kheli, Phys. Rev. B 12, 1796, (1975).

40. R.A. Tahir-Kheli, T. Fujiwara and R.J. Elliott, J. Phys. C 11, 497 (1978).

41. L.M. Roth, J. Phys. C 12, 4879 (1979).

42. W. Butler and B. Nickel, Phys. Rev. Lett. 30, 373 (1973).

43. W.K. Holcomb and A.B. Harris, AIP Conf. Proc. 24, 402 (1975).

44. R. Alben and M.F. Thorpe, J. Phys. C 8, L275 (1975); AIP Conf. Proc. 29, 250 (1976); M.F. Thorpe and R. Alben, J. Phys. C 9, 2555 (1976).

45. R. Alben, S. Kirkpatrick and D. Beeman, Phys. Rev. B 15, 346 (1977).

46. B.N. Brockhouse, Proceedings of the Symposium on Inelastic Scattering of Neutrons in Solids and Liquids, 113 (1961).

47. B.N. Brockhouse, G.A. de Wit, E.D. Hallman and J.M. Rowe, Proceedings of the Symposium on Inelastic Scattering of Neutrons, 259 (1968).

48. M.J. Cooper and R. Nathans, Acta Cryst. 23, 357 (1967).

49. H.B. Callen, Phys. Rev. 130, 890 (1963).

50. F. Keffer, Handb. Phys. 18, 2 (1967).

51. Y. Noda and Y. Ishikawa, J. Phys. Soc. Japan 40, 699 (1976).

52. W. Marshall and S.W. Lovesey, Theory of Thermal Neutron Scattering, Oxford: Clarendon Press (1971).

53. F. Holstein and H. Primakoff, Phys. Rev. 58, 1908 (1940).

54. D.W. Taylor, Private communication.

55. Y. Izyumov, Proc. Phys. Soc. Lond. 87, 505 (1966).

APPENDIX

Program DILUTC

DILUTC is a computer program that calculates the scattering function, $S(\vec{Q},E)$, for a diluted, ferromagnetic lattice of spins which is fcc. The interaction between the spins is of the Heisenberg form and the program includes up to third n.n. interactions. This program description has been added to complete the discussion of the computer simulation technique given in Chapter 4. There are six sections to the appendix. Section A.1 introduces the arrays involved in calculating the $h_{i\vec{Q}}(t)$ and Section A.2 gives equations involving these arrays. Section A.3 describes how the array of spins is set up and indexed, Section A.4 is an outline of DILUTC and Section A.5 describes the variables and constants used in the time Fourier transform. The last section is a listing of the program.

A.1 The Arrays Involved in Calculating $h_{i\vec{Q}}(t)$

The array of spin sites has $\frac{N1}{2} \times \frac{N2}{2} \times \frac{N3}{2}$ fcc unit cells. If CC is the number of spin sites in the array then

$$CC = \frac{N1 \times N2 \times N3}{2} \qquad (A.1)$$

$h_{i\vec{Q}}$ is a complex number. Two complex arrays, G(I) and G1(I), of dimension CC are required in the program, one to contain

$h_{i\vec{Q}}(t)$ and the other to contain $h_{i\vec{Q}}(t+\Delta t)$. Another array, C(I), which is real and of dimension CC is required to contain the information as to whether or not a spin site is occupied. (In the program a spin site I is not occupied if C(I) contains the number 10000.0. If site I is occupied, then C(I) is used to contain additional information (see below).) Thus a total of $5 \times CC$ memory locations are required to contain these arrays. CC is usually $\sim$ 16000 so the required memory approaches the usable core memory limit of many computers. Both the computer memory and time required are directly proportional to the number of spins present in the array.

A.2 Equations Involving C(I), G(I) and G1(I)

For the program, eqn. (4.9) is written

$$\frac{dh_{i\vec{Q}}}{dt} = \frac{2}{\hbar}\left[\left(SJ1\cdot Z1_i + SJ2\cdot Z2_i + SJ3\cdot Z3_i - \frac{\hbar\omega'}{2}\right)\cdot h_{i\vec{Q}}\right.$$

$$\left. - SJ1\cdot \sum_{j_1} h_{j_1\vec{Q}} - SJ2\cdot \sum_{j_2} h_{j_2\vec{Q}} - SJ3\cdot \sum_{j_3} h_{j_3\vec{Q}}\right] . \qquad (A.2)$$

Here, SJ1, SJ2 and SJ3 are S times the exchange constant between a spin and its n.n.'s, n.n.n.'s and third n.n.'s respectively. $Z1_i$, $Z2_i$ and $Z3_i$ are the number of n.n.'s, n.n.n.'s and third n.n.'s to spin i that are present. The sums over j_1, j_2 and j_3 are sums over n.n. sites, n.n.n. sites and third n.n. sites. ω' is read into the program as a frequency, ENORMP, in THz such that

$$\omega' = 2\pi\cdot ENORMP\cdot 10^{12} . \qquad (A.3)$$

If we define

$$ENORPP = \hbar\pi \cdot ENORMP \cdot 10^{12} \qquad (A.4)$$

and let C(I) contain the information in the round brackets in eqn. (A.2) then

$$C(I) = \begin{cases} SJ1 \cdot Z1_i + SJ2 \cdot Z2_i + SJ3 \cdot Z3_i - ENORPP & \text{(magnetic site)} \\ 10000.0 & \text{(non-magnetic site)} \end{cases} \qquad (A.5)$$

The random lattice is set up and the C(I) array is calculated at the beginning of the program. The number, 10000.0, is arbitrary but large compared to the magnetic site values of C(I). SJ1, SJ2 and SJ3 are also in THz.

Let us assume that G(I) contains $h_{i\vec{Q}}(t-\Delta t)$, G1(I) contains $h_{i\vec{q}}(t)$ and G(I) will contain $h_{i\vec{Q}}(t+\Delta t)$. If the following complex constants are defined

$$F = 2/i\hbar \qquad (A.6a)$$

$$F1 = 2F \cdot \Delta t \qquad (A.6b)$$

$$F2 = F \cdot \Delta t \qquad (A.6c)$$

$$F3 = (F \cdot \Delta t)^2/2 \ , \qquad (A.6d)$$

then the integration formula to calculate $h_{i\vec{Q}}$, eqn. (4.5), becomes

$$G(I) = G(I) + F1 \cdot [C(I) \cdot G1(I) - SJ1 \cdot \sum_{j_1} G1(j_1) - SJ2 \cdot \sum_{j_2} G1(j_2) - SJ3 \cdot \sum_{j_3} G1(j_3)] \ . \qquad (A.7)$$

Note that if the site I is unoccupied then G(I) = Gl(I) = (0,0) for all time.

For the first time step, if G(I) contains $\frac{d^2 h_{i\vec{Q}}(0)}{dt^2}$, if Gl(I) contains $\frac{dh_{i\vec{Q}}(0)}{dt}$ and if G(I) is to contain $h_{i\vec{Q}}(\Delta t)$, then eqn. (4.6) becomes

$$G(I) = e^{i\vec{Q}\cdot\vec{R}(I)} + F2\cdot Gl(I) + F3\cdot G(I) \ . \qquad (A.8)$$

A.3 Indexing

Each site in the array is specified by giving either the indices J, K and L or the corresponding index, I. The one-dimensional arrays C(I), G(I) and Gl(I) can also be viewed as the three-dimensional matrices, C(J,K,L), G(J,K,L) and Gl(J,K,L). Both methods of indexing are used in the program, whichever is most convenient for the purpose. The transformation from J,K and L to I is

$$I = ((L-1)\cdot N2\cdot N1 + (K-1)\cdot N1 + J + 1)/2 \qquad (A.9)$$

where integer division is implied.

In the program, the one-dimensional array index must be determined for all neighbours of each site, I. The 12 n.n. indices are labeled I1, I2,...,I9,IA,IB, IC; the 6 n.n.n. indices are II1, II2, ..., II6; and the 24 third n.n. indices are III1, III2, ..., III0. The positions of the neighbours that correspond to these indices are given in Table A.1. The value of the indices for a given I can easily be obtained by adding or subtracting certain integers. For example, III1, the index

Table A.1

The location of neighbours to the spin at site I. A neighbour is located at the position $\frac{a}{2}(X\hat{x}+Y\hat{y}+Z\hat{z})$ from the site.

(a) nearest neighbours

	X	Y	Z
I1	1	1	0
I2	1	-1	0
I3	-1	1	0
I4	-1	-1	0
I5	1	0	1
I6	1	0	-1
I7	-1	0	1
I8	-1	0	-1
I9	0	1	1
IA	0	1	-1
IB	0	-1	1
IC	0	-1	-1

(b) next nearest neighbours

	X	Y	Z
II1	2	0	0
II2	-2	0	0
II3	0	2	0
II4	0	-2	0
II5	0	0	2
II6	0	0	-2

(c) third neighbours

	X	Y	Z
III1	1	1	2
III2	1	-1	2
III3	-1	1	2
III4	-1	-1	2
III5	1	1	-2
III6	1	-1	-2
III7	-1	1	-2
III8	-1	-1	-2
III9	1	2	1
IIIA	1	2	-1
IIIB	-1	2	1
IIIC	-1	2	-1
IIID	1	-2	1
IIIE	1	-2	-1
IIIF	-1	-2	1
IIIG	-1	-2	-1
IIIH	2	1	1
IIII	2	1	-1
IIIJ	2	-1	1
IIIK	2	-1	-1
IIIL	-2	1	1
IIIM	-2	1	-1
IIIN	-2	-1	1
IIIO	-2	-1	-1

of the third n.n. at $\frac{a}{2}(1,1,2)$ from the site I is given by

$$III1 = I + N1 \cdot N2 + N1/2 + 1 \qquad (A.10)$$

However, for sites near the boundaries of the array, the neighbours are not so easy to locate. For these points, the DO LOOPS are set up to make the necessary modifications to the indices. The modifications are organized in groups. For example, GROUP 2L (J=N1) is the group of modifications to the n.n.n. indices that occur when J = N1.

A.4 Program Outline

The following outline describes the function of the major blocks of code in DILUTC. Please refer to the program listing in section A.6.

Line	
1-89	Variables are dimensioned, data is read in and constants, defined in Section A.5, are calculated.
90-96	The random lattice is set up. A fraction X of the spins are removed using a random number generator. Sets C(I) = 10000.0 if site is non-magnetic.
97-113	This section insures that exactly X·CC spins are removed.
114-127	The exponentials are calculated, and the look-up table is created for determining $e^{i\vec{Q}\cdot\vec{R}_i}$.

Line

133-149 (a) $h_{i\vec{Q}}$ is put into G(I); i.e. sets

$$G(I) = \begin{cases} e^{i\vec{Q}\cdot\vec{R}_i} & \text{(magnetic site)} \\ 0 & \text{(non-magnetic site)} \end{cases}$$

(b) FT(1) is calculated where

$$FT(1) = \sum_i e^{-i\vec{Q}\cdot\vec{R}_i} \cdot e^{i\vec{Q}\cdot\vec{R}_i} = X.CC$$

150-572 This is a two-pass DO LOOP system. The program passes twice through the J,K,L DO LOOPS. On the first pass (IO = 1) the section

(a) sets C(I), for a magnetic site, to

$$C(I) = SJ1\cdot Z1(I)+SJ2\cdot Z2(I)+SJ3\cdot Z3(I)-ENORPP$$

(b) puts $\frac{dh_{i\vec{Q}}}{dt}$ into G1(I), i.e. sets

$$G1(I) = \begin{cases} \frac{dh_{i\vec{Q}}}{dt} & \text{(magnetic site)} \\ 0 & \text{(non-magnetic site)} \end{cases}$$

On the second pass (IO = 2) puts $\frac{d^2h_{i\vec{Q}}}{dt^2}$ into G(I), i.e. sets

$$G(I) = \begin{cases} \frac{d^2h_{i\vec{Q}}}{dt^2} & \text{(magnetic site)} \\ 0 & \text{(non-magnetic site)} \end{cases}$$

Line

573-591 Puts $h_{i\vec{Q}}(\Delta t)$ into G(I) and $h_{i\vec{Q}}(0)$ into Gl(I), i.e. sets

$$G(I) = \begin{cases} e^{i\vec{Q}\cdot\vec{R}_i} + F2\cdot Gl(I) + F3\cdot G(I) & \text{(magnetic site)} \\ 0 & \text{(non-magnetic site)} \end{cases}$$

and

$$Gl(I) = \begin{cases} e^{i\vec{Q}\cdot\vec{R}_i} & \text{(magnetic site)} \\ 0 & \text{(non-magnetic site)} \end{cases}$$

Calculates FT(2).

592-974 This is an alternating pass DO LOOP system. On odd passes (IK=1) $h_{i\vec{Q}}(t+\Delta t)$ is put into Gl(I), i.e. sets

$$Gl(I) = Gl(I) + F1\cdot[C(I)\cdot G(I) - SJ1\cdot \sum_{j_1} G(j_1)$$

$$- SJ2\cdot \sum_{j_2} G(j_2) - SJ3\cdot \sum_{j_3} G(j_3)] .$$

On even passes (IK = 2) $h_{i\vec{Q}}(t+\Delta t)$ is put into G(I). The contribution of $h_{i\vec{Q}}$ to FT(t) is calculated as soon as each new $h_{i\vec{Q}}$ is known .

975-988 If FLAG3 = 1, FT(t) is printed out. Note that

$$FT(t) = \sum_i e^{-i\vec{Q}\cdot\vec{R}_i} h_{i\vec{Q}}(t) .$$

989-998 FT(t) is multiplied by $e^{-\lambda t^2}$, $e^{-i\omega' t}$ and $e^{-i\text{EXPANDX}\cdot 10^{12}\cdot t}$

999-1021 Fast Fourier Transform (FFT) routine.

1022-1028 The program calculates $S(\vec{Q},E)$ for NCELLS arrays. This section calculates the average of $S(\vec{Q},E)$, given by

Line

AVSQ(I), over the arrays and the index of the maximum AVSQ(I) array element.

1029-1035 GFT(I) is loaded with the real part of the FFT integral, normalized by N, the total number of spins present. The variable FFFF is equal to N. The index of the maximum GFT(I) array element, IIT, is found.

1036-1045 Prints out GFT(I). GFT(I) contains the function s.t.

$$S(\vec{Q},E) = \frac{1}{\pi\hbar} GFT(\vec{Q},E) \ .$$

The frequency that corresponds to the index I, ENORM(I), in THz, is given by

$$ENORM(I) = DENORM\cdot(I-1)-EXPANDX \ .$$

1046-1056 Prints out $S(\vec{Q},E)$ averaged over NCELLS arrays.

1059-1073 A printer plot of $S(\vec{Q},E)$ is produced.

1074-end Plots of $S(\vec{Q},E)$ are produced. Curves for each of the arrays considered are plotted on the same graph. The average is plotted on another graph.

A.5 Definition of Variables and Constants

The purpose of the program is to obtain a graph of $S(\vec{Q},E)$ vs. E for a particular $\vec{Q}$. $S(\vec{Q},E)$ at a finite energy resolution is given by

$$S(\vec{Q},E) = \frac{1}{\pi N\hbar} \mathrm{Re} \int_0^T dt \exp(\frac{iEt}{\hbar}) [\sum_i e^{-i\vec{Q}\cdot\vec{R}_i} h_{i\vec{Q}}] \exp(-i\omega' t) \exp(-\lambda t^2) \quad . \tag{A.11}$$

Evaluating this integral is equivalent to taking the Fourier transform of the function F where

$$F = \begin{cases} 0 & (t < 0) \\ [\sum_i e^{-i\vec{Q}\cdot\vec{R}_i} h_{i\vec{Q}}] \exp(-i\omega' t) \exp(-\lambda t^2) & (0 \leq t < T) \\ 0 & (t \geq T) \quad . \end{cases} \tag{A.12}$$

The quantity in square brackets is calculated at finite time intervals in the first part of the program. In the second part of the program, this quantity is multiplied by the factors $\exp(-i\omega' t)$ and $\exp(-\lambda t^2)$ to obtain F which is Fourier transformed to obtain $S(\vec{Q},E)$.

A fast Fourier Transform (FFT) routine is used. It calculates the Fourier transforms.

$$X_{k+1} = \sum_{j=0}^{N-1} A_{j+1} e^{2\pi ijk/N} \qquad (k = 0,1,\cdots,N-1) \tag{A.13}$$

where A_{j+1} corresponds to F at the time $t = j\cdot\Delta t$ and X_{k+1} is the value of the Fourier transform of F at the frequency $\omega = 2\pi k/N\Delta T$. N is the number of times at which F is known.

(N ≡ IMAXP in DILUTC).

Referring to Fig. A.1(a), F is known at the times $t = 0, \Delta t, 2\Delta t, \cdots, (IMAXP-1)\Delta t$. The FFT routine is run for ICON time intervals. ICON is large to obtain a smooth Fourier transform spectrum. The values of F from $t = IMAXP \cdot \Delta t$ to $(ICON-1) \cdot \Delta t$ are set to zero. The frequency step in the spectrum is

$$\Delta\omega = \frac{2\pi}{ICON \cdot \Delta t} . \qquad (A.14)$$

A value for the Fourier transform is obtained at the frequencies $\omega = 0, \Delta\omega, \cdots, (ICON-1)\Delta\omega$, however, only part of this range is of interest because there is an upper frequency bound to the spin-waves as discussed below.

The upper frequency bound, EMAX, for the response of a diluted crystal corresponds to the maximum energy that a spin wave can have in the perfect crystal. For a crystal with ferromagnetic n.n., n.n.n. and third neighbour interactions the spin-wave at the zone boundary in the [111] direction has the largest energy which is given by

$$EMAX = 24 \cdot SJ1 + 24 \cdot SJ2 + 48 \cdot SJ3 . \qquad (A.15)$$

For this program the energies are specified by giving the corresponding frequencies in THz. Thus the SJ's and EMAX are in THz. Therefore, whenever $\hbar$ occurs with any of these, $\hbar$ must be expressed in THz.sec. i.e.

Fig. A.1 Series of graphs to illustrate the use of the Fast Fourier Transform routine to evaluate the integral in eqn. (A.11) for $S(\vec{Q},E)$. (a) F (eqn. A.12) is calculated at the times 0, Δt, $2\cdot\Delta t$, ..., $(IMAXP-1)\Delta t$. The values for the times $IMAXP\cdot\Delta t$ to $(ICON-1)\Delta t$ are set to zero to obtain more points in the Fourier transform plot. (b) The Fourier transform of F (proportional to $S(\vec{Q},E)$) is calculated at the angular frequencies, 0, $\Delta\omega$, $2\cdot\Delta\omega$, ..., $(ICON-1)\Delta\omega$. Only those transforms for ENORM = 0 to EMAX are physically meaningful. (c) The Fourier transform of F is calculated and plotted for a slightly extended range, ENORM = -EXPANDX to EMAX + EXPANDX to show any response beyond the physically meaningful limits which may arise due to the broadening function or numerical errors.

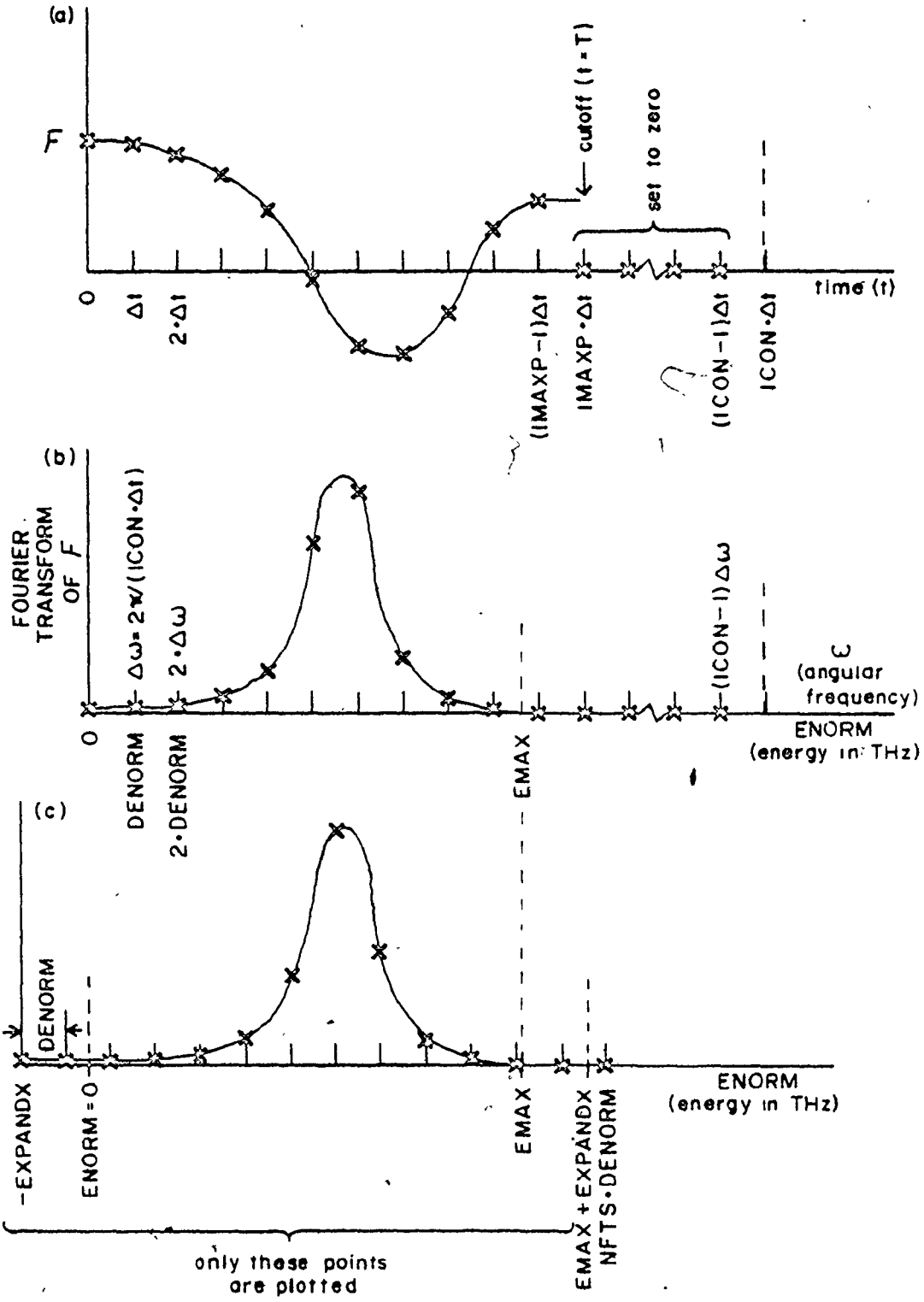
(a)
F
cutoff (I = T)
set to zero
time (t)
0
Δt
2·Δt
(IMAXP−1)Δt
IMAXP·Δt
(ICON−1)Δt
ICON·Δt
(b)
FOURIER TRANSFORM OF F
Δω = 2π/(ICON·Δt)
2·Δω
(ICON−1)Δω
ω (angular frequency)
0
DENORM
2·DENORM
EMAX
ENORM (energy in THz)
(c)
DENORM
-EXPANDX
ENORM = 0
EMAX
EMAX + EXPANDX
NFTS·DENORM
ENORM (energy in THz)
only these points are plotted

$$\text{HBAR} = \frac{1.05445\times10^{-27}\ \text{erg.sec.}}{1.60208\times10^{-12}\ \text{erg/eV}} \times 241.813\ \text{THz/eV} \ . \qquad (A.16)$$

This happens, for example, in eq. (A.2)

It is possible to express Δt (DELT in program) in terms of EMAX. Let NCMF (number of cycles of the maximum frequency) be the number of periods of the frequency EMAX which can occur in the time interval 0 to T. If NTSPC is the number of time steps per period, then the total number of times at which FT is known, IMAXP, can be written as

$$\text{IMAXP} = \text{NCMF}\cdot\text{NTSPC} \ . \qquad (A\text{-}17)$$

T is defined by

$$T = \text{IMAXP}\cdot\text{DELT} \ . \qquad (A.18)$$

From eqn. (4.7) it can be seen that

$$\text{DELT} = 1.0/(\text{NTSPC}\cdot\text{EMAX}\cdot1.0\text{E+12}) \ .$$

$S(\vec{Q},E)$ is plotted as a function of E in THz. Let ENORM be the energy in THz. If the step size in the response is DENORM, then from eqn. (A.14)

$$\text{DENORM} = \frac{\text{NTSPC}\cdot\text{EMAX}}{\text{ICON}} \ . \qquad (A.19)$$

So far the plot runs from ENORM = 0 to EMAX. However, because of the finite resolution and numerical errors, there may be some response for ENORM < 0 or ENORM > EMAX. It is therefore desirable

to expand the ENORM scale by a constant, EXPANDX, so that the energy runs from -EXPANDX to EMAX+EXPANDX. To shift from zero to -EXPANDX, FT must be multiplied by FSHIFT before being Fourier transformed where

$$\begin{aligned} \text{FSHIFT} &= \exp\{-2\pi i \cdot \text{EXPANDX} \cdot 10^{12} \cdot t\} \\ &= \text{CEXP}(Z2 \cdot 2.0 \cdot \text{EXPANDX} \cdot (I-1)/(\text{NTSPC} \cdot \text{EMAX})) \ . \end{aligned} \tag{A.20}$$

It is now apparent that the first Fourier transform, X_1, will be the value of the response at the energy -EXPANDX (see Fig. A.1(c)). For the plot to extend from -EXPANDX to EMAX+EXPANDX the number of transforms plotted, NFTS, must be

$$\begin{aligned} \text{NFTS} &= \frac{\text{EMAX}+2 \cdot \text{EXPANDX}}{\text{DENORM}} + 1 \\ &= \left[1 + \frac{2 \cdot \text{EXPANDX}}{\text{EMAX}}\right] \cdot \frac{\text{ICON}}{\text{NTSPC}} + 1 \ . \end{aligned} \tag{A.21}$$

Now we come to the other factors in eqn. (A.12) that FT must be multiplied by to obtain F. The first is $\exp(-i\omega' t)$. Since $t = (I-1) \cdot \text{DELT}$ and $\omega' = 2\pi \cdot \text{ENORMP}$ then

$$\begin{aligned} \text{FSHIFF} \equiv e^{-i\omega' t} &= \exp(-2\pi i \cdot \text{ENORMP} \cdot (I-1) \cdot \text{DELT}) \\ &= \text{CEXP}(Z2 \cdot 2.0 \cdot \text{ENORMP} \cdot (I-1)/(\text{NTSPC EMAX})) \ . \end{aligned} \tag{A.22}$$

Finally, there is the Gaussian apodization factor, $\exp(-\lambda t^2)$. The Fourier transform of $e^{-\lambda t^2}$ is proportional to $e^{-\omega^2/4\lambda}$. The FWHM of this function is

$$\text{FWHM} = 2\sqrt{4\lambda(-\ell n\ 0.5)} = 3.3302184\sqrt{\lambda}\ . \qquad \text{(A.23)}$$

For the FWHM to be $\sim$ 2% EMAX then

$$\lambda \equiv \text{APDC} = (\pi \cdot \text{EMAX} \cdot 10.\text{E+12}/(25.0 \cdot 3.3302184))^2 \qquad \text{(A.24)}$$

FT is then multiplied by $\text{EXP}(-\text{APDC} \cdot T^2)$ where $T = (I-1) \cdot \text{DELT}$.

A.6 Program Listing

```
      PROGRAM DIELEC (INPUT,OUTPUT,PLOT,TAPE5=INPUT,TAPE6=OUTPUT)

C     DIMENSION GFT(NFTS),ENORM(NFTS),AVSQ(NFTS)
      DIMENSION GFT(498),ENORM(498),AVSQ(498)
C     PLOT VARIABLES
      DIMENSION GF(100),FFF(5)
      DIMENSION FORM(5),FORMA(2),QMAT(3)
      INTEGER A,B,BB,CC
      COMPLEX F,F1,F2,F3,Z1,Z2,FSHIFT,FSHIFF

C     COMPLEX FT(IMAXF)
      COMPLEX FT(500)

      COMPLEX EZY,EZYCC
C     COMPLEX EX(N1),EXCC(N1),EY(N2),EYCC(N2),EZ(N3),EZCC(N3)
      COMPLEX EX(52),EXCC(52),EY(52),EYCC(52),EZ(52),EZCC(52)

C     DIMENSION C(CC),D(42)
      DIMENSION C(15840),D(42)
C     COMPLEX G1(I),G(I) WHERE I=MAX(CC,ICON)
      COMPLEX G(15840),G1(15840)
      READ (5,202) NCELLS
  202 FORMAT (I1)
      DO 203 LIFT=1,NCELLS
      READ (5,200) N1,N2,N3,NGX,NGY,NGZ, ISPC,NCNF,ISEED,FLAG1,FLAG2,X,E
     1XPANDX,ENORMP
  200 FORMAT (5I2,I10,5F4.1)
      WRITE (6,300) N1,N2,N3, NGX,NGY,NGZ
  300 FORMAT (1X,5HN1 = ,I2,7H  N2 = ,I2,7H  N3 = ,I2,8H  NGX = ,I2,8H
     1NGY = ,I2,8H  NGZ = ,I2)
      WRITE (6,301) ISPC,NCNF,ISEED,FLAG1,FLAG2,EXPANDX,ENORMP
  301 FORMAT (1X,8HNISPC = ,I2,9H  NCNF = ,I2,10H  ISEED = ,I10,10H  FLA
     1G1 = ,F4.1,10H  FLAG2 = ,F4.1,12H  EXPANDX = ,F4.1,11H  ENORMP = ,
     2F4.1)
      RN1=NGX
      RN2=NGY
      RN3=NGZ
      QMAT(1)=RN1/N1*2.0
      QMAT(2)=RN2/N2*2.0
      QMAT(3)=RN3/N3*2.0
      WRITE (6,302) QMAT(1),QMAT(2),QMAT(3)
  302 FORMAT (1X,12HQ = (2PI/A)(,F8.5,1H,,F8.5,1H,,F8.5,1H))
      WRITE (6,303) X
  303 FORMAT (1X,4HX = ,F4.1)
C     PROGRAM REQUIRES SJ=5 I.E. THZ
      S=2.0
      SJ1=5*0.696*0.241813
      SJ2=5*0.283*0.241813
      SJ3=5*0.110*0.241813
      EMAX=24.0*SJ1+24.0*SJ2+48.0*SJ3
      PI=4.0*ATAN(1.0)
      HBAR=1.05445E-27*241.813/1.6020E-12
      ICON=4096

      NFTS=(1.0+2.0*EXPANDX/EMAX)*ICON/NTSPC+1
      WRITE (6,305) NFTS
  305 FORMAT (1X,7HNFTS = ,I4)
```

```
      IF(LIFT.NE.1) GO TO 1204
      DO 204 I=1,NFTS
60    AVSG(I)=0.0
  204 CONTINUE
 1204 CONTINUE
      EMAX=ENMF*NTSPC/2
      EMAXP=ENMF*NTSPC
      DELT=1.0/(NTSPC*EMAX*1.0E+12)
      APOC=(PI*EMAX*1.0E+12/(25.0*3.3302184))**2
      DENORM=NTSPC*EMAX/ICOL
      ENORMP=PI*ENORMP*1.0E+12*HBAR
      WRITE (6,306) SJ1,SJ2,SJ3,EMAX,ENORMP
70  306 FORMAT (1X,6HSJ1 = ,E12.5,8H  SJ2 = ,E12.5,8H  SJ3 = ,E12.5,9H  EM
     1AX = ,E12.5,11H  ENORMP = ,E12.5)
      WRITE (6,304) EMAXP,DELT,APOC,DENORM
  304 FORMAT (1X,8HEMAXP = ,I4,9H  DELT = ,E17.10,9H  APOC = ,E17.10,11H
     1  DENORM = ,E17.10)
75    F=2.0/((0.0+1.0)*HBAR)
      F1=F*DELT*2.0
      F2=DELT*F
      F3=(DELT*F)**2/2.0
      A=N1/2
80    B=N1*N2/2
      BB=N1*N2
      CC=N1*N2*N3/2
      L1=A*B
      L2=A-B
85    L3=B-CC
      L6=A-1
      L7=BB-CC
      L8=N1-B

90    CALL RANSET(ISEED)
      DO 8 I=1,CC
      C(I)=10000.0
      YFL=RANF(ISEED)
      IF (YFL.GT.X) C(I)=1.0
95    IF (YFL.GT.X) ADD=ADD+1.0
    8 CONTINUE
C     TO ENSURE THAT THE FRACTION OF SPINS MISSING IS EXACTLY X
      NETTLE=CC*(1.0-X)-ADD
      IF (NETTLE) 2,3,4
100   2 NICKLE=-NETTLE
      DO 6 NUCKLE=1,NICKLE
    5 LUCK=RANF(ISEED)*CC
      IF (C(LUCK).NE.1.0) GO TO 5
      C(LUCK)=0.1
105   6 CONTINUE
      GO TO 3
    4 DO 7 NUCKLE=1,NETTLE
    1 LUCK=RANF(ISEED)*CC
      IF (C(LUCK).NE.0.1) GO TO 1
      C(LUCK)=1.0
    7 CONTINUE
    3 CONTINUE

      Z1=CMPLX(0.0,PI)
```

```
      ZZ=CMPLX(0.0,-PI)
      DO 9 I=1,N1
      EX(I)=CEXP(Z1*2.0*I*NDX/N1)
      EXCC(I)=CEXP(ZZ*2.0*I*NDX/N1)
    9 CONTINUE
      DO 10 I=1,N2
      EY(I)=CEXP(Z1*2.0*I*NDY/N2)
      EYCC(I)=CEXP(ZZ*2.0*I*NDY/N2)
   10 CONTINUE
      DO 11 I=1,N3
      EZ(I)=CEXP(Z1*2.0*I*NDZ/N3)
      EZCC(I)=CEXP(ZZ*2.0*I*NDZ/N3)
   11 CONTINUE

      DO 12 I=1,IMAXP
      FT(I)=(0.0,0.0)
   12 CONTINUE

      I=0
      DO 14 L=1,N3
      DO 14 K=1,N2
      EZY=EZ(L)*EY(K)
      EZYCC=EZCC(L)*EYCC(K)
      KP=L+K
      KC=1.5+(-1.0)**KP/2.0
      DO 14 J=KC,N1,2
      I=I+1
      IF (G(I).NE.10000.0) GO TO 114
      G(I)=(0.0,0.0)
      GO TO 14
  114 G(I)=EZY*EX(J)
      FT(I)=FT(I)+G(I)*EZYCC*EXCC(J)
   14 CONTINUE


      DO 31 I0=1,2
      I=0
      DO 30 L=1,N3
      IF (L-2) 15,16,17

C     GROUP 1A (L=1)
   15 IA5=IA7=IA9=IAB=0
      IA6=IA8=IAA=IAC=-L3

C     GROUP 2A (L=1)
      IIA1=BB
      IIA2=-L7

C     GROUP 3A (L=1)
      IIIA1=IIIA2=IIIA3=IIIA4=BB
      IIIA5=IIIA6=IIIA7=IIIA8=-L7
      IIIA9=IIIAB=IIIAD=IIIAF=IIIAH=IIIAJ=IIIAL=IIIAN=0
      IIIAA=IIIAC=IIIAE=IIIAG=IIIAI=IIIAK=IIIAM=IIIAO=-L3
      GO TO 18

C     GROUP 1B (L=2)
   16 IA6=IA8=IAA=IAC=-M
```

```
C     GROUP 3B (L=2)
      IIIAA=IIIAC=IIIAL=IIIAG=IIIAI=IIIAF=IIIAM=IIIAC=-B
175   GO TO 18
   17 IF (L.NE.3) GO TO 115

C     GROUP 2B (L=3)
      IIA2=-BB
180
C     GROUP 3C (L=3)
      IIIA5=IIIA6=IIIA7=IIIA8=-BB
      GO TO 18
  115 IF (L-N3+1) 18,116,117
185
C     GROUP 2C (L=N3-1)
  116 IIA1=L7

C     GROUP 3D (L=N3-1)
190   IIIA1=IIIA2=IIIA3=IIIA4=L7
      GO TO 18

C     GROUP 1C (L=N3)
  117 IA5=IA7=IA9=IAB=L3
195
C     GROUP 3E (L=N3)
      IIIA9=IIIAB=IIIAD=IIIAF=IIIAH=IIIAJ=IIIAL=IIIAN=L3

   18 DO 29 K=1,2
200   K0=1.5+(-1.0)**(L+K)/2.0
      IF (K-2) 19,20,21

C     GROUP 1D (K=1)
   19 IB1=A
205   IB2=-L2
      IB3=A
      IB4=-L2
      IB5=IA9+A
      IBA=IAA+A
210   IB6=IAB-L2
      IBC=IAC-L2

C     GROUP 2D (K=1)
      IIB3=N1
215   IIB4=-L8

C     GROUP 3F (K=1)
      IIIB1=IIIA1+A
      IIIB2=IIIA2-L2
220   IIIB3=IIIA3+A
      IIIB4=IIIA4-L2
      IIIB5=IIIA5+A
      IIIB6=IIIA6-L2
      IIIB7=IIIA7+A
225   IIIB8=IIIA8-L2
      IIIB9=IIIA9+N1
      IIIBA=IIIAA+N1
      IIIBC=IIIAB+N1
```

```
                IIIBC=IIIAC+N1
230             IIIBD=IIIAD-L8
                IIIBE=IIIAE-L8
                IIIBF=IIIAF-L8
                IIIBG=IIIAG-L8
                IIIBH=IIIAH+A
235             IIIBI=IIIAI+A
                IIIBJ=IIIAJ-L2
                IIIBK=IIIAK-L2
                IIIBL=IIIAL+A
                IIIBM=IIIAM+A
240             IIIBN=IIIAN-L2
                IIIBO=IIIAO-L2
                GO TO 22

          C     GROUP 1E (K=2)
245          20 IB2=-A
                IB4=-A
                IB6=IAB-A
                IBC=IAC-A

250       C     GROUP 3G (K=2)
                IIIB2=IIIA2-A
                IIIB4=IIIA4-A
                IIIB6=IIIA6-A
                IIIB8=IIIAB-A
255             IIIBJ=IIIAJ-A
                IIIBK=IIIAK-A
                IIIBL=IIIAL-A
                IIIBO=IIIAO-A
                GO TO 22
260          21 IF (K.NE.3) GO TO 118

          C     GROUP 2E (K=3)
                IIB4=-N1

265       C     GROUP 3H (K=3)
                IIIBD=IIIAD-N1
                IIIBE=IIIAE-N1
                IIIBF=IIIAF-N1
                IIIBG=IIIAG-N1
270             GO TO 22
             118 IF (K-N2+1) 22,120,121

          C     GROUP 2F (K=N2-1)
             120 IIB3=L8

275       C     GROUP 3I (K=N2-1)
                IIIB9=IIIA9+L8
                IIIBA=IIIAA+L8
                IIIBB=IIIAB+L8
280             IIIBC=IIIAC+L8
                GO TO 22

          C     GROUP 1F (K=N2)
             121 IB1=L2
285             IB3=L2
```

```
                IC9=IA9+L2
                ICA=IAA+L2
      C         GROUP 3J (K=N2)
  290           III01=III1+L2
                III03=III3+L2
                III05=III5+L2
                III07=III7+L2
                III0H=III+L2
  295           III0I=III1+L2
                III0L=III+L2
                III0N=III+L2
             22 DO 28 J=KO,N1,2
  300           I=I+1
                IF (KO-2) 122,123
            122 IF (J-3) 23,24,25
      C         GROUP 1G (J=1)
  305        23 IC1=IB1
                IC2=IB2
                IC3=IB3+L6
                IC4=IB4+L6
                IC5=IA5
  310           IC6=IA6
                IC7=IA7+L6
                IC8=IA8+L6
      C         GROUP 2G (J=1)
  315           III5=1
                III6=L6
      C         GROUP 3K (J=1)
                III1=III1
  320           III2=III2
                III3=III3+L6
                III4=III4+L6
                III5=III5
                III6=III6
  325           III7=III7+L6
                III8=III8+L6
                III9=III9
                IIIA=IIIA
                III8=III8+L6
  330           III0=III0+L6
                III0=III0
                III1=III1
                III2=III2+L6
                III3=III3+L6
  335           III4=III4+1
                III1=III1+1
                III1=III1+1
                III1=III1+1
                III1=III1+L6
  340           III1=III1+L6
                III1=III1+L6
                III1=III1+L6
```

```
                GO TO 27
345         C   GROUP 1I (J=3)
           24   IC3=IB3-1
                IC4=IB4-1
                IC7=IA7-1
                IC8=IA8-1
350
            C   GROUP 2I (J=3)
                IIC6=-1

            C   GROUP 3M (J=3)
355             IIIC3=IIIB3-1
                IIIC4=IIIB4-1
                IIIC7=IIIB7-1
                IIIC8=IIIB8-1
                IIIC9=IIIB9-1
360             IIICC=IIIBC-1
                IIICF=IIIBF-1
                IIIC6=IIIB6-1
                IIICL=IIIBL-1
                IIICM=IIIBM-1
365             IIICN=IIIBN-1
                IIICO=IIIBO-1
                GO TO 27
           25   IF (J.NE.N1-1) GO TO 27
370         C   GROUP 2K (J=N1-1)
                IIC5=-L6

            C   GROUP 3O (J=N1-1)
                IIICH=IIIBH-L6
375             IIIC1=IIIB1-L6
                IIICJ=IIIBJ-L6
                IIICK=IIIBK-L6
                GO TO 27
          123   IF (J-4) 124,125,126
380
            C   GROUP 1H (J=2)
          124   IC1=IB1+1
                IC2=IB2+1
                IC3=IB3
385             IC4=IB4
                IC5=IA5+1
                IC6=IA6+1
                IC7=IA7
                IC8=IA8
390
            C   GROUP 2H (J=2)
                IIC5=1
                IIC6=L6

395         C   GROUP 3L (J=2)
                IIIC1=IIIB1+1
                IIIC2=IIIB2+1
                IIIC3=IIIB3
                IIIC4=IIIB4
```

```
400               IIIC5=III+5+1
                  IIIC6=III+6+1
                  IIIC7=III+7
                  IIIC8=III+8
                  IIIC9=III+9+1
405               IIICA=III+A+1
                  IIICB=III+B
                  IIICC=III+C
                  IIICD=III+D+1
                  IIICE=III+E+1
410               IIICF=III+F
                  IIIC6=III+6
                  IIICH=III+H+1
                  IIIC1=III+1+1
                  IIICJ=III+J+1
415               IIICK=III+K+1
                  IIICL=III+L+L6
                  IIICM=III+M+L6
                  IIICN=III+N+L6
                  IIICO=III+O+L6
420               GO TO 27

C     GROUP 2J (J=4)
  125 IIC6=-1

425   C     GROUP 3M (J=4)
            IIICL=III+L-1
            IIICM=III+M-1
            IIICN=III+N-1
            IIICO=III+O-1
430         GO TO 27
  126 IF (J.NE.N1) GO TO 27

C     GROUP 1J (J=N1)
      IC1=IA1-L6
435   IC2=IA2-L6
      IC5=IA5-L6
      IC6=IA6-L6

C     GROUP 2L (J=N1)
440   IIC5=-L6

C     GROUP 3P (J=N1)
      IIIC1=III+1-L6
      IIIC2=III+2-L6
445   IIIC5=III+5-L6
      IIIC6=III+6-L6
      IIIC9=III+9-L6
      IIICA=III+A-L6
      IIICD=III+D-L6
450   IIICE=III+E-L6
      IIICM=III+M-L6
      IIICI=III+I-L6
      IIICJ=III+J-L6
      IIICK=III+K-L6
455
   27 II=I+IC1
```

```
      I2=I+IC2
      I3=I+IC3
      I4=I+IC4
460   I5=I+IC5
      I6=I+IC6
      I7=I+IC7
      I8=I+IC8
      I9=I+IC9
465   IA=I+ICA
      IB=I+ICB
      IC=I+ICC

      II1=I+IIA1
470   II2=I+IIA2
      II3=I+IIB3
      II4=I+IIB4
      II5=I+IIC5
      II6=I+IIC6
475
      III1=I+IIIC1
      III2=I+IIIC2
      III3=I+IIIC3
      III4=I+IIIC4
480   III5=I+IIIC5
      III6=I+IIIC6
      III7=I+IIIC7
      III8=I+IIIC8
      III9=I+IIIC9
485   IIIA=I+IIICA
      IIIB=I+IIICB
      IIIC=I+IIICC
      IIID=I+IIICD
      IIIE=I+IIICE
490   IIIF=I+IIICF
      IIIG=I+IIICG
      IIIH=I+IIICH
      IIII=I+IIICI
      IIIJ=I+IIICJ
495   IIIK=I+IIICK
      IIIL=I+IIICL
      IIIM=I+IIICM
      IIIN=I+IIICN
      IIIO=I+IIICO
500   IF (IO.EQ.2) GO TO 130
      DO 127 IJ=1,42
      D(IJ)=0.0
  127 CONTINUE
      IF (C(I).EQ.10000.0) GO TO 128
505   IF (C(I1).NE.10000.0) D(1)=1.0
      IF (C(I2).NE.10000.0) D(2)=1.0
      IF (C(I3).NE.10000.0) D(3)=1.0
      IF (C(I4).NE.10000.0) D(4)=1.0
      IF (C(I5).NE.10000.0) D(5)=1.0
510   IF (C(I6).NE.10000.0) D(6)=1.0
      IF (C(I7).NE.10000.0) D(7)=1.0
      IF (C(I8).NE.10000.0) D(8)=1.0
      IF (C(I9).NE.10000.0) D(9)=1.0
```

```
      IF (C(1A).NE.10000.0) D(10)=1.0
      IF (C(1B).NE.10000.0) D(11)=1.0
      IF (C(1C).NE.10000.0) D(12)=1.0
      IF (C(II1).NE.10000.0) D(13)=1.0
      IF (C(II2).NE.10000.0) D(14)=1.0
      IF (C(II3).NE.10000.0) D(15)=1.0
      IF (C(II4).NE.10000.0) D(16)=1.0
      IF (C(II5).NE.10000.0) D(17)=1.0
      IF (C(II6).NE.10000.0) D(18)=1.0
      IF (C(III1).NE.10000.0) D(19)=1.0
      IF (C(III2).NE.10000.0) D(20)=1.0
      IF (C(III3).NE.10000.0) D(21)=1.0
      IF (C(III4).NE.10000.0) D(22)=1.0
      IF (C(III5).NE.10000.0) D(23)=1.0
      IF (C(III6).NE.10000.0) D(24)=1.0
      IF (C(III7).NE.10000.0) D(25)=1.0
      IF (C(III8).NE.10000.0) D(26)=1.0
      IF (C(III9).NE.10000.0) D(27)=1.0
      IF (C(IIIA).NE.10000.0) D(28)=1.0
      IF (C(IIIB).NE.10000.0) D(29)=1.0
      IF (C(IIIC).NE.10000.0) D(30)=1.0
      IF (C(IIID).NE.10000.0) D(31)=1.0
      IF (C(IIIE).NE.10000.0) D(32)=1.0
      IF (C(IIIF).NE.10000.0) D(33)=1.0
      IF (C(IIIG).NE.10000.0) D(34)=1.0
      IF (C(IIIH).NE.10000.0) D(35)=1.0
      IF (C(IIII).NE.10000.0) D(36)=1.0
      IF (C(IIIJ).NE.10000.0) D(37)=1.0
      IF (C(IIIK).NE.10000.0) D(38)=1.0
      IF (C(IIIL).NE.10000.0) D(39)=1.0
      IF (C(IIIM).NE.10000.0) D(40)=1.0
      IF (C(IIIN).NE.10000.0) D(41)=1.0
      IF (C(IIIO).NE.10000.0) D(42)=1.0
      C(I)=SJ1*(D(1)+D(2)+D(3)+D(4)+D(5)+D(6)+D(7)+D(8)+D(9)+D(10)+D(11)
     1+D(12))+SJ2*(D(13)+D(14)+D(15)+D(16)+D(17)+D(18))+SJ3*(D(19)+D(20)
     2+D(21)+D(22)+D(23)+D(24)+D(25)+D(26)+D(27)+D(28)+D(29)+D(30)+D(31)
     3+D(32)+D(33)+D(34)+D(35)+D(36)+D(37)+D(38)+D(39)+D(40)+D(41)+D(42)
     4)-ENORPP
      G1(I)=C(I)*G(I)-SJ1*(G(I1)+G(I2)+G(I3)+G(I4)+G(I5)+G(I6)+G(I7)+G(I
     18)+G(I9)+G(IA)+G(IB)+G(IC))-SJ2*(G(III)+G(II2)+G(II3)+G(II4)+G(II5
     2)+G(II6))-SJ3*(G(III1)+G(III2)+G(III3)+G(III4)+G(III5)+G(III6)+G(I
     3II7)+G(III8)+G(III9)+G(IIIA)+G(IIIB)+G(IIIC)+G(IIID)+G(IIIE)+G(III
     4F)+G(IIIG)+G(IIIH)+G(IIII)+G(IIIJ)+G(IIIK)+G(IIIL)+G(IIIM)+G(IIIO)
     5+G(IIIO))
      GO TO 28
  128 G1(I)=(0.0,0.0)
      GO TO 28
  130 IF (C(I).EQ.10000.0) GO TO 28
      G(I)=C(I)*G1(I)-SJ1*(G1(I1)+G1(I2)+G1(I3)+G1(I4)+G1(I5)+G1(I6)+G1(
     1I7)+G1(I8)+G1(I9)+G1(IA)+G1(IB)+G1(IC))-SJ2*(G1(III)+G1(II2)+G1(II
     23)+G1(II4)+G1(II5)+G1(II6))-SJ3*(G1(III1)+G1(III2)+G1(III3)+G1(III
     34)+G1(III5)+G1(III6)+G1(III7)+G1(III8)+G1(III9)+C1(IIIA)+G1(IIIB)+
     4G1(IIIC)+G1(IIID)+G1(IIIE)+G1(IIIF)+G1(IIIG)+G1(IIIH)+G1(IIII)+G1(
     5IIIJ)+G1(IIIK)+G1(IIIL)+G1(IIIM)+G1(IIIN)+G1(IIIO))
   26 CONTINUE
   29 CONTINUE
   30 CONTINUE
```

```
   31 CONTINUE

      I=0
      DO 34 L=1,N3
575   DO 34 K=1,N2
      EZY=EZ(L)*EY(K)
      EZYCC=EZCC(L)*EYCC(K)
      KP=K+L
      KC=1.5+(-1.0)**KP/2.0
580   DO 34 J=NO,N1,2
      I=I+1
      IF (G(I).EQ.10000.0) GO TO 34
      G(I)=F3*G(I)+F2*G1(I)+EZY*EX(J)
      FT(2)=FT(2)+G(I)*EZYCC*EXCC(J)
585   G1(I)=EZY*EX(J)
   34 CONTINUE


      R=XTIME(1)
590   WRITE (6,666) R
  666 FORMAT (1X,16HCPU TIME USED = ,F10.5)
      DO 52 II=2,IMAX
      DO 51 IK=1,2
      IE=2*II+IK-2
595   I=0

      DO 50 L=1,L3
      IF (L-2) 35,36,37

600   C     GROUP 1A (L=1)
   35 IA5=IA7=IA9=IAB=8
      IA6=IA8=IAA=IAC=-L3

      C     GROUP 2A (L=1)
605   IIA1=BB
      IIA2=-L7

      C     GROUP 3A (L=1)
      IIIA1=IIIA2=IIIA3=IIIA4=88
610   IIIA5=IIIA6=IIIA7=IIIA8=-L7
      IIIA9=IIIAB=IIIAD=IIIAF=IIIAH=IIIAJ=IIIAL=IIIAN=8
      IIIAA=IIIAC=IIIAE=IIIAG=IIIAI=IIIAK=IIIAM=IIIAO=-L3
      GO TO 38

615   C     GROUP 1B (L=2)
   36 IA6=IA8=IAA=IAC=-8


      IIIAA=IIIAC=IIIAE=IIIAG=IIIAI=IIIAK=IIIAM=IIIAO=-8
620   GO TO 38
   37 IF (L.NE.3) GO TO 135

      C     GROUP 2B (L=3)
      IIA2=-88
625
      C     GROUP 3C (L=3)
      IIIA5=IIIA6=IIIA7=IIIA8=-88
```

```
                GO TO 38
  135 IF (L-N3+1) 38,136,137
630
C       GROUP 2C (L=N3-1)
  136 IIA1=L7

635         IIIA1=IIIA2=IIIA3=IIIA4=L7
            GO TO 38

C       GROUP 1C (L=N3)
  137 IA5=IA7=IA9=IAB=L3
640
C       GROUP 3E (L=N3)
            IIIA9=IIIAB=IIIAD=IIIAF=IIIAH=IIIAJ=IIIAL=IIIAN=L3

   38 DO 49 K=1,N2
645         EZYCC=EZCC(L)*EYCC(K)
            KP=L+K
            KQ=1.5+(-1.0)**KP/2.0
            IF (K-2) 39,40,41

650 C       GROUP 1D (K=1)
   39 IB1=A
            IB2=-L2
            IB3=A
            IB4=-L2
655         IB9=IA9+A
            IBA=IAA+A
            IBB=IAB-L2
            IBC=IAC-L2

660 C       GROUP 2D (K=1)
            IIB3=N1
            IIB4=-L8

C       GROUP 3F (K=1)
665         IIIB1=IIIA1+A
            IIIB2=IIIA2-L2
            IIIB3=IIIA3+A
            IIIB4=IIIA4-L2
            IIIB5=IIIA5+A
670         IIIB6=IIIA6-L2
            IIIB7=IIIA7+A
            IIIB8=IIIA8-L2
            IIIB9=IIIA9+N1
            IIIBA=IIIAA+N1
675         IIIBB=IIIAB+N1
            IIIBC=IIIAC+N1
            IIIBD=IIIAD-L8
            IIIBE=IIIAE-L8
            IIIBF=IIIAF-L8
680         IIIBG=IIIAG-L8
            IIIBH=IIIAH+A
            IIIBI=IIIAI+A
            IIIBJ=IIIAJ-L2
            IIIBK=IIIAK-L2
```

```
685               IIIBL=IIIAL+A
                  IIIBM=IIIAM+A
                  IIIBN=IIIAN-L2
                  IIIBO=IIIAO-L2
                  GO TO 42
690
                C     GROUP 1E (K=2)
                40 IB2=-A
                  IB4=-A
                  IBB=IAB-A
695               IBC=IAC+A

                C     GROUP 3G (K=2)
                  IIIB2=IIIA2-A
                  IIIB4=IIIA4+A
700               IIIB6=IIIA6-A
                  IIIB8=IIIA8-A
                  IIIBJ=IIIAJ-A
                  IIIBK=IIIAK-A
                  IIIBN=IIIAN-A
705               IIIBO=IIIAO-A
                  GO TO 42
                41 IF (K.NE.3) GO TO 136

                C     GROUP 2E (K=3)
710               IIB4=-N1

                C     GROUP 3H (K=3)
                  IIIBO=IIIAO-N1
                  IIIBE=IIIAE-N1
715               IIIBF=IIIAF-N1
                  IIIBG=IIIAG-N1
                  GO TO 42
                136 IF (K-N2+1) 42,140,141

720             C     GROUP 2F (K=N2-1)
                140 IIB3=L8

                C     GROUP 3I (K=N2-1)
                  IIIB9=IIIA9+L8
725               IIIBA=IIIAA+L8
                  IIIBB=IIIAB+L8
                  IIIBC=IIIAC+L8
                  GO TO 42

730             C     GROUP 1F (K=N2)
                141 IB1=L2
                  IB3=L2
                  IB9=IA9+L2
                  IBA=IAA+L2
735
                C     GROUP 3J (K=N2)
                  IIIB1=IIIA1+L2
                  IIIB3=IIIA3+L2
                  IIIB5=IIIA5+L2
740               IIIB7=IIIA7+L2
                  IIIBB=IIIAB+L2
```

```
                IIIBI=IIIAI+L2
                IIIBL=IIIAL+L2
                IIIBM=IIIAM+L2
745
             42 DO 46 J=KO,N1,2
                I=I+1
                IF (KO-2) 142,143
            142 IF (J-3) 43,44,45
750
C               GROUP 1G (J=1)
             43 IC1=IB1
                IC2=IB2
                IC3=IB3+L6
755             IC4=IB4+L6
                IC5=IA5
                IC6=IA6
                IC7=IA7+L6
                IC8=IA8+L6
760
C               GROUP 2G (J=1)
                IIC5=1
                IIC6=L6

765 C           GROUP 3K (J=1)
                IIIC1=IIIB1
                IIIC2=IIIB2
                IIIC3=IIIB3+L6
                IIIC4=IIIB4+L6
770             IIIC5=IIIB5
                IIIC6=IIIB6
                IIIC7=IIIB7+L6
                IIIC8=IIIB8+L6
                IIIC9=IIIB9
775             IIICA=IIIBA
                IIICB=IIIBB+L6
                IIICC=IIIBC+L6
                IIICD=IIIBD
                IIICE=IIIBE
780             IIICF=IIIBF+L6
                IIICG=IIIBG+L6
                IIICH=IIIBH+1
                IIICI=IIIBI+1
                IIICJ=IIIBJ+1
785             IIICK=IIIBK+1
                IIICL=IIIBL+L6
                IIICM=IIIBM+L6
                IIICN=IIIBN+L6
                IIICO=IIIBO+L6
790             GO TO 47

C               GROUP 1I (J=3)
             44 IC3=IB3-1
                IC4=IB4-1
795             IC7=IA7-1
                IC8=IA8-1

C               GROUP 2I (J=3)
```

```
                IIC6=-1.
800
C               GROUP 3M (J=3)
                IIIC3=IIIB3-1
                IIIC4=IIIB4-1
                IIIC7=IIIB7-1
805             IIIC8=IIIB8-1
                IIICB=IIIBB-1
                IIICC=IIIBC-1
                IIICF=IIIBF-1
                IIICG=IIIBG-1
810             IIICL=IIIBL-1
                IIICM=IIIBM-1
                IIICN=IIIBN-1
                IIICO=IIIBO-1
                GO TO 47
815          45 IF (J.NE.N1-1) GO TO 47

C               GROUP 2K (J=N1-1)
                IIC5=-L6

820  C          GROUP 3O (J=N1-1)
                IIICH=IIIBH-L6
                IIICI=IIIBI-L6
                IIICJ=IIIBJ-L6
                IIICK=IIIBK-L6
825             GO TO 47
             148 IF (J-4) 144,145,1145

C               GROUP 1H (J=2)
             144 IC1=IB1+1
830             IC2=IB2+1
                IC3=IB3
                IC4=IB4
                IC5=IA5+1
                IC6=IA6+1
835             IC7=IA7
                IC8=IA8

C               GROUP 2H (J=2)
                IIC5=1.
840             IIC6=L6

C               GROUP 3L (J=2)
                IIIC1=IIIB1+1
                IIIC2=IIIB2+1
845             IIIC3=IIIB3
                IIIC4=IIIB4
                IIIC5=IIIB5+1
                IIIC6=IIIB6+1
                IIIC7=IIIB7
850             IIIC8=IIIB8
                IIIC9=IIIB9+1
                IIICA=IIIBA+1
                IIICB=IIIBB
                IIICC=IIIBC
855             IIICD=IIIBD+1
```

```
                IIICE=IIIBE+1
                IIICF=IIIBF
                IIICG=IIIBG
                IIICH=IIIBH+1
      860       IIIGI=IIIBI+1
                IIICJ=IIIBJ+1
                IIICK=IIIBK+1
                IIICL=IIIBL+L6
                IIICM=IIIBM+L6
      865       IIICN=IIIBN+L6
                IIICO=IIIBO+L6
                GO TO 47

           C    GROUP 2J (J=4)
      870    145 IIC6=-1

           C    GROUP 3M (J=4)
                IIICL=IIIBL-1
                IIICM=IIIBM-1
      875       IIICN=IIIBN-1
                IIICO=IIIBO-1
                GO TO 47
             1145 IF (J.NE.N1) GO TO 47

      880   C    GROUP 1J (J=N1)
                IC1=IB1-L6
                IC2=IB2-L6
                IC5=IA5-L6
                IC6=IA6-L6
      885
           C    GROUP 2L (J=N1)
                IIC5=-L6

           C    GROUP 3P (J=N1)
      890       IIIC1=IIIB1-L6
                IIIC2=IIIB2-L6
                IIIC5=IIIB5-L6
                IIIC6=IIIB6-L6
                IIIC9=IIIB9-L6
      895       IIICA=IIIBA-L6
                IIICB=IIIBB-L6
                IIICE=IIIBE-L6
                IIICH=IIIBH-L6
                IIIC1=IIIBI-L6
      900       IIICJ=IIIBJ-L6
                IIICK=IIIBK-L6

             47 I1=I+IC1
                I2=I+IC2
      905       I3=I+IC3
                I4=I+IC4
                I5=I+IC5
                I6=I+IC6
                I7=I+IC7
      910       I8=I+IC8
                I9=I+IC9
                IA=I+ICA
```

```
      IB=I+IBB
      IC=I+IBC
915
      III=I+IIA1
      II2=I+IIA2
      II3=I+IIB3
      II4=I+IIB4
920   II5=I+IIC5
      II6=I+IIC6

      IIII=I+IIIC1
      III2=I+IIIC2
925   III3=I+IIIC3
      III4=I+IIIC4
      III5=I+IIIC5
      III6=I+IIIC6
      III7=I+IIIC7
930   III8=I+IIIC8
      III9=I+IIIC9
      IIIA=I+IIICA
      IIIB=I+IIICB
      IIIC=I+IIICC
935   IIID=I+IIICD
      IIIE=I+IIICE
      IIIF=I+IIICF
      IIIG=I+IIICG
      IIIH=I+IIICH
940   IIII=I+IIICI
      IIIJ=I+IIICJ
      IIIK=I+IIICK
      IIIL=I+IIICL
      IIIM=I+IIICM
945   IIIN=I+IIICN
      IIIO=I+IIICO
      IF (IK-1) 147,146
146 IF (G(I).EQ.10000.0) GO TO 48
      G1(I)=G1(I)+F1*
     +      (G(I)*G(I)-SJ1*(G(II)+G(I2)+G(I3)+G(I4)+G(I5)+G(I6)+G(I7)+G(I
     18)+G(I9)+G(IA)+G(IB)+G(IC))-SJ2*(G(III)+G(II2)+G(II3)+G(II4)+G(II5
     2)+G(II6))-SJ3*(G(IIII)+G(III2)+G(III3)+G(III4)+G(III5)+G(III6)+G(I
     3II7)+G(III8)+G(III9)+G(IIIA)+G(IIIB)+G(IIIC)+G(IIID)+G(IIIE)+G(III
     4F)+G(IIIG)+G(IIIH)+G(IIII)+G(IIIJ)+G(IIIK)+G(IIIL)+G(IIIM)+G(IIIN)
     5+G(IIIO)))
      FT(IE)=FT(IE)+G1(I)*EZYCC*FXCC(J)
      GO TO 48
147 IF (G(I).EQ.10000.0) GO TO 48
      G(I)=G(I)+F1*
     +      (G(I)*G1(I)-SJ1*(G1(II)+G1(I2)+G1(I3)+G1(I4)+G1(I5)+G1(I6)+G1(
     1I7)+G1(I8)+G1(I9)+G1(IA)+G1(IB)+G1(IC))-SJ2*(G1(III)+G1(II2)+G1(II
     23)+G1(II4)+G1(II5)+G1(II6))-SJ3*(G1(IIII)+G1(III2)+G1(III3)+G1(III
     34)+G1(III5)+G1(III6)+G1(III7)+G1(III8)+G1(III9)+G1(IIIA)+G1(IIIB)+
     4G1(IIIC)+G1(IIID)+G1(IIIE)+G1(IIIF)+G1(IIIG)+G1(IIIH)+G1(IIII)+G1(
     5IIIJ)+G1(IIIK)+G1(IIIL)+G1(IIIM)+G1(IIIN)+G1(IIIO))
      FT(IE)=FT(IE)+ G(I)*EZYCC*FXCC(J)
   48 CONTINUE
   49 CONTINUE
   50 CONTINUE
```

```
970            51 CONTINUE
               52 CONTINUE
                  R=ATIME(1)
                  WRITE (6,666) R

975               FLAG3=0.0
                  IF (FLAG3.NE.1.0) GO TO 201

               C     TO PRINT OUT FT
                  WRITE (6,320)
980            320 FORMAT (//1X,1X,5(8HREAL(FT),4X,8HIMAG(FT),4X),/)
                  ILL=IMAXP/5
                  IF (5*ILL.NE.IMAXP) ILL=ILL+1
                  DO 62 I=1,ILL
                  WRITE (6,321) FT(I),FT(I+ILL),FT(I+2*ILL),FT(I+3*ILL),FT(I+4*ILL)
985            62 CONTINUE
               201 CONTINUE
               321 FORMAT (1X,10G12.6)

               C     FREQUENCY SHIFTS
990               T=0.0
                  DO 59 I=1,IMAXP
                  FSHIFF=CEXP(Z2*2.0*FNORMF*(I-1)/(NTSPC*EMAX))
                  FSHIFT=CEXP(Z2*2.0*EXPANDX*(I-1)/(NTSPC*EMAX))
                  IF (FLAG1.NE.1.0) FSHIFT=(1.0,0.0)
995               FT(I)=FT(I)*EXP(-AL*DC*T**2)*FSHIFT*FSHIFF
                  T=T+DELT
               59 CONTINUE

               C     BELOW, THE MEMORY OF G AND G1 IS USED FOR FT AND ITS FOURIER XFORM
1000              DO 72 I=1,IMAXP
                  G(I)=FT(I)
                  G1(I)=(0.0,0.0)
               72 CONTINUE
                  IMAXPP=IMAXP+1
1005              DO 73 I=IMAXPP,ICON
                  G(I)=(0.0,0.0)
                  G1(I)=(0.0,0.0)
               73 CONTINUE

1010           C     FFFF(LIFT) IS THE NUMBER OF SPIKES PRESENT
                  FFFF(LIFT)=REAL(FT(1))
                  WRITE(6,207) FFFF(LIFT)
               207 FORMAT (/1X,8HFT(1) = ,F7.0)
                  R=ATIME(1)
1015              WRITE (6,666) R

               C     FOURIER TRANSFORM SUBROUTINE
                  CALL FFT(G1,G,ICON)
                  R=ATIME(1)
1020              WRITE (6,666) R

               C     TO AVERAGE THE FT'S OVER NCELLS CELLS
                  ILLI=1
                  DO 206 I=1,NFTS
1025              AVSQ(I)=REAL(G1(I))+AVSQ(I)
                  IF (AVSQ(I).GT.AVSQ(ILLI)) ILLI=I
```

```
  206 CONTINUE

C     TO NORMALIZE GFT AND FIND GFTMAX
1030      IIT=1
          DO 69 I=1,NFTS
          GFT(I)=REAL(G1(I))/FFFF(LIFT)
          IF (GFT(I).GT.GFT(IIT)) IIT=I
   69 CONTINUE
1035
C     TO PRINT OUT GFT
          WRITE (6,322)
  322 FORMAT (//1X,1A,10(3HGFT,9X))
          ILL=NFTS/10
1040      IF (10*ILL.NE.NFTS) ILL=ILL+1
          DO 63 I=1,ILL
          WRITE (6,321) GFT(I),GFT(I+ILL),GFT(I+2*ILL),GFT(I+3*ILL),GFT(I+4*
         1ILL),GFT(I+5*ILL),GFT(I+6*ILL),GFT(I+7*ILL),GFT(I+8*ILL),GFT(I+9*
         2ILL)
1045   63 CONTINUE
          IF (LIFT.NE.NCELLS) GO TO 205

C     TO PRINT OUT AVERAGED S(G,F) AFTER NCELLS RUNS
          WRITE (6,210)
1050  210 FORMAT (//1X,9HAVERAGED)
          DO 208 I=1,ILL
          WRITE (6,321) AVSQ(I),AVSQ(I+ILL),AVSQ(I+2*ILL),AVSQ(I+3*ILL),AVSQ
         1(I+4*ILL),AVSQ(I+5*ILL),AVSQ(I+6*ILL),AVSQ(I+7*ILL),AVSQ(I+8*ILL),
         2AVSQ(I+9*ILL)
1055  208 CONTINUE
  209 CONTINUE
          IF (FLAG2.NE.1) GO TO 64

C     GIVES A PRINTER PLOT OF FFT IF (FLAG2.EQ.1.0)
1060      JCE=NFTS/100+1
          DO 61 JIM=1,JCE
          DO 60 K=1,100
          JACK=K+(JIM-1)*100
          GF(K)=REAL(G1(JACK))
1065   60 CONTINUE
          GF(1)=GFT(IIT)
          GF(2)=0.0
          CALL GRAPH (GF)
   61 CONTINUE
1070   64 CONTINUE



C     TO NORMALIZE GFT TO 100
C     TO SET UP X-AXIS VALUES OF E (=ENORM)
1075      IF (LIFT.NE.1) GO TO 222
          GFTMAX=GFT(IIT)
  222 DO 71 I=1,NFTS
          GFT(I)=GFT(I)*100.0/GFTMAX
1080      ENORM(I)=DINORM*I-EXPAND
   71 CONTINUE
C     TO PLOT THE ABOVE MESS
          IF (LIFT.NE.1) GO TO 205
```

```
      XL=8.5
1085  YL=6.5
      XMIN=-EXPANDX
      XMAX=EMAX+EXPANDX
      YMIN=0.0
      YMAX=110.0
1090  TICX=1.0
      TICY=10.0
      CALL PLOT (1,XL,YL,XMIN,XMAX,YMIN,YMAX,TICX,TICY)
      CALL AXLIN (10H("E(TH-Z)"),6,30H("S(W,E) (NORMALIZED TO 100)"),26,6
     1H(F4.1),4,6H(F5.0),5)
1095  FORM(1)=10H(13H6 = (2
      FORM(2)=10HPI/A)(,F8.
      FORM(3)=10H5,1H,,F8.5
      FORM(4)=10H,1H,,F8.5,
      FORM(5)=4H1H))
1100  SIZE=2.0
      DIR=0.0
      XLOC=-EXPANDX+0.7
      YLOC=101.25
      CALL PLOT (3,FORM,SIZE,DIR,XLOC,YLOC,CHAT,3)
1105  FORMA(1)=10H(4HX = ,F4
      FORMA(2)=3H.1)
      YLOC=96.25
      CALL PLOT (3,FORMA,SIZE,DIR,XLOC,YLOC,X,1)
      PEN=1.0
1110  SYMB=0.0
  205 CALL PLOT (2,PEN,SYMB,ENORM,GET,NPTS)
  203 CONTINUE
      AVSQM=AVSQ(ILL1)
      DO 211 I=1,NPTS
1115  AVSQ(I)=AVSQ(I)*100.0/AVSQM
  211 CONTINUE
      CALL PLOT (1,XL,YL,XMIN,XMAX,YMIN,YMAX,TICX,TICY)
      CALL AXLIN (10H("E(TH-Z)"),6,30H("S(W,E) (NORMALIZED TO 100)"),26,6
     1H(F4.1),4,6H(F5.0),5)
1120  YLOC=101.25
      CALL PLOT (3,FORM,SIZE,DIR,XLOC,YLOC,CHAT,3)
      YLOC=96.25
      CALL PLOT (3,FORMA,SIZE,DIR,XLOC,YLOC,X,1)
      CALL PLOT (2,PEN,SYMB,ENORM,AVSQ,NPTS)
1125

      CALL EXIT
      END
```